NANOPIPET ELECTRODES FOR THE DETECTION OF NEUROTRANSMITTERS USING THE INTERFACE BETWEEN TWO IMMISCIBLE ELECTROLYTE SOLUTIONS

BY

MICHELLE LYNNE COLOMBO

THESIS

Submitted in partial fulfillment of the requirements
for the degree of Master of Science in Chemistry
in the Graduate College of the
University of Illinois at Urbana-Champaign, 2016

Urbana, Illinois

Advisers:

Professor Jonathan Sweedler
Research Assistant Professor Mei Shen

ABSTRACT

The ability to chemically characterize small domains in living systems is an important yet unmet goal. Specifically, there is still much to learn regarding the vital process of cell-to-cell communication, or neurotransmission. A nanoscale interface between two immiscible electrolyte solutions (ITIES) provides a unique analytical platform for the detection of ionic species of biological interest such as neurotransmitters and neuromodulators, especially those that are otherwise difficult to detect directly on a carbon electrode without electrode modification.

In this thesis, the detection of acetylcholine, serotonin, and tryptamine is reported using nanopipet electrode probes with radii on the order of tens of nanometers. The transfer of these analytes across a 1,2-dichloroethane/water interface was studied by cyclic voltammetry and amperometry. Well-defined sigmoidal voltammograms were observed on the nanopipet electrodes within the potential window of artificial seawater for acetylcholine and tryptamine. The half-wave transfer potential of acetylcholine, tryptamine, and serotonin were examined and found to be distinct from one another, allowing for qualitative detection. The detection of these analytes was linear in the mM concentration range, and the limits of detection for acetylcholine and serotonin were found to be below the expected concentrations within a synaptic cleft.

Next, the detection of dopamine (DA) at nanopipet electrodes with radii of hundreds of nanometers is presented. Dibenzo-18-crown-6 was employed as an ionophore to facilitate DA transfer, allowing for DA to be detected in a solution of $MgCl_2$, where well-defined steady-state sigmoidal cyclic voltammograms were observed for the transfer of DA. The detection is linear for concentrations of DA ranging from 0.25 mM to 2 mM. The diffusion

coefficient at these nanopipet electrodes was calculated both with and without the presence of the common interferent ascorbic acid. DA detection still shows linear behavior with well-defined sigmoidal CVs even when up to 20 mM ascorbic acid is present in solution, though the observed diffusion coefficient of DA decreases with increasing ascorbic acid concentrations. However, the physiological concentration of 0.1 mM AA had no effect on DA's diffusion coefficient.

Finally, cultured neurons from *Aplysia californica* were interrogated using these ITIES-based nanopipet electrodes in combination with scanning electrochemical microscopy. No external mediator was required for this process, as the assisted transfer of ASW produced successful negative feedback. This technique allowed for highly spatially resolved topographical images of neuronal processes using constant height imaging. Furthermore, cells were stimulated with a solution of high potassium and the intracellular response was recorded at the nanopipet electrodes. While significant future work is still necessary, these preliminary results show potential for these electrodes to examine the dynamics of neurotransmission in real-time.

ACKNOWLEDGMENTS

I would like express my deep gratitude to Professor Mei Shen for allowing me to work with her and learn from her, and to Professor Jonathan Sweedler for all of his guidance and advice that he has given me over the past several years. I am extremely appreciative of all of the opportunities that Professor Shen and Professor Sweedler have provided me.

I wish to extend thanks to Professor Joaquín Rodríguez-López and his group members for including me in scientific discussions and allowing me to share their work space, particularly Mark Burgess and Teresa Cristarella for the scientific input and encouraging conversations. I am especially thankful to Scott Dubowsky for the many conversations regarding chemistry and careers, and for providing support and encouragement daily.

I would also like to express gratitude to Xiying Wang and Dr. Stanislav Rubakhin for their continued support in the cell culturing process. Finally I would like to thank the many undergraduate researchers who have assisted me with this work, especially Swami McNeil, Albert Chang, Nicholas Iwai, Theresa Welle, and Natalie Ibe.

TABLE OF CONTENTS

CHAPTER 1

INTRODUCTION

1.1 GENERAL OVERVIEW

Neurotransmission is the process by which cell to cell communication occurs, governing many aspects of nervous system activity. While we have learned a lot about this process over the past few decades, there is still a great deal of information that is unknown regarding the dynamics of synaptic release. Given that neurotransmission is involved in regulating so much of nervous system functioning, and that numerous neurological disorders are caused by disruptions in synaptic function (1-7), it is important to learn how both healthy and diseased cells behave during this process. To do this, it is likely that the analytical technique used should be able to probe the various small spaces in which neurotransmission occurs, so that the process can be studied at the appropriate scale (see section 1.2).

Electrochemical techniques have been very useful in probing the intricacies of neurotransmission (8-18). Traditional electrochemical analyses within neuroscience rely on the use of a carbon fiber microelectrode, where the species of interest is detected via reduction or oxidation upon contact with the solid carbon surface. While these studies have provided neuroscientists with invaluable information, there is still much to be explored. Of particular interest is the study of neurotransmitters that cannot be detected at traditional electrodes, such as acetylcholine, glutamate, and γ-aminobutyric acid. Because these analytes do not go through the processes of reduction or oxidation, carbon electrodes need to be modified in various ways to detect them (19-22). However, these surface modifications can introduce further complications to the system, such as delayed time response.

A different type of electrode exists, which does not rely on redox processes for the detection of analytes. Rather, it relies on the transfer of ions across an "Interface between Two Immiscible Electrolyte Solutions" (ITIES; see section 1.3) (23-26). When the interface is sufficiently polarized upon the application of a certain potential, ions will transfer across the interface and this charge transfer is read as a current response that can be analyzed analogously to traditional carbon microelectrodes. This mode of detection means that as long as an analyte is in ionic form, it can be detected whether it is redox-active or not, and without the use of electrode surface modifications. Here we present the use of nanometer-sized ITIES-based pipet electrodes for the detection of both redox active and non-redox active neurotransmitters and neuromodulators.

1.2 LITERATURE REVIEW: CARBON NANOELECTRODES FOR THE DETECTION OF NEUROTRANSMITTERS[1]

Reports of carbon electrodes with dimensions on the submicron scale can be traced back to the late 1980's (27-30). Most are based on the typical fabrication process for carbon fiber microelectrodes (CFMEs) (31-33), followed by further etching to achieve nm scale dimensions, as follows (Figure 1.1): a carbon fiber with a diameter on the micron scale is aspirated into a glass capillary, which is then pulled to form two glass pipets with the fiber between the two nm sized openings. This fiber is then cut and electrical contact is made with a conductive liquid and a metal wire. From here, the carbon fiber can be etched down to nm dimensions in a variety of ways.

[1] This section appeared in Analytical Methods with the following citation: Shen, M. and Colombo, M.L. "Electrochemical nanoprobes for the chemical detection of neurotransmitters." *Anal. Methods.* **2015**, *7*, 7095-7105, and portions have been edited or removed for clarity and brevity. This article is reprinted with the permission of the publisher and is available using DOI: 10.1039/c5ay00512d.

In 1992, Ewing's group reported a method for the fabrication of carbon fiber nanoelectrodes (CFNEs) whereby an oxygen/ methane flame was used to etch the carbon fiber down to as small as 100 nm, followed by an extremely thin copolymer film coating of 2-allylphenol and phenol for insulation (34). This insulating layer was then removed from the very tip of the fiber, typically via scalpel, to create a disk-shaped electroactive area. Dopamine concentrations down to 99 mM were detected using a probe of electroactive diameter of about 200 nm. Besides the disk shaped carbon nanoelectrode as described above (34), the majority of literature employing carbon nanoelectrode for neurotransmitter detection are conical shape, with a length most often in micrometer scale exposed. Since the exposed electroactive area is much larger compared to disk shaped nanoelectrode, typically much lower LODs are achieved on these conical carbon fiber nanoelectrodes. In 1996, Zhang et al. reported a method employing argon ion beam etching to fabricate smooth cone shaped CFNEs with a success rate of 50–80% depending on tip diameter, using argon ion beam etching (35). Using differential pulse voltammetry (DPV), these CFNEs were able to detect down to 100 nM DA and 500 nM 5-HT in a phosphate buffer solution. While no selectivity study was reported on these conical CFNEs; a decrease in 5-HT steady-state oxidation current was observed with multiple scans due to an insulating film that forms on the surface of the electrode from the oxidation products of 5-HT, as reported in other works (36, 37).

In 2001, the Cheng group of Wuhan University reported a new method for creating carbon nanoelectrodes in which the carbon fibers are flame fuse sealed to the tip of a pulled glass capillary (with inner diameter of ~20 mm) and flame etched and in order to reduce etching time while maintaining a smooth fiber/glass interface (38). These CFNEs were used to detect several catecholamines (dopamine, epinephrine, and norepinephrine) in a phosphate

buffer solution using cyclic voltammetry as well as DPV, with detection limits for dopamine, epinephrine, and norepinephrine in the mid-nanomolar range. The electrooxidation of serotonin formed an insulating film on the surface of the electrode (38), which can be overcome by using fast scan rates such as those used in fast scan cyclic voltammetry (FSCV) (12).

These nanoelectrodes were later used in combination with FSCV to amperometrically monitor dopamine release from live PC12 cells (39). The tip diameter of the probes, around 100 nm, nicely corresponds to the average size of a PC12 vesicle, around 99 nm. A nanoelectrode placed < 500 nm above a cellular release site was able to detect amperometric spikes corresponding to the release of content from individual vesicles. The high spatial resolution obtained by these nanoelectrodes showed that most sites on a cell surface are actually inactive, supporting previous results that used a 2 mm diameter microelectrode to image chromaffin cell release sites (40). Additionally, this was the first report of direct electrochemical detection of sequential dopamine release from multiple vesicles at the same release site (Figure 1.2).

Recently, Li et al. reported on CFNEs that were able to fit inside an apparent synapse, specifically inside the space between a neuron's soma and a neuronal varicosity (41). Inside the apparent synapse, complex sequences of events were detected, which were distinctly different from single spike events that are typically detected using carbon fiber microelectrodes (Figure 1.3B). Furthermore, using a CFNE inside the apparent synapse and a CFNE above the same varicosity (semi-artificial synapse), significantly more amperometric spikes corresponding to vesicle release were detected at the probe inside the synapse than at the one above (Figure 1.3B), confirming non-uniform distribution of active hot spots at the

synapse (42). While this study is insightful regarding vesicular release at the synapse, no information was obtained in terms of the chemical makeup of the release detected.

Most recently, Jill Venton's group has reported on the use of carbon nanopipette electrodes (CNPEs), which are fabricated without the use of a carbon fiber, making them more robust for applications involving tissue implantation (43). Briefly, after laser pulling quartz capillaries, chemical vapor deposition was used to selectively deposit carbon inside the pipette. Next, 5:1 buffered hydrofluoric acid was used to etch away quartz at the tip of the electrode. FSCV of 1 mM dopamine was used to compare CNPEs to CFMEs. While the ratio of background current to peak oxidative current was higher at CNPEs, the average difference between the oxidative and reductive peak potentials was significantly lower for CNPEs. Octopamine and serotonin were also detected using FSCV at the CNPEs, each with a waveform specialized for the respective analyte that reduces electrode fouling. Octopamine showed a larger secondary peak at the CNPE compared to the CFME, indicating possible oxidation product adsorption at the surface of the CNPE. Based on the ratio of background current to peak oxidative current, the CNPEs show a higher sensitivity to serotonin and the same sensitivity to octopamine relative to the CFMEs. Finally, the CNPEs were used for *in vivo* FSCV measurements of endogeneous extracellular dopamine in the *Drosophila melanogaster* (43).

1.3 ITIES-BASED PIPET ELECTRODES[2]

Despite the advantages of carbon nanoelectrodes, they have been slow to become routine probes in electroanalytical chemistry due to technical challenges in preparing electrodes with sizes that are two to three orders of magnitude smaller than traditionally used microelectrodes. Other limitations include the lack of availability for nanometer sized carbon fiber or metal wires. However, the use of ITIES-based pipet electrodes may overcome this difficulty, because preparing nanopipets uses the same technique as preparing micro- or macropipets, by adjusting puller parameters.

The process of nanopipet fabrication relies on three basic steps: (1) creation of nanometer orifice at the end of pipet, (2) surface treatment of the generated nanopipet and (3) assembly the nanopipet electrode. This process is summarized in Figure 1.4 and described in more detail below.

The surface treatment of the nanopipet is very critical for the formation of stable ITIES. During surface treatment, a silane, such as chlorotrimethylsilane, reacts with –OH group on the surface of the glass, and the glass surface changes from hydrophilic to hydrophobic, eventually yielding $–O–Si(CH_3)_3$ groups. Once a nanopipet has been prepared, the next step is to fill the nanopipet with an electrolyte solution of 1,2-dichloroethane or nitrobenzene. Sometimes, an ionophore will be used to facilitate the transfer of certain ions. The last step of nanopipet preparation is insertion of an inner reference electrode, typically a Pt wire.

This thesis describes the characterization and use of nano-scale ITIES pipet electrodes. Chapter 2 describes the characterization of these electrodes for the voltammetric and

[2] This section appeared in Analytical Methods with the following citation: Shen, M. and Colombo, M.L. "Electrochemical nanoprobes for the chemical detection of neurotransmitters." *Anal. Methods.* **2015**, *7*, 7095-7105, and portions have been edited or removed for clarity and brevity. This article is reprinted with the permission of the publisher and is available using DOI: 10.1039/c5ay00512d.

amperometric detection of acetylcholine, tryptamine, and serotonin using simple ion transfer. Chapter 3 describes the electrodes that have been modified to include an ionophore, which allows for the facilitated transfer and detection of dopamine using cyclic voltammetry; and it examines the effect of ascorbic acid interference. Chapter 4 describes the use of these probes in combination with scanning electrochemical microscopy for the imaging and chemical stimulation of cultured *Aplysia californica* neurons, and Chapter 5 summarizes the work described here and details future work for this project.

1.4 FIGURES

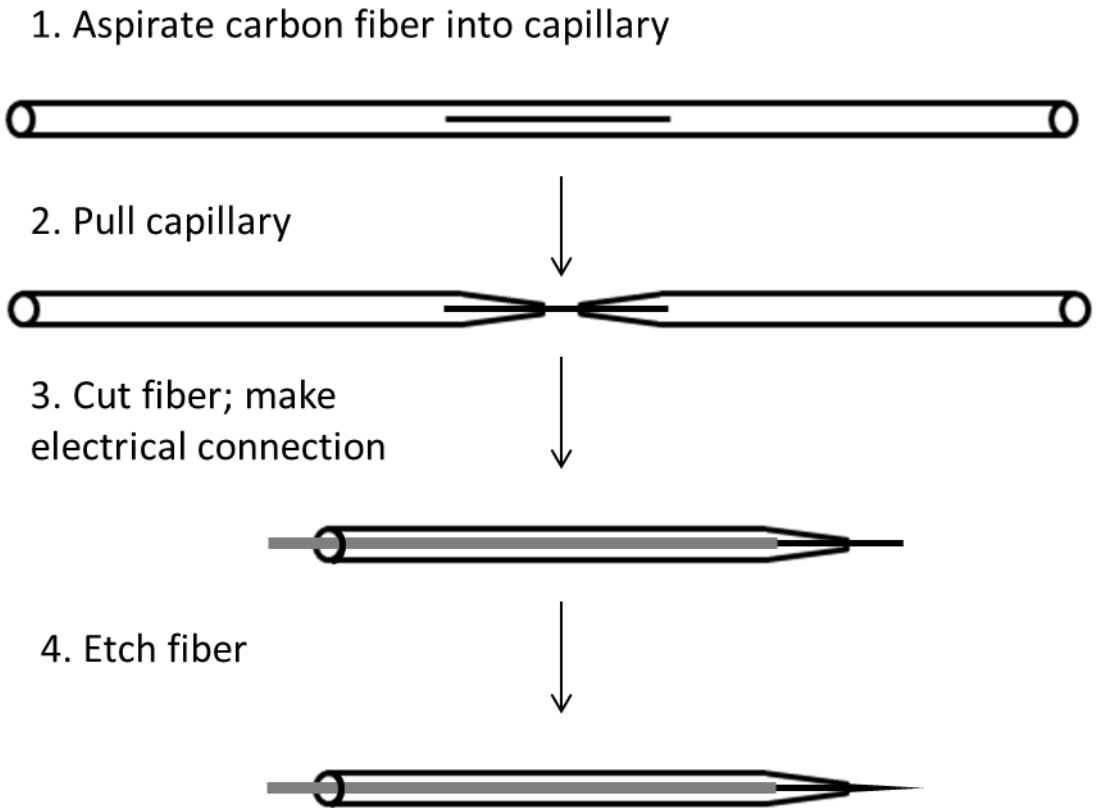

Figure 1.1. General procedure for producing carbon fiber nanoelectrodes, which can then be further modified according to specific detection needs. Order may be rearranged, as noted in the main text.

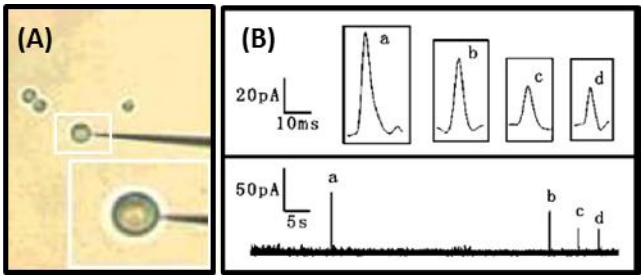

Figure 1.2. (A) Photograph of nanoelectrode-cell arrangement. (B) Spikes corresponding to sequential dopamine release from multiple vesicles with the electrode placed over the same position on the cell. Graphs a-d show magnified pictures of the individual current spikes. Modified from ref. 39.

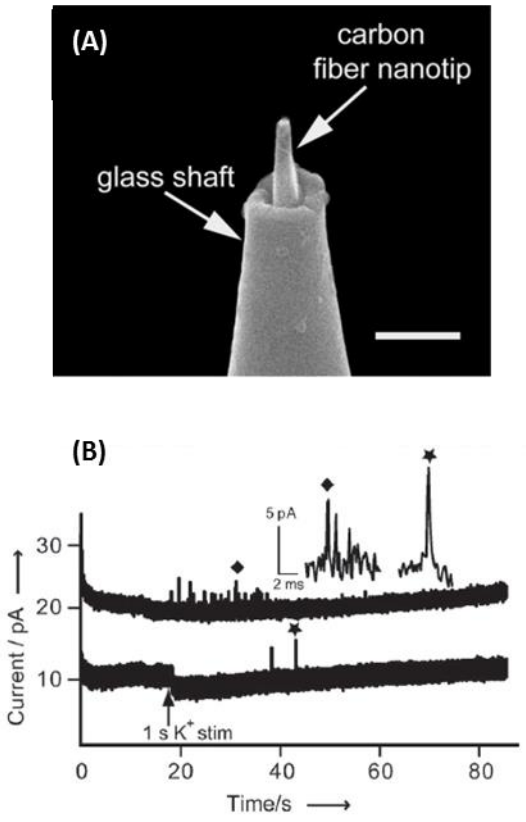

Figure 1.3. (A) Scanning electron micrograph of flame etched carbon fiber fused inside a sub-micropipette; scale bar is 1 µm. (B) Quantal amperometric spikes recorded inside the synapse (upper trace) and above the synapse (lower trace). Modified from ref. 41.

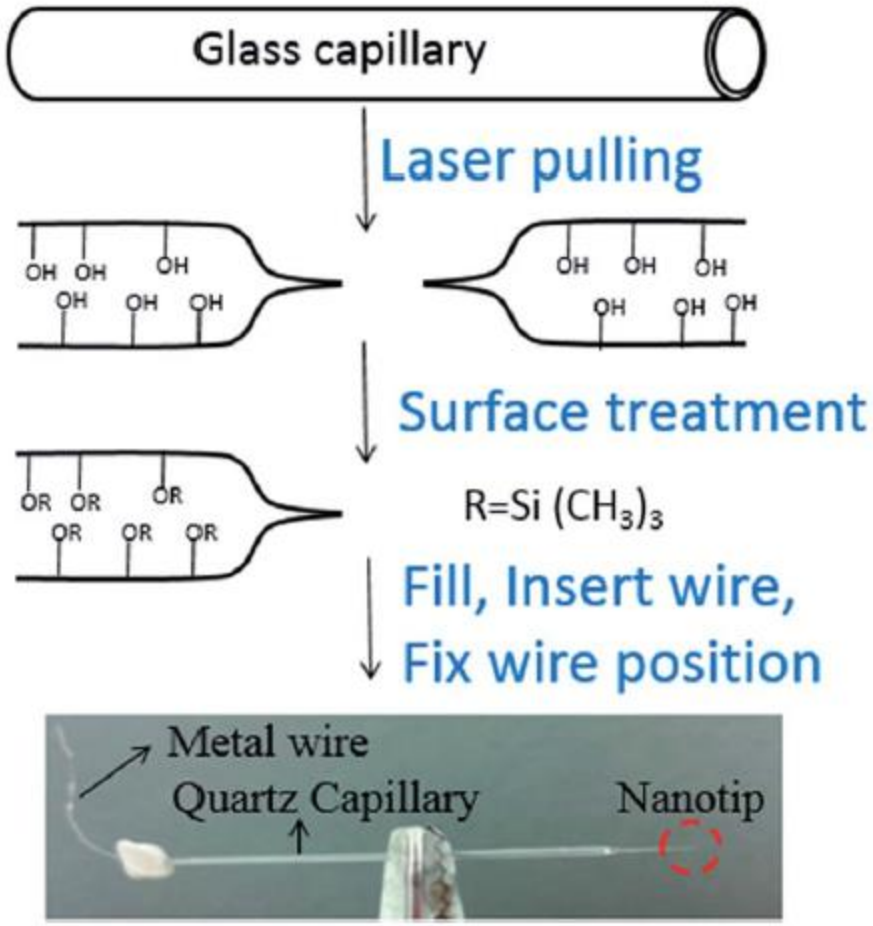

Figure 1.4. Fabrication process of a nanopipet electrode. In the surface treatment process, listed here is trimethylsilyl (-Si$(CH_3)_3$) as an example, however other types of silanes can be used as well.

1.5 REFERENCES

1. A. S. Brown and S. Gershon, *Journal of Neural Transmission-General Section*, **91**, 75 (1993).
2. T. Sawaguchi and P. S. Goldmanrakic, *Science*, **251**, 947 (1991).
3. B. E. Jones, *Trends in Pharmacological Sciences*, **26**, 578 (2005).
4. K. P. Lesch, D. Bengel, A. Heils, S. Z. Sabol, B. D. Greenberg, S. Petri, J. Benjamin, C. R. Muller, D. H. Hamer and D. L. Murphy, *Science*, **274**, 1527 (1996).
5. T. Kihara and S. Shimohama, *Acta Neurobiologiae Experimentalis*, **64**, 99 (2004).
6. T. A. Slotkin, C. B. Nemeroff, G. Bissette and F. J. Seidler, *Journal of Clinical Investigation*, **94**, 696 (1994).
7. E. A. Kravitz, *Science*, **241**, 1775 (1988).
8. B. D. Bath, D. J. Michael, B. J. Trafton, J. D. Joseph, P. L. Runnels and R. M. Wightman, *Analytical Chemistry*, **72**, 5994 (2000).

9. M. P. Brazell, R. J. Kasser, K. J. Renner, J. Feng, B. Moghaddam and R. N. Adams, *Journal of Neuroscience Methods*, **22**, 167 (1987).
10. G. A. Gerhardt, A. F. Oke, G. Nagy, B. Moghaddam and R. N. Adams, *Brain Research*, **290**, 390 (1984).
11. P. Hashemi, E. C. Dankoski, J. Petrovic, R. B. Keithley and R. M. Wightman, *Analytical Chemistry*, **81**, 9462 (2009).
12. B. P. Jackson, S. M. Dietz and R. M. Wightman, *Analytical Chemistry*, **67**, 1115 (1995).
13. M. C. Rodriguez, M. D. Rubianes and G. A. Rivas, *Journal of Nanoscience and Nanotechnology*, **8**, 6003 (2008).
14. P. S. Cahill, Q. D. Walker, J. M. Finnegan, G. E. Mickelson, E. R. Travis and R. M. Wightman, *Analytical Chemistry*, **68**, 3180 (1996).
15. A. S. Cans and A. G. Ewing, *J. Solid State Electrochem.*, **15**, 1437 (2011).
16. E. L. Ciolkowski, B. R. Cooper, J. A. Jankowski, J. W. Jorgenson and R. M. Wightman, *Journal of the American Chemical Society*, **114**, 2815 (1992).
17. J. M. Finnegan and R. M. Wightman, *Journal of Biological Chemistry*, **270**, 5353 (1995).
18. R. M. Wightman, *Science*, **311**, 1570 (2006).
19. P. D. Hale and R. M. Wightman, *Molecular Crystals and Liquid Crystals*, **160**, 269 (1988).
20. J. L. Kawagoe, D. E. Niehaus and R. M. Wightman, *Analytical Chemistry*, **63**, 2961 (1991).
21. E. Tamiya, Y. Sugiura, E. N. Navera, S. Mizoshita, K. Nakajima, A. Akiyama and I. Karube, *Analytica Chimica Acta*, **251**, 129 (1991).
22. T. V. Barkhimer, J. R. Kirchhoff, R. A. Hudson, W. S. Messer and L. M. V. Tillekeratne, *Anal. Bioanal. Chem.*, **392**, 651 (2008).
23. S. Amemiya, J. Kim, A. Izadyar, B. Kabagambe, M. Shen and R. Ishimatsu, *Electrochimica Acta*, **110**, 836 (2013).
24. Z. k. Samec, V. Mareček, and D. Homolka, *Journal of Electroanalytical Chemistry and Interfacial Electrochemistry*, **158**, 25 (1983).
25. Y. X. Wang, J. Velmurugan, M. V. Mirkin, P. J. Rodgers, J. Kim and S. Amemiya, *Analytical Chemistry*, **82**, 77 (2010).
26. P. J. Rodgers, S. Amemiya, Y. X. Wang and M. V. Mirkin, *Analytical Chemistry*, **82**, 84 (2010).
27. T. Abe, K. Itaya and I. Uchida, *Chemistry Letters*, 399 (1988).
28. A. Schulte and R. H. Chow, *Analytical Chemistry*, **70**, 985 (1998).
29. M. Armstrongjames, K. Fox and J. Millar, *Journal of Neuroscience Methods*, **2**, 431 (1980).
30. A. Meulemans, B. Poulain, G. Baux, L. Tauc and D. Henzel, *Analytical Chemistry*, **58**, 2088 (1986).
31. M. A. Dayton, J. C. Brown, K. J. Stutts and R. M. Wightman, *Analytical Chemistry*, **52**, 946 (1980).
32. J. L. Ponchon, R. Cespuglio, F. Gonon, M. Jouvet and J. F. Pujol, *Analytical Chemistry*, **51**, 1483 (1979).
33. A. G. Ewing, M. A. Dayton and R. M. Wightman, *Analytical Chemistry*, **53**, 1842 (1981).
34. T. G. Strein and A. G. Ewing, *Analytical Chemistry*, **64**, 1368 (1992).
35. X. J. Zhang, W. M. Zhang, X. Y. Zhou and B. Ogorevc, *Analytical Chemistry*, **68**, 3338 (1996).

36. Y. Y. Lau, D. K. Y. Wong, G. Luo and A. G. Ewing, *Electroanalysis*, **4**, 865 (1992).
37. M. C. Henstridge, G. G. Wildgoose and R. G. Compton, *Journal of Physical Chemistry C*, **113**, 14285 (2009).
38. W. H. Huang, D. W. Pang, H. Tong, Z. L. Wang and J. K. Cheng, *Analytical Chemistry*, **73**, 1048 (2001).
39. W. Z. Wu, W. H. Huang, W. Wang, Z. L. Wang, J. K. Cheng, T. Xu, R. Y. Zhang, Y. Chen and J. Liut, *Journal of the American Chemical Society*, **127**, 8914 (2005).
40. I. M. Robinson, J. M. Finnegan, J. R. Monck, R. M. Wightman and J. M. Fernandez, *Proceedings of the National Academy of Sciences of the United States of America*, **92**, 2474 (1995).
41. Y. T. Li, S. H. Zhang, L. Wang, R. R. Xiao, W. Liu, X. W. Zhang, Z. Zhou, C. Amatore and W. H. Huang, *Angewandte Chemie-International Edition*, **53**, 12456 (2014).
42. T. C. Sudhof, *Neuron*, **75**, 11 (2012).
43. H. R. Rees, S. E. Anderson, E. Privman, H. H. Bau and B. J. Venton, *Analytical Chemistry*, **87**, 3849 (2015).

CHAPTER 2

NANOPIPET-BASED LIQUID-LIQUID INTERFACE PROBES FOR THE ELECTROCHEMICAL DETECTION OF ACETYLCHOLINE, TRYPTAMINE, AND SEROTONIN VIA IONIC TRANSFER[3]

2.1 INTRODUCTION

Neurotransmitters, acting as chemical messengers, play an important role in neurotransmission, which governs many functional aspects of nervous system activity, including behaviors, emotional responses, learning, and memory. Specifically, acetylcholine (ACh) is a key regulator in sleep and wakefulness (1, 2), as well as consciousness (3), and promotes sustained attention (4). Similarly, disruptions in the serotonergic system have been shown to be involved in disorders such as anxiety and depression (5-7), and the neuromodulator tryptamine (T) has been shown to enhance serotonin (5-HT) release (8).

The use of pipet electrodes based on ionic transfer across an interface between two immiscible electrolyte solutions (ITIES) has been an important method to detect ionic analytes (9-22). Ionic transfer of neurotransmitters across ITIES, mainly micro- and macrointerfaces has been reported (23-25). NanoITIES-based sensor probes have significantly improved spatial resolution compared to microelectrodes and have been proven to be useful for imaging a single nanopore (26).

To the best of our knowledge, the ionic transfer of neurotransmitters across a nanointerface has not been reported. Herein we describe the direct quantitative and

[3] This chapter appeared in its in Analytical Chemistry with the following citation: Colombo, M.L., Sweedler, J.V., Shen, M. "Electrochemical nanoprobes for the chemical detection of neurotransmitters." *Anal. Chem.* **2015**, *87*, 5095-5100, and portions have been edited or removed for clarity and brevity. This article is reprinted with the permission of the publisher and is available using DOI: 10.1021/ac504151e.

qualitative detection of both electrochemically nonredox-active (ACh) and redox-active neurotransmitters (T and 5-HT) with nanoITIES based pipet sensor probes. Such an approach has the advantage of being able to detect both electrochemically nonredox-active neurotransmitters (e.g., ACh) and redox-active neurotransmitters (e.g., T and 5-HT) (Scheme 2.1).

2.2 EXPERIMENTAL SECTION

2.2.1 Reagents

Potassium tetrakis(pentafluorophenyl)borate (TFAB) was obtained from Boulder Scientific Company (Mead, CO). Tetradodecylammonium (TDDA) chloride, tetraethylammonium chloride (TEACl), 1,2-dichloroethane (1,2-DCE), and chlorotrimethylsilane were purchased from Sigma-Aldrich (St. Louis, MO). The TFAB salt of TDDA (TDDATFAB) was prepared by metathesis. Potassium chloride (KCl) was from VWR (Radnor, PA), calcium chloride ($CaCl_2$) was from Sigma-Aldrich (St. Louis, MO), and magnesium chloride ($MgCl_2$) was from Amresco (Solon, OH). Magnesium sulfate (MgSO4), HEPES, and lithium chloride (LiCl) were from Fisher Scientific (Pittsburgh, PA). Artificial seawater (ASW) contained (in mM) the following: 460 NaCl, 10 KCl, 10 $CaCl_2$, 22 $MgCl_2$, 26 $MgSO_4$, and 10 HEPES (pH 7.8). Acetylcholine (ACh) chloride and tryptamine (T) hydrochloride were from Sigma-Aldrich (St. Louis, MO), and serotonin (5-HT) hydrochloride was purchased from Alfa Aesar (Ward Hill, MA). All reagents were used as received, and solutions were prepared using 18.3 MΩ cm deionized water (ELGA, Woodridge, IL). The prepared solutions were passed through a 0.2 μm filter (Thermo Scientific, Waltham, MA) before use.

2.2.2 Nanopipet electrode preparation and characterization

Nanometer-scale pipet probes were fabricated by laser pulling of quartz capillaries (O.D. = 1.0 mm, I.D. = 0.7 mm, length = 10 cm, Sutter Instrument, Novato, CA) using a P-2000 capillary puller (Sutter Instrument) using the parameters listed in Table A.1 in Supporting Information (Appendix A). To make sure a stable interface was formed at the orifice of the nanopipet, we applied a surface treatment through a chemical vapor silanization process via chlorotrimethylsilane to the pulled nanopipet. Figure 2.1A shows one nanopipet probe with a radius ≈ 15 nm, and Figure 2.1B shows an SEM image of the orifice of the pipet tip. The prepared nanopipets were filled with a 1,2-DCE solution of organic supporting electrolytes and immersed in an aqueous solution of either ACh, T, or 5-HT.

2.2.3 Electrochemical experiments

The transfer of protonated ACh, T, and 5-HT across the 1,2-DCE/water interface was studied by cyclic voltammetry and amperometry. All electrochemical measurements were recorded using a CHI1205B Electrochemical Analyzer (CH Instruments, Austin, TX). A nanopipet was filled with 5 mM TDDATFAB in 1,2-DCE and immersed into an aqueous solution for the detection of neurotransmitters (NT). NTs were detected in an aqueous solution of ASW. ASW was used, as it is a relevant biological media for our commonly used neuronal model, *Aplysia californica* (27, 28); by optimizing our detection in this media, future biological experiments will be facilitated. When NT cannot be transferred within the potential window of ASW, an aqueous media with a potential window larger than that of ASW was used, i.e., LiCl. A Pt wire (diameter = 50 μm) was inserted inside the pipet, and either a Ag wire (diameter = 250 μm) coated with AgCl or a Au wire (diameter = 50 μm) coated with polypyrrole (Ppy) was placed outside the pipet used as an external reference

electrode; the voltage was applied between the platinum wire and the external reference electrode. The Pt wire was electrochemically etched until the end was small enough to be placed approximately 200 μm away from the pipet tip. cell 1, cell 2, and cell 3 represent the electrochemical cells for different aqueous background solutions and reference electrodes used in this study. At the end of each experiment, TEACl was added as an internal standard to determine the transfer potentials of each analyte.

cell 1: Pt | 5 mM TDDATFAB + 1,2 DCE || ASW + mM NT | Ppy | Au

cell 2: Pt | 5 mM TDDATFAB + 1,2 DCE || 10 mM LiCl + mM NT | AgCl | Ag

cell 3: Pt | 5 mM TDDATFAB + 1,2 DCE || ASW + mM NT | AgCl | Ag

The diffusion coefficients of ACh, T (in ASW), and 5-HT (in LiCl) were calculated using pipets with radii on the scale of hundreds of nanometers, which were easily verified via SEM. Several pipets of this size were used to measure the steady-state current response for each analyte at 1 mM concentration (Figures A.1, A.2, and A.3 in Supporting Information, Appendix A) show the cyclic voltammogram for one of the pipets used, e.g., radius = 360, 450, and 340 nm for ACh, T, and 5-HT, respectively). Diffusion coefficients could then be calculated using the expression (29):

$$i = 4xnFDca \quad (1)$$

where i is the steady-state limiting current, x is a function of the quantity RG = rg/a (rg and a are outer and inner tip radii, respectively) (30), n is the number of transferred charges in the tip reaction, F is Faraday's constant, a is the radius of the pipet, D is the diffusion coefficient of the neurotransmitter measured, and c is the concentration of analyte in solution. A proposed disk geometry for the nanopipet tip was used for the calculation. The diffusion coefficients of ACh and T in ASW were found to be $7.5 \pm 1.2 \times 10^{-6}$ cm^2/s and $6.1 \pm 0.4 \times$

10^{-6} cm^2/s at 24 °C, respectively, in ASW. The diffusion coefficient for 5-HT in 10 mM LiCl was found to be $6.3 \pm 0.8 \times 10^{-6}$ cm^2/s at 24 °C. The same relationship was then used in determining the radius of each of the smaller scale pipets used for the detection of neurotransmitters.

Limits of detection (LODs) were calculated by 3s/m (31), where s is equal to the standard deviation of background solution without neurotransmitters present and m is equal to the slope of the calibration curve. In the case of cyclic voltammetry, s was determined by the standard deviation of the average current at a potential on the limiting current from three replicate cyclic voltammograms of background solution. In the case of amperometry, s was determined by the standard deviation of the average current obtained over a 50 s amperometric i−t curve of background solution.

2.3 RESULTS AND DISCUSSION

Cyclic voltammetry was used to determine the half-wave transfer potentials ($E_{1/2}$) of acetylcholine (ACh), tryptamine (T), and serotonin (5-HT). Upon applying a potential, the neurotransmitters were transferred voltammetrically across the nanopipet-supported ITIES tip, and their cyclic voltammograms are shown in Figure 2.2; the transfer of all three neurotransmitters investigated produced sigmoidal voltammograms, with $E_{1/2}$ as −0.11, −0.25, and −0.47 vs $E_{1/2,TEA}$ for ACh, T, and 5-HT, respectively. As shown in Figure 2.2, the transfer of ACh and T occurred well before the background, while 5-HT is much more difficult to be transferred, and its transfer has slight overlap with background. For this reason, background subtraction is used to increase the accuracy of measurements.

Because ACh transfers early within the potential window of ASW, it can achieve a steady-state current for up to 200 mV before background interference from ASW occurs. Some capacitance is seen in the cyclic voltammogram of ACh, due the small pipet radius of 7 nm and the fact that it was scanned at a rate of 50 mV/s rather than 20 mV/s (Figure 2.2a). T has a moderate $E_{1/2}$ and was also able to achieve a steady state in ASW (Figure 2.2b). It is worth noting that the observed difference in the transfer potentials between T and 5-HT corresponds well with that reported in the literature at a much larger nitrobenzene/water interface (25). Because 5-HT requires a much larger overpotential for its transfer, ASW background interference proves to be an issue for the detection of low concentrations of 5-HT. A 2 mM addition of 5-HT has only a small response relative to ASW, because the two transfer at similar potentials (Figure A.4, Supporting Information, Appendix A). Steady-state transfer of lower concentrations of 5-HT was achieved when a background solution of 10 mM LiCl was used in place of ASW, due to the larger potential window of LiCl (Figure 2.2c).

The different transfer potentials of these protonated analytes on the nano-ITIES probes provide the basis for their qualitative detection. Additionally, the ITIES probes presented here are selective toward the detection of ACh, T, and 5-HT compared to other neurotransmitters that could coexist in vivo, such as dopamine, γ-aminobutyric acid (GABA), and ascorbic acid, a redox-active compound present at high levels in many neuronal systems. The response of these nanopipet probes to these possible interferents are shown in Figures A.5 and A.6, Supporting Information (Appendix A). The tests were performed both in ASW and LiCl, background solutions used in this study. It can be seen from Figures A.5 and A.6 that no change occurred in the shape of the cyclic voltammograms of ASW and LiCl within

the relevant potential window when 5 mM DA, 5 mM GABA, or 100 mM AA were added. TEA was added at the end of these interferent tests to verify that each nanopipet electrode was working properly, ensuring that the lack of interferent signal was due to the fact that it does not transfer. Overall, at the ITIES of nanopipet electrodes presented here, ascorbic acid, dopamine, and GABA cannot be transferred within the potential window and thus are not detected. In contrast, surface modifications on the traditionally used carbon electrode are often needed to enhance NTs detection selectivity against ascorbic acid, e.g., carbon electrodes modified with Nafion were used for 5-HT detection in the presence of ascorbic acid (32-35).

Figure 2.3 shows the quantitative detection of ACh (Figure 2.3a and 2.3b) and T (Figure 2.3c and 2.3d) on nanopipet-supported ITIES probes. As shown in Figure 2.3a, even with such a small interface radius of ≈ 7 nm, we were able to use cyclic voltammetry to detect ACh quantitatively in the range of 0.25−6 mM, resulting in a steady-state current that was linearly proportional to concentration (Figure A.7, $R^2 = 0.994$, Supporting Information, Appendix A). T also showed linear detection using cyclic voltammetry (Figure 2.3c), in the range of 0.5−10 mM at a ≈ 19 nm radius interface, with a steady-state current linearly proportional to the concentration (Figure A.8, $R^2 = 0.989$, Supporting Information, Appendix A). Amperometry was also used for the quantification of ACh and T, as shown in Figures 2.3b and 2.3d, respectively. Using this technique, probes were held at a potential at which a steady-state current occurred for ACh and T. The resulting average current over a period of 50 s was linearly proportional to ACh concentration from 0.25 to 6 mM (Figure A.9, $R^2 = 0.995$, Supporting Information, Appendix A) and linearly proportional to T concentration from 0.5 to 10 mM (Figure A.10, $R^2 = 0.992$, Supporting Information, Appendix A). The

LODs for ACh and T were calculated to be 205 μM and 86 μM, respectively, based on i−t curves. The quantitative detection of 5-HT in LiCl with both cyclic voltammetry and amperometry are shown in Figure 2.4a and 2.4b, respectively. The response is linear over the concentration range of 0.15−8 mM for 5-HT. On the basis of results shown in Figure 2.4a, limiting current corresponding to detection of 5-HT at −0.51 V is changing linearly with its concentration in the range of 0.15−8 mM (Figure A.11, $R^2 = 0.995$, Supporting Information, Appendix A). Similarly, linear calibration curve (Figure A.12, $R^2 = 0.999$, Supporting Information, Appendix A) for this concentration range was obtained using amperometry on a radius of ≈ 21 nm nanopipet electrode by holding the probe at −0.52 V vs $E_{1/2,\ TEA}$ (Figure 2.4b), with an LOD of 77 μM. In order for 5-HT to be detected in the potential window of biological media, e.g., ASW, an ionophore can be used to facilitate the transfer of 5-HT; thus, the transfer potential of 5-HT can be shifted to be within the potential window of biological media, namely with the mechanism of facilitated ion transfer. Work is currently in progress to facilitate earlier transfer of 5-HT so that it can be detected in biological media.

2.4 CONCLUSIONS

Acetylcholine (ACh), tryptamine (T), and serotonin (5-HT) have been successfully detected quantitatively and qualitatively at a nanopipet-supported interface between 1,2-DCE and aqueous solutions via ionic transfer. Transfer potentials at $E_{1/2}$ were compared between ACh, T, and 5-HT, with the following transfer potential order: ACh < T < 5-HT, with ACh being transferred at the least negative potential. A lower detection limit for the detection of 5-HT was observed using a 1,2-DCE/ LiCl interface compared to a 1,2-DCE/ASW interface, because transfer of serotonin occurs at a similar potential as ASW background. The local

concentrations of ACh and 5-HT from an exocytotic event are well above the LODs of these probes (36, 37). Nanoelectrodes coupled with scanning electrochemical microscopy (38) have successfully provided nanometer spatial resolution imaging of single nanopore (26) and single nanoparticles (39). The nanopipet electrodes presented here have great potential to be used in detecting neurotransmitters for nanometer scale biological structures, such as synapses and in single vesicles. Overall, as shown in our work, nanopipet-supported ITIES probes can be used as multifunctional sensors to detect both electrochemically nonredox-active and redox-active neurotransmitters in both a qualitative and quantitative manner. The nano-ITIES electrodes presented here are selective toward the detection of ACh, T, and 5-HT against other neurotransmitters that could coexist in vivo, such as dopamine, γ-aminobutyric acid (GABA), and ascorbic acid.

2.5 NOTES AND ACKNOWLEDGMENTS

Research reported in this chapter was supported by the National Institute of Neurological Disorders and Stroke of the National Institutes of Health under award number R21NS085665 to M.S. (PI), J.V.S. (Co-PI). The content is solely the responsibility of the authors and does not necessarily represent the official views of the National Institutes of Health. J.V.S. is grateful for the support from the National Institutes of Health under award number P30 DA018310. All experimental work was performed by Michelle Colombo at the University of Illinois at Urbana-Champaign, School of Chemical Sciences. SEM was carried out in the Frederick Seitz Materials Research Laboratory Central Facilities, University of Illinois. Scientific background and methods were input by Mei Shen and Jonathan Sweedler. Writing

was completed by Michelle Colombo and Mei Shen. We thank Prof. Joaquín Rodríguez-López for helpful discussions.

2.6 FIGURES AND SCHEMES

Scheme 2.1. Molecular structure of (a) acetylcholine (ACh), (b) tryptamine (T), and (c) serotonin (5-HT).

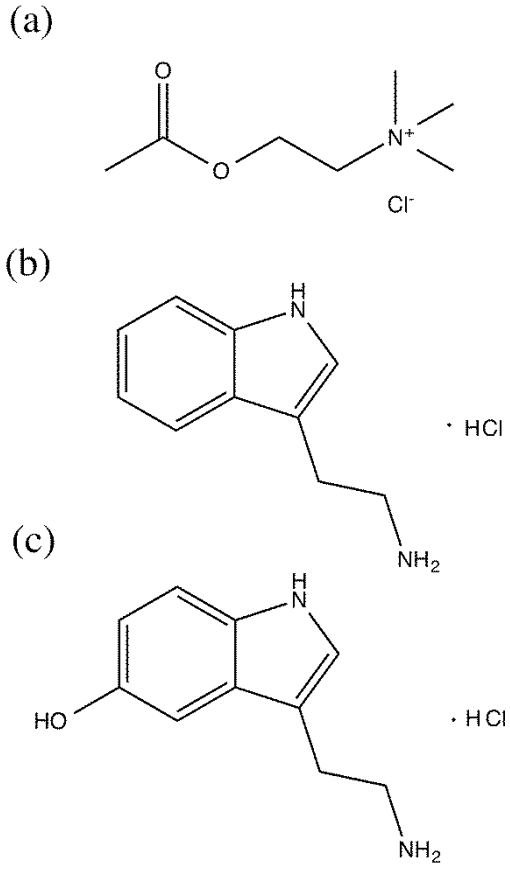

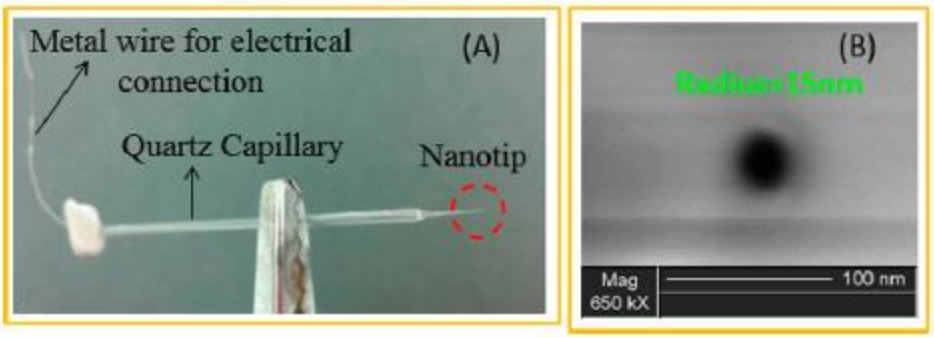

Figure 2.1. Photograph (A) and SEM image (B) of a nanopipet prepared in the lab. The pipet was prepared by laser pulling a quartz capillary.

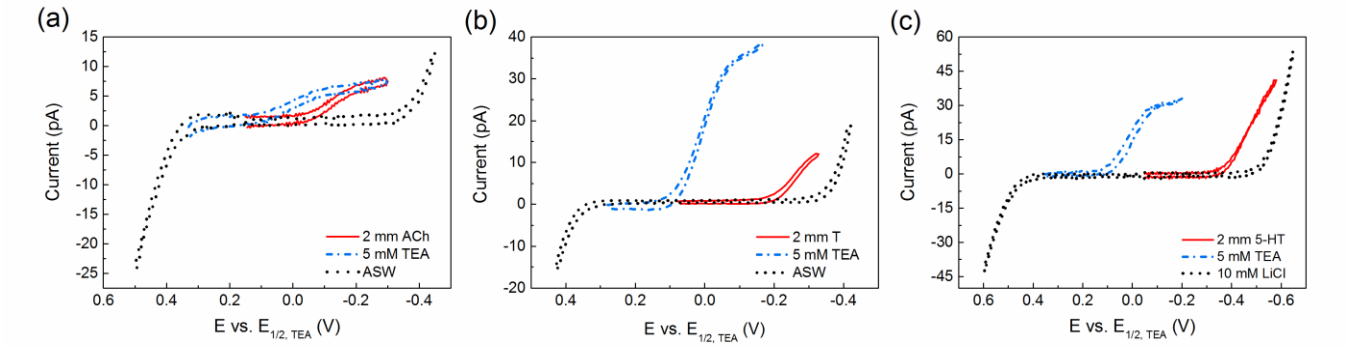

Figure 2.2. Cyclic voltammograms of acetylcholine (ACh), tryptamine (T), and serotonin (5-HT) on a nanopipet electrode. (a) 2 mM acetylcholine transfer across a radius ≈7 nm interface in cell 1; scan rate = 0.05 V/s. (b) 2 mM tryptamine transfer across a radius ≈19 nm interface in cell 1; scan rate = 0.02 V/s. (c) 2 mM serotonin transfer across a radius ≈35 nm interface in cell 2; scan rate = 0.05 V/s. For comparison, the cyclic voltammogram of tetraethylammonium is shown in each overlay.

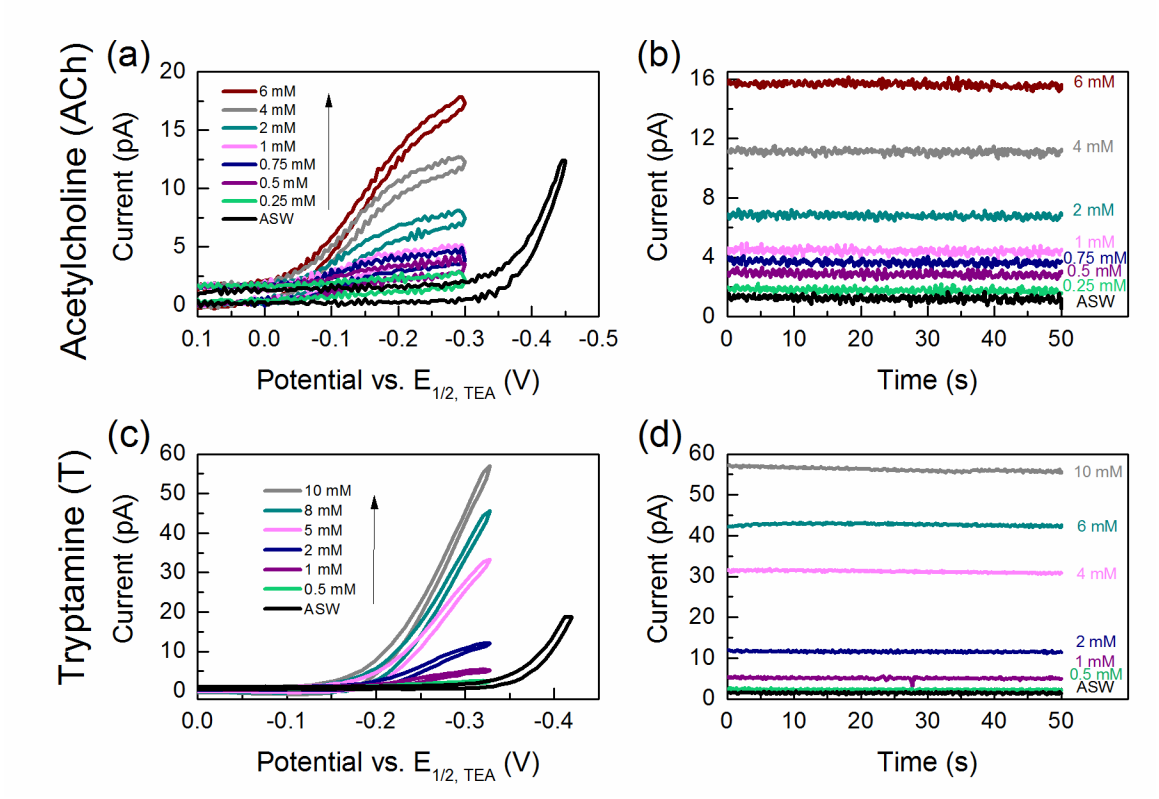

Figure 2.3. (a) Cyclic voltammograms and (b) amperometric i−t curves for 0.25−6 mM acetylcholine (ACh) using a nanopipet probe with a radius of 7 nm in cell 1; applied potential E = −0.25 V vs $E_{1/2,\ TEA}$ for i−t curves. (c) Cyclic voltammograms and (d) amperometric i−t curves for 0.5−10 mM tryptamine (T) using a nanopipet probe with a radius of 19 nm in cell 1; applied potential E = −0.32 V vs $E_{1/2,\ TEA}$ for i−t curves.

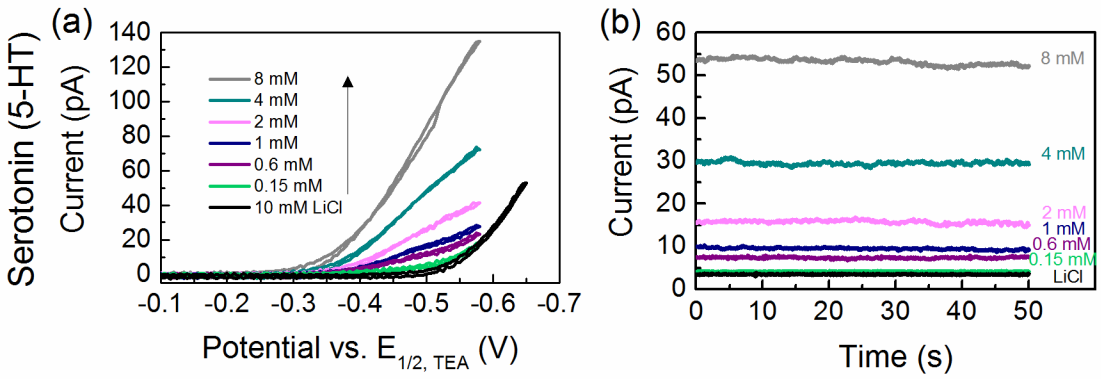

Figure 2.4. (a) Cyclic voltammograms of 0.15−8 mM serotonin (5-HT) on a nanopipet electrode with a radius of 35 nm in cell 2. (b) Amperometric i−t curves for 0.15−8 mM 5-HT using a nanopipet probe with a radius of 21 nm in cell 2; applied potential E = −0.52 V vs $E_{1/2,\ TEA}$.

2.7 REFERENCES

1. B. Platt and G. Riedel, *Behavioural Brain Research*, **221**, 499 (2011).
2. B. E. Jones, *Trends in Pharmacological Sciences*, **26**, 578 (2005).
3. E. Perry, M. Walker, J. Grace and R. Perry, *Trends in Neurosciences*, **22**, 273 (1999).
4. A. M. Himmelheber, M. Sarter and J. P. Bruno, *Cognitive Brain Research*, **9**, 313 (2000).
5. K. P. Lesch, D. Bengel, A. Heils, S. Z. Sabol, B. D. Greenberg, S. Petri, J. Benjamin, C. R. Muller, D. H. Hamer and D. L. Murphy, *Science*, **274**, 1527 (1996).
6. L. Pezawas, A. Meyer-Lindenberg, E. M. Drabant, B. A. Verchinski, K. E. Munoz, B. S. Kolachana, M. F. Egan, V. S. Mattay, A. R. Hariri and D. R. Weinberger, *Nature Neuroscience*, **8**, 828 (2005).
7. A. Caspi, K. Sugden, T. E. Moffitt, A. Taylor, I. W. Craig, H. Harrington, J. McClay, J. Mill, J. Martin, A. Braithwaite and R. Poulton, *Science*, **301**, 386 (2003).
8. S. Shimazu and I. Miklya, *Progress in Neuro-Psychopharmacology & Biological Psychiatry*, **28**, 421 (2004).
9. S. Amemiya, J. Kim, A. Izadyar, B. Kabagambe, M. Shen and R. Ishimatsu, *Electrochimica Acta*, **110**, 836 (2013).
10. S. Amemiya, in *Scanning Electrochemical Microscopy*, 2 ed., A. J. Bard and M. V. Mirkin Editors, p. 127, Taylor and Francis, New York (2012).
11. Z. Samec, E. Samcova and H. H. Girault, *Talanta*, **63**, 21 (2004).
12. Z. Samec, *Pure and Applied Chemistry*, **76**, 2147 (2004).
13. M. Senda, T. Kakiuchi and T. Osakai, *Electrochimica Acta*, **36**, 253 (1991).
14. Y. X. Wang, J. Velmurugan, M. V. Mirkin, P. J. Rodgers, J. Kim and S. Amemiya, *Analytical Chemistry*, **82**, 77 (2010).
15. F. Reymond, D. Fermin, H. J. Lee and H. H. Girault, *Electrochimica Acta*, **45**, 2647 (2000).
16. P. J. Rodgers and S. Amemiya, *Analytical Chemistry*, **79**, 9276 (2007).
17. S. Amemiya and A. J. Bard, *Analytical Chemistry*, **72**, 4940 (2000).
18. P. Vanysek, *Analytical Chemistry*, **62**, A827 (1990).
19. B. Liu and M. V. Mirkin, *Electroanalysis*, **12**, 1433 (2000).
20. B. Liu and M. V. Mirkin, *Analytical Chemistry*, **73**, 670A (2001).
21. T. J. Stockmann, A.-M. Montgomery and Z. Ding, *Journal of Electroanalytical Chemistry*, **684**, 6 (2012).
22. T. J. Stockmann, J. Zhang, A.-M. Montgomery and Z. Ding, *Analytica Chimica Acta*, **821**, 41 (2014).
23. D. W. M. Arrigan, M. Ghita and V. Beni, *Chemical Communications*, 732 (2004).
24. G. Herzog, B. McMahon, M. Lefoix, N. D. Mullins, C. J. Collins, H. A. Moynihan and D. W. M. Arrigan, *Journal of Electroanalytical Chemistry*, **622**, 109 (2008).
25. H. Tatsumi and T. Ueda, *J. Electroanal. Chem.*, **655**, 180 (2011).
26. M. Shen, R. Ishimatsu, J. Kim and S. Amemiya, *Journal of the American Chemical Society*, **134**, 9856 (2012).
27. J. A. Jing, J. V. Sweedler, E. C. Cropper, V. Alexeeva, J. H. Park, E. V. Romanova, F. Xie, N. C. Dembrow, B. C. Ludwar, K. R. Weiss and F. S. Vilim, *Journal of Neuroscience*, **30**, 16545 (2010).

28. Y. Fan, S. S. Rubakhin and J. V. Sweedler, *Analytical Chemistry*, **83**, 9557 (2011).
29. C. Lefrou, *Journal of Electroanalytical Chemistry*, **592**, 103 (2006).
30. J. Kim, M. Shen, N. Nioradze and S. Amemiya, *Analytical Chemistry*, **84**, 3489 (2012).
31. D. C. Harris, *Quantitative Chemical Analysis*, W. H. Freeman and Company, New York (2010).
32. G. A. Gerhardt, A. F. Oke, G. Nagy, B. Moghaddam and R. N. Adams, *Brain Research*, **290**, 390 (1984).
33. M. P. Brazell, R. J. Kasser, K. J. Renner, J. Feng, B. Moghaddam and R. N. Adams, *Journal of Neuroscience Methods*, **22**, 167 (1987).
34. B. P. Jackson, S. M. Dietz and R. M. Wightman, *Analytical Chemistry*, **67**, 1115 (1995).
35. P. Hashemi, E. C. Dankoski, J. Petrovic, R. B. Keithley and R. M. Wightman, *Analytical Chemistry*, **81**, 9462 (2009).
36. A. Y. Aidoo and K. Ward, *Mathematical and Computer Modelling*, **44**, 952 (2006).
37. M. A. Bunin and R. M. Wightman, *Journal of Neuroscience*, **18**, 4854 (1998).
38. A. J. Bard and M. V. Mirkin, *Scanning Electrochemical Microscopy*, Marcel Dekker, New York (2001).
39. T. Sun, Y. Yu, B. J. Zacher and M. V. Mirkin, *Angewandte Chemie-International Edition*, **53**, 14120 (2014).

CHAPTER 3

ELECTROCHEMICAL DETECTION OF DOPAMINE VIA ASSISTED ION TRANSFER AT NANOPIPET ELECTRODE USING CYCLIC VOLTAMMETRY[4]

3.1 INTRODUCTION

Dopamine (DA) is a small molecule that has many functions throughout the body. More specifically, DA functions as a neurotransmitter in the brain, and acts as a chemical messenger between neurons. DA has been attributed to playing a role in such processes as memory (1), motor control (2, 3), and reward (4, 5). When the dopaminergic system is altered, certain disease states may occur, such as Parkinson's disease (6) or Schizophrenia (7, 8).

Electrochemical measurements, mainly on a carbon microelectrode, have proven to be a very useful technique for studying DA release during neurotransmission (9-22). There are however, several issues with the traditional electrochemical detection via the oxidation of DA, which primarily involve the presence of ascorbic acid (AA). Ascorbic acid is present in the brain at much higher concentrations compared to DA, and the two compounds are oxidized at similar potentials, thus ascorbic acid is a major interferent for the electrochemical detection of DA (23). Furthermore, ascorbic acid can reduce dopamine's oxidation product back into DA, causing a signal larger than that is representative of the actual amount of DA in solution (18). Electrode modifications are needed to circumvent this issue, including the use of charge-selective polymer films, which can provide improved selectivity (18, 24-27).

[4] This chapter appeared in the Journal of The Electrochemical Society, with the following citation: Colombo, M.L., McNeil, S., Iwai, N.; Chang, A.; Shen, M. "Electrochemical detection of dopamine via assisted ion transfer at nanopipet electrode using cyclic voltammetry." *J. Electrochem. Soc.* **2015**, *163*, H3072-H3076, and portions have been edited or removed for clarity and brevity. This article is reprinted with the permission of the publisher and is available using DOI: 10.1149/2.0091604jes.

Pipet supported Interface between Two Immiscible Electrolyte Solutions (ITIES) provides a unique platform for detecting ionic species, such as DA, which has a pKa of 8.8–8.9 and 10.4–10.6 and is protonated under biological pH (28-30). The detection is based on ion transfer across a liquid-liquid interface rather than a redox process. Because of this, side reactions involving dopamine's oxidation product are not an issue. Furthermore, ion transfer at the ITIES offers the selectivity against AA that is necessary in DA detection without the use of modified electrode surfaces (31-34).

The transfer of DA across the macroITIES (e.g. area ≈1 cm^2) has been demonstrated by Arrigan et al. (31-34), as well as by Samec and colleagues (35, 36); and across the microITIES by Shao's group (37), using ionophores such as dibenzo-18-crown-6 ether (DB18C6) to facilitate dopamine's transfer. DB18C6 complexes with dopamine via hydrogen bonds between the hydrogen atoms in DA's amino group and the oxygen atoms from the crown ether. This can lower the Gibbs energy of DA transfer (38), allowing dopamine transfer to occur within the potential window of the background solution (34, 39).

To the best of our knowledge, facilitated transfer of neurotransmitters at the nanometer scale ITIES has not yet been reported. Though DA transfer has been reported at macro and micro interfaces, the kinetic scaling of all processes involved in the facilitated transfer needs to be demonstrated in the challenging mass transfer conditions imposed by a nanoelectrode. Study at nano-ITIES provides insight regarding how the ion complexation reaction at the interface aligns with ion transfer and ion diffusion to the ITIES surface. This is critical at nanoelectrodes because when we decrease the size of the interface, the diffusion time decreases as well, (proportional to square of electrode radius divided by diffusion coefficient, a^2/D), thus challenging the kinetics of many processes involved, but importantly that of the

interfacial formation of a complex. Here we report the detection of DA via assisted ion transfer by DB18C6 at nanopipet electrode with sizes on the hundreds of nanometer scale. We also investigated selective detection of DA with the presence of ascorbic acid, a major interferent that co-exists with dopamine in the brain at high concentrations.

3.2 EXPERIMENTAL

3.2.1 Reagents

Potassium tetrakis(pentafluorophenyl)borate (TFAB) was obtained from Boulder Scientific Company (Mead, CO). Dopamine hydrochloride, dibenzo-18-crown-6 (DB18C6), tetradodecylammonium (TDDA) chloride, tetrabutylammonium chloride (TBACl), 1,2-dichloroethane (DCE), chlorotrimethylsilane were purchased from Sigma-Aldrich (St. Louis, MO). The TFAB salt of TDDA (TDDATFAB) was prepared by metathesis, as described elsewhere (40). Magnesium chloride ($MgCl_2$) was from Amresco (Solon, OH). Ascorbic acid was from Fisher Scientific (Pittsburgh, PA). All reagents were used as received, and solutions were prepared using 18.3 MΩ cm deionized water (ELGA, Woodridge, IL). The prepared solutions were passed through a 0.2 μm filter (Thermo Scientific, Waltham, MA) before use.

3.2.2 Nanopipet electrode preparation and charaterization

Nanometer-scale pipet electrodes were fabricated by laser pulling of I.D.=0.7 mm, length=10 cm) using a P-2000 capillary puller (Sutter Instrument Co., Novato, CA). The pulled pipets were then silanized via vapor deposition as described elsewhere (41, 42). Pipets were characterized using Scanning Electron Microscopy (SEM) and ion-transfer voltammetry. For SEM imaging, the nanopipets were coated with a thin Au/Pd film by a

high-resolution sputter coater (Quorum Technologies LTD, Kent, UK), and the orifices were observed by high resolution field emission SEM (FEI dual-beam 235, FEI Co., Hillsboro OR, USA) under a 20 kV electron beam.

3.2.3 Electrochemical experiments

The transfer of protonated DA across the 1,2-DCE/water interface was studied by cyclic voltammetry. All electrochemical measurements were recorded using a CHI1205B Electrochemical Analyzer (CH Instruments, Austin, TX). The prepared nanopipets were backfilled with a solution of 5 mM TDDATFAB + 25 mM DB18C6 in 1,2-DCE using a 10 μL Hamilton syringe, and the organic solution was pushed to the tip of the pipet by creating a gentle vibration. When immersed in an aqueous solution, a liquid-liquid interface is formed at the tip of the pipet. Voltage was applied between two reference electrodes: one inside the pipet and one outside, which is immersed in the aqueous solution. A Pt wire (50 μm diameter) was used as the inner reference, and the external reference was a AgCl coated Ag wire (250 μm diameter). Cell diagrams representing each experimental setup used are the following:

cell 1: Pt | 5 mM TDDATFAB + DCE + 25 mM DB18C6 || 10 mM $MgCl_2$ + x mMDA | AgCl | Ag

cell 2: Pt | 5 mM TDDATFAB + DCE + 25 mM DB18C6 || 10 mM $MgCl_2$ + x mMDA + x mM AA | AgCl | Ag

3.2.4 Characterization of steady-state limiting current

Nanopipet electrodes with radii of hundreds of nanometers were used to measure the steady-state current response for a range of dopamine concentrations, represented by (43):

$$i = 4xnFDca \quad (1)$$

where i is the steady-state limiting current, x is a function of the quantity RG = rg /a (rg and a are outer and inner tip radii, respectively) (44), here approximately RG = 1.4 and x = 1.23, n is the number of transferred charges in the tip reaction, F is Faraday's constant, a is the inner radius of the pipet, D is the diffusion coefficient of the neurotransmitter measured, and c is the concentration of neurotransmitter in solution. A proposed disk geometry for the nanopipet tip was used for the calculation. The slope, m = i /c, of calibration curves can be used in combination with Eq. 1 to determine the diffusion coefficient of dopamine.

3.2.5 Other calculations

To determine the half-wave transfer potential ($E_{1/2}$) of dopamine, TBACl was added at the end of experiments as an internal standard. This was calculated by subtracting the highest point of the first derivative of the DA CVs from the highest point of the first derivative of the TBA CV.

3.2.6 pH experiment

The pH of the bulk solution was monitored after subsequent additions of DA and AA. pH measurements were performed using a pH meter (Model # AB15, Fischer Scientific, Pittsburg, PA).

3.3 RESULTS AND DISCUSSION

3.3.1 Overall matrix considerations

Here we report the detection of dopamine in a background solution of 10 mM $MgCl_2$, which provides a large potential window because divalent matrix cations (such as Mg^{2+}) typically transfer at more negative potentials than monovalent matrix cations (such as Li^{+}) (33). A background solution with a large potential window such as $MgCl_2$ was used in our

study to provide the best condition in terms of background potential window to allow DA transfer at nanoITIES to be studied in a controlled manner. The study of this process facilitated by DB18C6 is possible in principle in other matrices, however it may prove more challenging given a larger overlap with the potential window.

Maintaining an appropriate pH environment for dopamine detection is a critical aspect of experimentation (39). The electrochemical detection of DA at the ITIES is dependent on that dopamine, when protonated at its amine group, is cationic (39). This allows dopamine to be detected by ion transfer at the ITIES (39). Furthermore, it is necessary for dopamine to be positively charged in order to form a complex with DB18C6, the ionophore used in our study for the facilitated ion transfer of DA (35). In aqueous solution at physiological pH or lower, dopamine is protonated (31), since the pH of the environment is lower than the pKa of DA's amino group, which is reported to be 8.8 to 8.9 and 10.4 to 10.6 in the literature (28-30). In order to ensure that DA will be in its cationic state for relevant ITIES experiments, the pH of the solution was monitored during various additions of DA and AA (Table B.1, Supporting Information, Appendix B). These results indicate that DA exists in its cationic form in all of the experiments discussed below.

3.3.2 Dopamine detection using probes with radii of hundreds of nanometers

We present here dopamine detection with nanopipet electrodes with radii of hundreds of nanometers, ranging from 160 to 480 nm, using DB18C6 as an ionophore present in the organic phase. In the absence of DB18C6, DA does not transfer across the interface, and therefore is not detected (data not shown). Figure 3.1 shows the cyclic voltammograms for the facilitated DA detection with concentrations ranging from 0.25 mM to 2 mM in a background solution of 10 mM $MgCl_2$ at nanopipet electrodes with radii of 210 nm, 225 nm,

and 480 nm for Figures 3.1a, 3.1b, and 3.1c, respectively. It can be seen that sigmoidal voltammograms with steady-state limiting currents were achieved for 0.25 – 2 mM DA at all of these nanoITIES pipets. The results shown in Figure 3.1 are representative of typical results that we observed in the lab for similar size ITIES, and it is important to note that all values reported in this paper were calculated from the results of pipets that were characterized via the electrochemistry of TBA as well as SEM imaging, to ensure that the pipets were working properly. The measured half-wave transfer potential for DA at these nanopipet electrodes is −0.322 ± 0.020 V vs. $E_{1/2,\,TBA}$ (n = 5). The insets of Figure 3.1 show the SEM micrographs of the nano-orifice at the end of nanopipet electrode (cross section) as well as the side view of the nanopipet positioned at 45 degrees with respect to the detector. These images allow for the pipet radius, r, and taper angle, θ, to be determined.

The current response corresponding to DA detection increases linearly with increasing concentration of DA for all of the nanopipet electrodes with various sizes studied, up to 2 mM. Past 2 mM, the current response still increases, but the response starts to slow down (data not shown). Calibration curves of the limiting current with respect to DA concentration shows an R^2 value of 0.99 for Figure 3.1a, of 0.98 for Figure 3.1b, and of 0.99 for Figure 3.1c, indicating linear response from the nanopipet electrodes for the detection of DA (Figure B.1-B.3, Supporting Information, Appendix B). Using calibration curves for these pipets and others (n = 6), in combination with Eq. 1, the calculated diffusion coefficient for DA transfer is 4.87 (±0.28) × 10^{-10} m^2/s for pipets with radii ranging from 175 to 480 nm. This value is very close to the value determined by flow injection analysis, 6 (±0.25) × 10^{-10} m^2/s (45).

The taper angle, θ, is reported to influence the attainment of steady-state at the nanopipet-based ITIES; as θ increased from 0° to 90°, there is a gradual transition from linear to

hemispherical ion diffusion in the internal solution (46). Using SEM images in the Figure 3.1 insets, θ was calculated to be 16.2°, 17.5°, and 17.5° for the nanopipets used in Figures 3.1a, 3.1b, 3.1c, respectively. These θ values observed in our quartz nanopipets are within the range of that reported typically for quartz nanopipets, i.e. 9° to 22° (47). These values of θ could allow for the ingress and egress of DA transfer to reach steady-state, resulting in well-defined sigmoidal behavior in the voltammogram as observed with Figure 3.1. The taper angles of all pipets tested in this study ranged from 16° to 21°, with no effect in transfer behavior observed within this range of angles.

3.3.3 Dopamine detection with the presence of ascorbic acid using nanopipet electrodes with radii of hundreds of nanometers

As ascorbic acid is a substance present in the brain at high concentrations and is a known interferent for DA detection; we present here the detection of DA with AA present in the aqueous solution (Figure 3.2) at nanopipet electrodes with radii of 223 nm and 258 nm. As shown in Figure 3.2, there is no change on the potential window at the positive potential side after adding AA to background solution of $MgCl_2$, indicating that ascorbate ion was not detected at our nanopipet electrode, thus not interfering with DA detection. However, the potential window on the negative side is slightly narrowed upon addition of AA, similar to previous reports at larger interfaces (33), which is likely due to the transfer of protons evidenced as decrease in pH with addition of AA (Table B.1, Supporting Information, Appendix B). After the addition of 2 mM AA, DA with concentrations varying from 0.25 mM to 2 mM was added to the cell, where transfer behavior is similar to that shown in Figure 3.1 when no AA was present during DA detection. Cyclic voltammograms corresponding to transfer of DA with presence of AA show sigmoidal shape and steady-state limiting current

increases linearly with increasing concentration of DA in multiple independent measurements (n = 5) on nanopipet electrodes with various radii ranging from 161 to 263 nm with R^2 values ≥ 0.98, e. g. R^2 for Figures 3.2a and 3.2b are 0.99 and 0.98, respectively (Figure B.4-B.5, Supporting Information, Appendix B). The measured half wave transfer potential for DA detection with presence of 2 mM AA was calculated to be −0.328 ± 0.029 V vs. $E_{1/2,\,TBA}$ (n = 6), showing no significant change in the presence of ascorbic acid. Based on calibration curves and Eq. 1, the diffusion coefficient for DA transfer with the presence of 2 mM AA was measured to be 1.93 (±0.59) × 10^{-10} m^2/s from multiple independent measurements on nanopipet electrodes with various radii ranging from 161 nm to 263 nm (n = 5).We found few papers studying DA transfer at macro-ITIES (31-33, 35, 36) and micro-ITIES (37), with no diffusion coefficient reported based on calibration curves with the presence of AA. In the previously reported transient detection of DA at large pipet electrodes with radii on the scale of mm, the diffusion coefficient of DA with presence of 10 mM ascorbate was calculated from plots of peak current versus the square root of sweep rate (32). The results from Ref 32 indicated no significant change in D whether ascorbate is present in solution or not. The observed decrease in D of DA in our study with the presence of high concentration of AA, 2 mM, could be related to pH change in background solution after adding 2 mM AA (Table B.1, Appendix B); in Ref 37, when the authors added $Mg(OH)_2$ to a solution of DA in $MgCl_2$ after adding AA, not much change in dopamine current was observed with the addition of 20 mM AA. Although we observe a decrease in the diffusion coefficient of DA when 2 mM AA is present, it is important to note that detection of DA is still linear with respect to its concentration, so determining an unknown concentration of dopamine in a solution with the presence of AA simply requires the use of this modified D in

Eq. 1. Most importantly, steady state current of dopamine remains the same with presence of physiological concentration of 0.1 mM AA, as discussed in next paragraph. While the concentration of AA present in biological environment is typically in the range of 0.1 mM (48), we also investigated the electrode's response when AA was in even larger excess to DA, at 20 mM (Figure 3.3). As shown in Figure 3.3, there is no change on the potential window at the positive potential side after adding AA to background solution of $MgCl_2$, indicating that even at 20 mM, ascorbate ion was not detected at our nanopipet electrode, thus not interfering with DA detection. Although the DA steady-state limiting current wave is cut off a little sooner than when compared to the presence of 2 mM AA, detection was still linear from 0.25 – 2 mM DA (R^2 = 0.97; Figure B.6, Supporting Information, Appendix B). Interestingly, we measured D of DA in the presence of 20 mM AA to be 1.93 ± 0.33 m^2/s (n = 5), a value not statistically different from D when only 2 mM AA is present. In order to further explore the effect of AA, we performed experiments in which the current for 2 mM DA was monitored with respect to the addition of various concentrations of AA, ranging from 0.1 – 20 mM AA. The results are shown in Figure B.7 of the Supporting Information (Appendix B), which show no significant change in DA current when 0.1 mM AA was added. This is important to note, because as mentioned previously, 0.1 mM is the typical AA concentration reported in biological environments. A steep drop in current is seen between 0.1 and 0.5 mM AA, but the decrease slows down with additions of higher concentrations.

3.4 CONCLUSIONS

We have shown the DB18C6 facilitated detection of dopamine at a nanopipet-supported ITIES interface consisting of water and 1,2- DCE using cyclic voltammetry. The steady-state

limiting current corresponding to dopamine (DA) detection increases linearly with respect to concentration of DA. The diffusion coefficient of DA at interfaces of hundreds of nanometers was found to be 4.87 (± 0.28) × 10^{-10} m^2/s calculated based on independent measurements with nanopipets with radii ranging from 175 nm to 480 nm (n = 6), with a half-wave transfer potential of −0.322 ± 0.020 V vs. $E_{1/2,\,TBA}$ (n = 5). We also show that with the presence of ascorbic acid (2 mM), DA detection at nanopipet electrodes still shows well-defined steady-state cyclic voltammograms, with current increasing linearly with respect to concentration of DA as well; no ascorbate was detected at nanopipet electrode. The half-wave transfer potential of DA was measured to be −0.328 ± 0.029 V vs. $E_{1/2,\,TBA}$ (n = 6) with the presence of ascorbic acid. The presence of ascorbic acid doesn't affect the detection potential of DA at the nanopipet electrodes reported. These nano-ITIES electrodes provide an alternative to traditional DA detection at carbon electrodes, minimizing effects of ascorbic acid interference.

3.5 NOTES AND ACKNOWLEDGMENTS

Research reported in this publication was supported by the National Institute of Neurological Disorders and Stroke of the National Institutes of Health under award number R21NS085665 to M.S. (PI), J.V.S. (Co-PI). The content is solely the responsibility of the authors and does not necessarily represent the official views of the National Institutes of Health. Michelle L. C. acknowledges the support from the Coleman Fellowship and the NIH Chemical Biology Interface Training Program under training grant number 2T32GM070421-11. SEM was carried out in the Frederick Seitz Materials Research Laboratory Central Research Facilities, University of Illinois. Albert C. is grateful for the support from John E.

Gieseking Scholarship for undergraduate summer research. All experimental work was performed by Michelle Colombo, Swami McNeil, Nicholas Iwai, and Albert Chang at the University of Illinois at Urbana-Champaign, School of Chemical Sciences. SEM was carried out in the Frederick Seitz Materials Research Laboratory Central Facilities, University of Illinois. Writing was completed by Michelle Colombo, Swami McNeil, and Mei Shen.

3.6 FIGURES

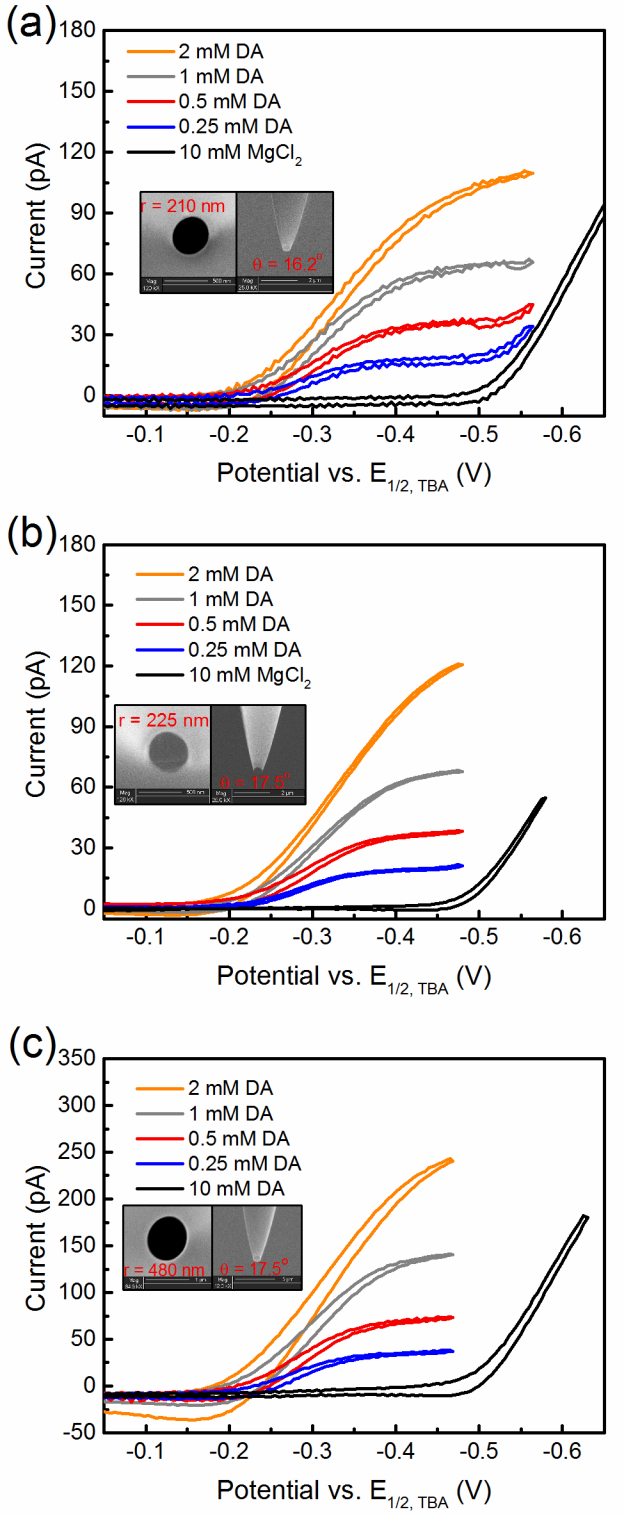

Figure 3.1. Cyclic voltammograms showing transfer of 0.25 –2 mM dopamine (DA) across an ITIES with a radius of (a) 210 nm, (b) 225 nm, and (c) 480 nm using Cell 1. Insets: SEM micrographs of the pipet used for these experiments, showing tip geometry (radius, r, and taper angle, θ) with both cross-section view and side view at 45 degrees.

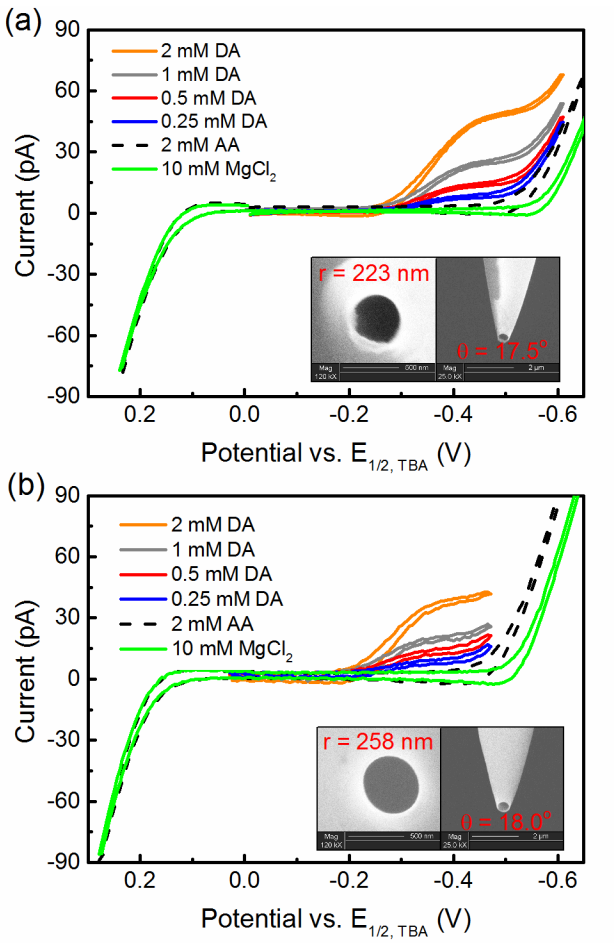

Figure 3.2. Cyclic voltammograms showing transfer of 2 mM ascorbic acid (AA) followed by 0.25–2 mM dopamine (DA) across ITIES with radii of (a) 223 nm and (b) 258 nm, using 25mMDB18C6; cell 2. Inset: SEM micrographs of the pipet used for these experiments, showing tip geometry (radius, r, and taper angle, θ) with both cross-section view and side view at 45 degrees.

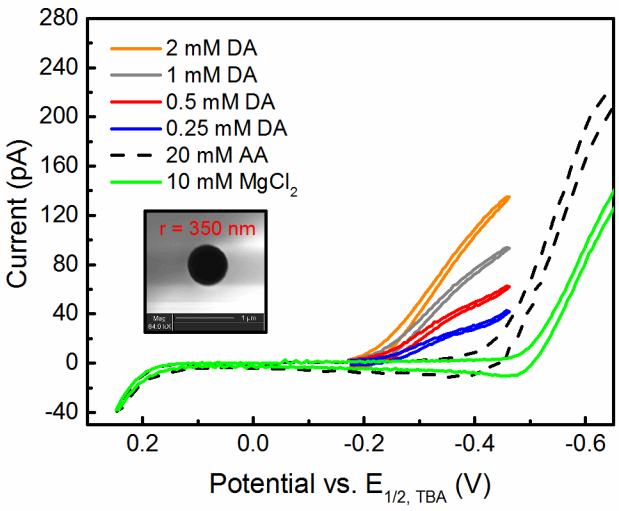

Figure 3.3. Cyclic voltammograms showing transfer of 20 mM ascorbic acid (AA) followed by 0.25–2 mM dopamine (DA) across an ITIES with radius = 350 nm using 25 mM DB18C6; cell 2. Inset: SEM micrograph showing cross section view of pipet used for this experiment.

3.7 REFERENCES

1. T. Sawaguchi and P. S. Goldmanrakic, *Science*, **251**, 947 (1991).
2. M. S. Cousins and J. D. Salamone, *Neuroscience*, **70**, 849 (1996).
3. A. M. Graybiel, T. Aosaki, A. W. Flaherty and M. Kimura, *Science*, **265**, 1826 (1994).
4. K. C. Berridge and T. E. Robinson, *Brain Research Reviews*, **28**, 309 (1998).
5. W. Schultz, *Journal of Neurophysiology*, **80**, 1 (1998).
6. S. J. Kish, K. Shannak and O. Hornykiewicz, *New England Journal of Medicine*, **318**, 876 (1988).
7. K. L. Davis, R. S. Kahn, G. Ko and M. Davidson, *American Journal of Psychiatry*, **148**, 1474 (1991).
8. A. A. Grace, *Neuroscience*, **41**, 1 (1991).
9. R. N. Adams, *Analytical Chemistry*, **48**, 1126 (1976).
10. M. D. Hawley, Tatawawa.Sv, Piekarsk.S and R. N. Adams, *Journal of the American Chemical Society*, **89**, 447 (1967).
11. R. M. Wightman, J. A. Jankowski, R. T. Kennedy, K. T. Kawagoe, T. J. Schroeder, D. J. Leszczyszyn, J. A. Near, E. J. Diliberto and O. H. Viveros, *Proceedings of the National Academy of Sciences of the United States of America*, **88**, 10754 (1991).
12. R. W. Holz, R. A. Senter and R. A. Frye, *Journal of Neurochemistry*, **39**, 635 (1982).
13. L. A. Sombers, M. M. Maxson and A. G. Ewing, *Journal of Neurochemistry*, **93**, 1122 (2005).
14. G. A. Detoledo, R. Fernandezchacon and J. M. Fernandez, *Nature*, **363**, 554 (1993).
15. R. T. Kurulugama, D. O. Wipf, S. A. Takacs, S. Pongmayteegul, P. A. Garris and J. E. Baur, *Analytical Chemistry*, **77**, 1111 (2005).
16. E. L. Ciolkowski, B. R. Cooper, J. A. Jankowski, J. W. Jorgenson and R. M. Wightman, *Journal of the American Chemical Society*, **114**, 2815 (1992).

17. M. Heien, M. A. Johnson and R. M. Wightman, *Analytical Chemistry*, **76**, 5697 (2004).
18. D. C. S. Tse, R. L. McCreery and R. N. Adams, *Journal of Medicinal Chemistry*, **19**, 37 (1976).
19. A. C. Michael and L. M. Borland, *Electrochemical Methods for Neuroscience*, CRC Press/Taylor & Francis (2007).
20. B. J. Venton and R. M. Wightman, *Analytical Chemistry*, **75**, 414A (2003).
21. C. Amatore, S. Arbault, Y. Bouret, M. Guille, F. Lemaitre and Y. Verchier, *Analytical Chemistry*, **81**, 3087 (2009).
22. J. A. Stamford, *Analytical Chemistry*, **58**, 1033 (1986).
23. R. M. Wightman, M. R. Deakin, P. M. Kovach, W. G. Kuhr and K. J. Stutts, *Journal of the Electrochemical Society*, **131**, 1578 (1984).
24. G. A. Gerhardt, A. F. Oke, G. Nagy, B. Moghaddam and R. N. Adams, *Brain Research*, **290**, 390 (1984).
25. M. P. Brazell, R. J. Kasser, K. J. Renner, J. Feng, B. Moghaddam and R. N. Adams, *Journal of Neuroscience Methods*, **22**, 167 (1987).
26. B. P. Jackson, S. M. Dietz and R. M. Wightman, *Analytical Chemistry*, **67**, 1115 (1995).
27. P. Hashemi, E. C. Dankoski, J. Petrovic, R. B. Keithley and R. M. Wightman, *Analytical Chemistry*, **81**, 9462 (2009).
28. A. E. Sanchez-Rivera, S. Corona-Avendano, G. Alarcon-Angeles, A. Rojas-Hernandez, M. T. Ramirez-Silva and M. A. Romero-Romo, *Spectrochimica Acta Part a-Molecular and Biomolecular Spectroscopy*, **59**, 3193 (2003).
29. J. Armstrong and R. B. Barlow, *British Journal of Pharmacology*, **57**, 501 (1976).
30. G. P. Lewis, *British Journal of Pharmacology and Chemotherapy*, **9**, 488 (1954).
31. G. Herzog, B. McMahon, M. Lefoix, N. D. Mullins, C. J. Collins, H. A. Moynihan and D. W. M. Arrigan, *Journal of Electroanalytical Chemistry*, **622**, 109 (2008).
32. D. W. M. Arrigan, M. Ghita and V. Beni, *Chemical Communications*, 732 (2004).
33. V. Beni, M. Ghita and D. W. M. Arrigan, *Biosensors & Bioelectronics*, **20**, 2097 (2005).
34. A. Berduque, R. Zazpe and D. W. M. Arrigan, *Analytica Chimica Acta*, **611**, 156 (2008).
35. O. Dvorak, V. Marecek and Z. Samec, *Journal of Electroanalytical Chemistry*, **300**, 407 (1991).
36. D. Homolka, V. Marecek, Z. Samec, K. Base and H. Wendt, *Journal of Electroanalytical Chemistry*, **163**, 159 (1984).
37. D. P. Zhan, S. N. Mao, Q. Zhao, Z. Chen, H. Hu, P. Jing, M. Q. Zhang, Z. W. Zhu and Y. H. Shao, *Analytical Chemistry*, **76**, 4128 (2004).
38. J. A. Ribeiro, I. M. Miranda, F. Silva and C. M. Pereira, *Physical Chemistry Chemical Physics*, **12**, 15190 (2010).
39. D. W. M. Arrigan, *Analytical Letters*, **41**, 3233 (2008).
40. J. D. Guo and S. Amemiya, *Analytical Chemistry*, **78**, 6893 (2006).
41. M. L. Colombo, J. V. Sweedler and M. Shen, *Analytical chemistry*, **87**, 5095 (2015).
42. M. Shen and M. L. Colombo, *Analytical Methods*, **7**, 7095 (2015).
43. C. Lefrou, *Journal of Electroanalytical Chemistry*, **592**, 103 (2006).
44. J. Kim, M. Shen, N. Nioradze and S. Amemiya, *Analytical Chemistry*, **84**, 3489 (2012).
45. G. Gerhardt and R. N. Adams, *Analytical Chemistry*, **54**, 2618 (1982).
46. P. J. Rodgers, S. Amemiya, Y. X. Wang and M. V. Mirkin, *Analytical Chemistry*, **82**, 84 (2010).

47. Y. X. Wang, J. Velmurugan, M. V. Mirkin, P. J. Rodgers, J. Kim and S. Amemiya, *Analytical Chemistry*, **82**, 77 (2010).
48. C. M. E. Tallaksen, T. Bohmer and H. Bell, *American Journal of Clinical Nutrition*, **56**, 559 (1992).

CHAPTER 4

NANOPIPET ELECTRODES FOR THE DETECTION OF NEUROTRANSMITTER RELEASE FROM CULTURED *APLYSIA CALIFORNICA* NEURONS

4.1 INTRODUCTION

We have previously shown the detection of several neurotransmitters, both redox active and non-redox active, using nano-ITIES based pipet electrodes (1, 2). The small size of these electrodes gives many advantages over larger electrodes that have traditionally been used, including high diffusive mass transport; low background current; and most importantly in this case, superior spatial resolution for interrogating biological structures. Scanning Electrochemical Microscopy (SECM) is a scanning probe technique that when combined with micro- or nanoelectrodes, is able to create highly spatially resolved images based on chemical diffusion or reactivity (3-7). The spatial resolution here depends directly on electrode size, where a smaller tip radius yields higher resolution.

The high spatial resolution afforded by this method allows for highly targeted studies of exocytosis (8-13). This type of work has the potential to provide neuroscientists with important information regarding the dynamics of neurotransmission, as there is still much unknown or disputed about the process (14-19).

An excellent model system for linking neural activity and behavior is the *Aplysia californica*, a sea slug found off the coast of Mexico and California (20). This animal's nervous system has been examined and described extensively in numerous neurobiological studies, and therefore many cell clusters or even individual cells have already been linked to specific physiological functions (20-28). Furthermore, *A. californica* has relatively large

neurons that form large axons and synapses (29, 30), making it easier to probe specific targets within a cell culture. Here, SECM in combination with ITIES-based pipet electrodes is used to explore neurotransmission from cultured *A. californica* neurons.

4.2 METHODOLOGY

4.2.1 Reagents

Potassium tetrakis(pentafluorophenyl)borate (TFAB) was obtained from Boulder Scientific Company (Mead, CO). Fast green FCF, tetradodecylammonium (TDDA) chloride, tetraethylammonium chloride (TEACl), tetrabutylammonium chloride (TBACl), dibenzo-18-crown-6 (DB18C6), 1,2-dichloroethane (1,2-DCE), and chlorotrimethylsilane were purchased from Sigma-Aldrich (St. Louis, MO). The TFAB salt of TDDA (TDDATFAB) was prepared by metathesis. Potassium chloride (KCl) was from VWR (Radnor, PA), calcium chloride ($CaCl_2$) was from Sigma-Aldrich (St. Louis, MO), and magnesium chloride ($MgCl_2$) was from Amresco (Solon, OH). Magnesium sulfate (MgSO4), HEPES, and lithium chloride (LiCl) were from Fisher Scientific (Pittsburgh, PA). Artificial seawater (ASW) contained (in mM) the following: 460 NaCl, 10 KCl, 10 $CaCl_2$, 22 $MgCl_2$, 26 $MgSO_4$, and 10 HEPES (pH 7.8). All reagents were used as received, and solutions were prepared using 18.3 MΩ cm deionized water (ELGA, Woodridge, IL). The prepared solutions were passed through a 0.2 μm filter (Thermo Scientific, Waltham, MA) before use.

4.2.2 Fabrication and characterization of electrochemical probes

Nanometer-scale pipet electrodes were fabricated by laser pulling of quartz capillaries (O.D. = 1.0 mm, I.D. = 0.7 mm, length = 10 cm) using a P-2000 capillary puller (Sutter Instrument Co., Novato, CA). The pulled pipets were then silanized via vapor deposition as

described elsewhere (1, 31). Pipets were characterized using Scanning Electron Microscopy (SEM) and ion-transfer voltammetry. For SEM imaging, the nanopipets were coated with a thin Au/Pd film by a high-resolution sputter coater (Quorum Technologies LTD, Kent, UK), and the orifices were observed by high resolution field emission SEM (FEI dual-beam 235, FEI Co., Hillsboro OR, USA) under a 20 kV electron beam. The prepared nanopipets were backfilled with a supporting electrolyte solution 1,2-DCE using a 10 μL Hamilton syringe, and the organic solution was pushed to the tip of the pipet by creating a gentle vibration. When immersed in an aqueous solution, a liquid-liquid interface is formed at the tip of the pipet. Voltage was applied between two reference electrodes: one inside the pipet and one outside, which is immersed in the aqueous solution. A Pt wire (50 μm diameter) was used as the inner reference, and the external reference was a AgCl coated Ag wire (250 μm diameter). Cell diagrams representing each experimental setup used are the following:

cell 1: Pt | 5 mM TDDATFAB + DCE || ASW + 4 mm TEA| AgCl | Ag

cell 2: Pt | 5 mM TDDATFAB + DCE + 1 mM DB18C6 || ASW | AgCl | Ag

4.2.3 *Aplysia californica* neuronal culture

A. californica, weighing 20 – 100 g, were obtained from the University of Miami/NIH National Resource for Aplysia and kept in an aquarium containing aerated and filtered artificial seawater (Instant Ocean, Aquarium Systems Inc., Mentor, OH) maintained at 14 °C. Animals were anesthetized by injection of isotonic $MgCl_2$ into the body cavity at 30 – 50% of body weight before dissection. The pedal ganglia were extracted and placed in a 1% protease solution prepared in ASW for 45-60 minutes at 34 °C to help remove connective tissues and reduce adherence between cells. The ganglia were then washed in ASW for 2-3 hours before cell isolation. Cells were manually isolated under the guidance of a Zeiss Stemi

2000-C stereomicroscope (Carl Zeiss Microscopy, LLC, Thornwood, NY). Isolated cells were plated on piranha-cleaned Si wafers that were coated with poly-L-lysine for at least 15 minutes, and left to grow overnight in an antibiotic containing solution of ASW (ASW containing penicillin G, gentamycin, and streptomycin) before beginning experiments.

4.2.4 Experimental setup

All electrochemical experiments were performed using a CHI920D Scanning Electrochemical Microscope (CH Instruments, Austin, TX), in a well-grounded Faraday cage atop a vibration isolation table to minimize noise. After taking initial cell images with a Zeiss Axio Lab.A1 (Carl Zeiss Microscopy, LLC, Thornwood, NY), regions of interest were found using a video microscope (Caltex Scientific Inc., Irvine, CA) located in the Faraday cage setup. The electrode was then lowered down to the region of interest using a probe approach curve, after which either a chemical stimulation experiment was performed, or an SECM image was taken.

4.2.5 Approach curves and SECM imaging

Electrodes were lowered to substrates using the Probe Approach Curve technique, positioned using piezo motors. Approaches were stopped when current level reached a given threshold percentage of the steady-state limiting current in bulk solution. All approach curve data were analyzed using the method described by Lefrou (32).

With the electrode placed less than five tip radii away from the substrate ($L < 5$), SECM images were taken by monitoring the current at a potential at which the mediator transferred, as the probe was rastered over the surface in the x,y directions. Changes in topography were reflected in fluctuations in current, where higher topography produced lower current due to limited diffusion of analyte to the electrode. Height data was extrapolated from the images by

determining the distance away from the surface using approach curve data and L=d/a, where L is the normalized distance, d is the distance away from the surface, and a is the inner radius of the electrode. d was divided by the current level at the first pixel of the image to create a normalization ratio, and all pixels within the image were normalized by multiplying the current by this ratio, then subtracting the result from d.

4.2.6 Chemical stimulation

Cells were stimulated with a solution of high potassium ASW, where the ASW described in section 4.2.1 was modified so that KCl concentration was increased to 50 mM, and NaCl was lowered to maintain osmolarity. Stimulation occurred via manually puffing a syringe connected to a borosilicate micropipette (O.D. = 1.0 mm, I.D. = 0.58 mm, length = 10 cm) pulled to a radius of 5 – 10 μm using a P-2000 capillary puller (Sutter Instrument, Novato, CA), with the tip placed near the cell of interest without direct contact. With the detection electrode placed inside the cell, amperometric i-t curves were taken to monitor the current response during stimulation, at a sample interval of 33 ms^{-1}. Fast green FCF was added to the stimulating solution to ensure that the target was reached with the high K^+ puffs. As of this writing, a total of five neurons from four different animals have been investigated in this manner.

4.3 RESULTS AND DISCUSSION

4.3.1 Culturing *Aplysia californica* neurons

Neurons were isolated and cultured from the pedal ganglia of *Aplysia californica* according to the procedure described in the experimental section. Culturing conditions were optimized in order to create ideal conditions that resulted clean, simple connections between

the processes of the neurons. Placing neurons in groups of two or three per cluster, with each cell body within the clusters approximately 100-300 μm apart created the best possibility for simple connections to form. Creating clean cultures with minimal cellular debris and glial cells required the optimization of the enzyme treatment process. Small animals typically produce healthier cultures than large ones, and therefore *Aplysia* that weighed less than 80 g were typically used. Ganglia from larger animals could produce clean cultures if they were incubated in 0.1 mM DNAse for 15 min following protease treatment. A successful culture could typically live for 48 h if cells were in a solution of antibiotic-supplemented ASW.

4.3.2 Choice of mediator

An ion that acts as a mediator is required for approach curves and SECM imaging, where the current level of the mediator transfer is monitored during each experiment to determine the tip-substrate distance. TEA works as an excellent mediator for this purpose due to its well-defined transfer properties that fit well to theory for approaching with an ITIES electrode (33-36). Figures 4.1a and 4.1b show approach curves that were taken using TEA as a mediator, with electrodes with radii of 28 and 168 nm, respectively. In both cases, the experimental data corresponds nicely to the theoretical curve, and both were able to achieve approximately 30% feedback. In the case of the 28 nm radius electrode, the approach stop occurred at L = 0.0713, corresponding to a distance of 2 nm away from the substrate. The 168 nm radius electrode approach ends at L = 0.167, corresponding to a distance of 28 nm away from the substrate.

It must be considered that biological studies such as the one presented here require as few external influences as possible, and TEA is known to cause disruptions in neurotransmitter release or uptake (37-40). Therefore, one goal of this study was to determine if the

background solution alone, i.e. ASW, could work as a mediator for approaching and imaging purposes.

Modifications to the system can be made in order to achieve steady-state current from the ASW cations. By using DB18C6 as an ionophore present in the organic filling solution, assisted ASW cation transfer occurs, resulting in steady-state current. The composition of assisted ASW transfer was evaluated by obtaining cyclic voltammograms of each component of ASW separately to evaluate the potential at which each ion transfers, with respect to TBA. These potentials are described as half-wave transfer potentials ($E_{1/2}$), and are reported with respect to the $E_{1/2}$ of TBA as described elsewhere (1, 2). The $E_{1/2}$ for each component ion was then compared to the $E_{1/2}$ of ASW to determine which ions are assisted by DB18C6. The results from this study showed that K^+ and Na^+ are assisted by DB18C6, and make up the total composition of the steady-state wave of ASW (Figure 4.2). With the assisted wave composition now identified, this wave was used as a mediator for approaching an Si wafer, producing approach curves that fit very nicely to theory (Figure 4.3).

4.3.3 SECM imaging of *Aplysia californica* neurons

With the electrode placed within a few tip radii away from the substrate, SECM imaging of *A. californica* neurons was performed at a constant-height. Topographical images of cellular processes were obtained by monitoring the steady-state current of TEA as the electrode was rastered over the surface of the cells (Figure 4.4). The small size of the electrodes used resulted in images with very high spatial resolution, allowing for detailed topography of processes to be observed. In these images, pixel size is determined by electrode step size, manually input by the user to correlate to the tip radius. Information regarding the topography (i.e. the height of the cellular processes) can be calculated from the

current data as detailed in the experimental section. Based on the images obtained, typical pedal neuronal processes range from 0.5 – 1.5 μm in height. The size information obtained by these SECM images corresponds well to that reported in the literature (30, 41, 42).

While Figure 4.4 demonstrates that a nice SECM image may be obtained in this manner, this is one of the best results achieved in the present study due to some limitations of the current methodology. A home built optical microscope with commercial lens (highest magnification: 50x) was used to provide rough estimation of location of cellular structures during the SECM imaging. The best view of the cellular structures as well as the SECM tip was achieved at the magnification of 15x, where the cell body can be viewed clearly while observing fine neurite structures can be challenging. This caused problems confirming the location of the tip with respect to fine cellular structures, which posed challenges for constant height imaging. This can be conquered by employing a higher resolution optical lens for constant height SECM imaging, and an alternative strategy is constant distance imaging as discussed below. Of 89 attempted images in the present study (at 30 different cells and 30 individual electrodes) with electrodes of hundreds of nanometers, 29 showed feedback corresponding to topographical features.

Correlated to the limitation set by the currently used optical microscope for SECM imaging is the magnitude of change in cell topography relative to the size of the electrode. While most electrodes in this study were of a similar size as the expected heights of the cell processes examined, electrodes that are much smaller than the cell surface topography could encounter problems with constant-height imaging. For example, if the nanoelectrode originally approaches a low part of the cell and is moved over a higher area, the tip can crash into the cell either creating distortions in the image or clogging the pipet electrode.

Alternatively, if the nanoelectrode first approaches an area with medium-high topography and moves toward an area with much lower topography, the feedback interaction could be lost, and the lower portions will not show up in the image. This effect has previously been described by Schulte et al. (8).

Figure 4.5b is one of the SECM images achieved at constant height with an electrode of radius of 400 nm. A distortion can be seen near y = 15 µm, followed by a sudden decrease in current for the remainder of the image, indicating a possible crash between the electrode and the cell or substrate. Aside from the sudden current decrease, a gradual decrease can also be seen throughout the whole image when moving down in the y direction. It is possible that this is caused by a tilt in the substrate. The spike in current near L = 0 in the approach curve indicates that the interface likely touched the substrate before stopping (Figure 4.5a). Evaluating the TEA steady-state current from CVs before and after this approach shows that the current magnitude grew by 93% (data not shown), meaning that the electrode interface during imaging was likely larger than 400 nm. It is also important to note that this particular image was taken 4 µm above the approach stop. Given that the cell processes are only ~1 µm high, it is reasonable that the distortion was caused by something other than the cell itself, such as a broken glass shard that might have been formed from the crash during the approach curve.

An alternative to using a higher resolution optical microscope for constant height imaging is the use of constant-distance imaging as mentioned above. Constant-distance imaging is a mode in which the electrode is moved in the z-plane during the imaging process in order to maintain the same distance between the tip and the substrate as it moves. This motion in the z-plane is controlled by a computer-controlled feedback loop that allows the software to

determine the tip-substrate distance at all times. Possible feedback loops include amperometric current or impedance measurements at the tip (43-48), or the vibration amplitude of the tip, which could be measured with either optical (13, 49) or tuning fork methods (43, 50-52).

4.3.4 Chemical stimulation of *Aplysia californica* neurons

Control experiments were performed to ensure that the K^+ stimulation puffs alone would not induce fluctuations in current at the detection electrode. The tips of the stimulation pipet and detection electrode were placed near one another without direct contact over either a bare Si wafer or a dead *A. californica* neuron (<100 μm above surface of each), and the high K^+ ASW solution was puffed at various time intervals while the current at the detection electrode was being monitored via amperometry at various potentials. These experiments showed that the introduction of high K^+ had no effect on the current recorded at the detection electrode, even at a potential where the assisted ASW wave is observed. We are currently confirming this at closer distance between the stimulation electrode and detection electrode, as well as with the detection electrode immediately over the substrate surface (L<5). Although K^+ was shown to be detected in the assisted ASW wave, the introduction of additional K^+ here does not add to the current of the wave due to the fact that the concentration of K^+ in ASW is already in excess compared to the concentration of DB18C6 in the organic filling solution (53).

Several chemical stimulation experiments were performed using the same setup as described above, with *Aplysia* cells cultured on the surface of the Si wafer. The detection pipet was placed inside the cell body prior to stimulation. Amperometric recordings at a small overpotential yielded no observed spikes, as expected since most neurotransmitters are

detected at comparatively large negative overpotentials (Table 4.1). When the electrode was poised at more negative potentials, peaks were observed immediately following the K^+ stimulation (Figure 4.6) for three out of the five experiments of this type that were performed. These peaks lasted for approximately 10-20 s before the current level returned to baseline. It is possible that the measurements inside the cell recorded intracellular events leading up to neurotransmitter release. It was previously reported that Ca^{2+} uptake occurs within 15 s of K^+ stimulation of chromaffin cells (58). This timescale corresponds well to the events observed in the present study, though it is not likely that Ca^{2+} intake is what is directly causing the spikes observed inside the cell, but perhaps some other intracellular event that would be interesting to explore further. Several more replicates of this experiment will be necessary to ensure reproducibility of these results.

4.4 CONCLUSIONS

Here we have described the use of ITIES-based nanopipet electrodes for interrogating neurons cultured from *Aplysia californica*. Well-behaved approach curves were obtained by using the background solution of artificial sea water without the use of a mediator, which is the first time this has been reported, to the best of our knowledge. SECM images with high spatial resolution provided topographical information regarding the neuronal processes of cultured *A. californica* pedal neurons, though modification to the experimental setup could provide higher success rates in the future. Stimulation of these neurons showed varying response at the detection electrode depending on tip placement relative to the cell, indicating this technique is valuable in monitoring neurotransmitter release in real time at very targeted locations within a single cell. Significant future work will be required to evaluate

reproducibility and to confirm whether these peaks are due to neurotransmitter release. For more qualitative studies, cells with specific contents should be examined, such as the B1 and B2 neurons from *A. californica* buccal ganglia, which are known to release acetylcholine (23), and enzymatic control experiments should also be performed. Spikes with higher signal-to-noise ratios may be obtained with the addition of a lock-in amplifier to the instrument setup, which will also allow for higher sampling intervals. Overall, the results presented here provide preliminary evidence that ITIES-based nanopipet electrodes can offer valuable information regarding neurotransmitter release from cultured cells.

4.5 NOTES AND ACKNOWLEDGMENTS

Research reported in this chapter was supported by the National Institute of Neurological Disorders and Stroke of the National Institutes of Health under award number R21NS085665 to M.S. (PI), J.V.S. (Co-PI). The content is solely the responsibility of the authors and does not necessarily represent the official views of the National Institutes of Health. M. L. C. acknowledges the support from the Coleman Fellowship and the NIH Chemical Biology Interface Training Program under training grant number 2T32GM070421-11. All experimental work in this chapter was performed by Michelle Colombo, Theresa Welle, and Natalie Ibe at the University of Illinois at Urbana-Champaign, School of Chemical Sciences. SEM was carried out in the Frederick Seitz Materials Research Laboratory Central Facilities, University of Illinois. *A. californica* were provided partially by the National Resource for Aplysia funded by PHS grant P40 OD010952. Cell culture assistance was provided by Xiying Wang and Dr. Stanislav Rubakhin.

4.6 FIGURES AND TABLES

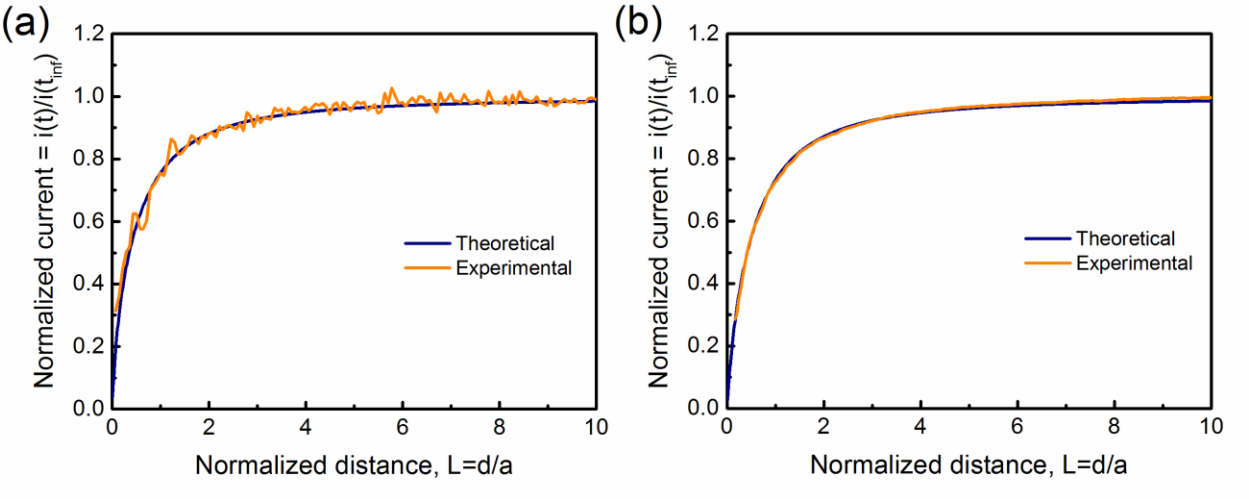

Figure 4.1. Approach curves using tetraethylammonium (TEA) as a mediator at pipet electrodes with radii of (a) 28 nm and (b) 168 nm.

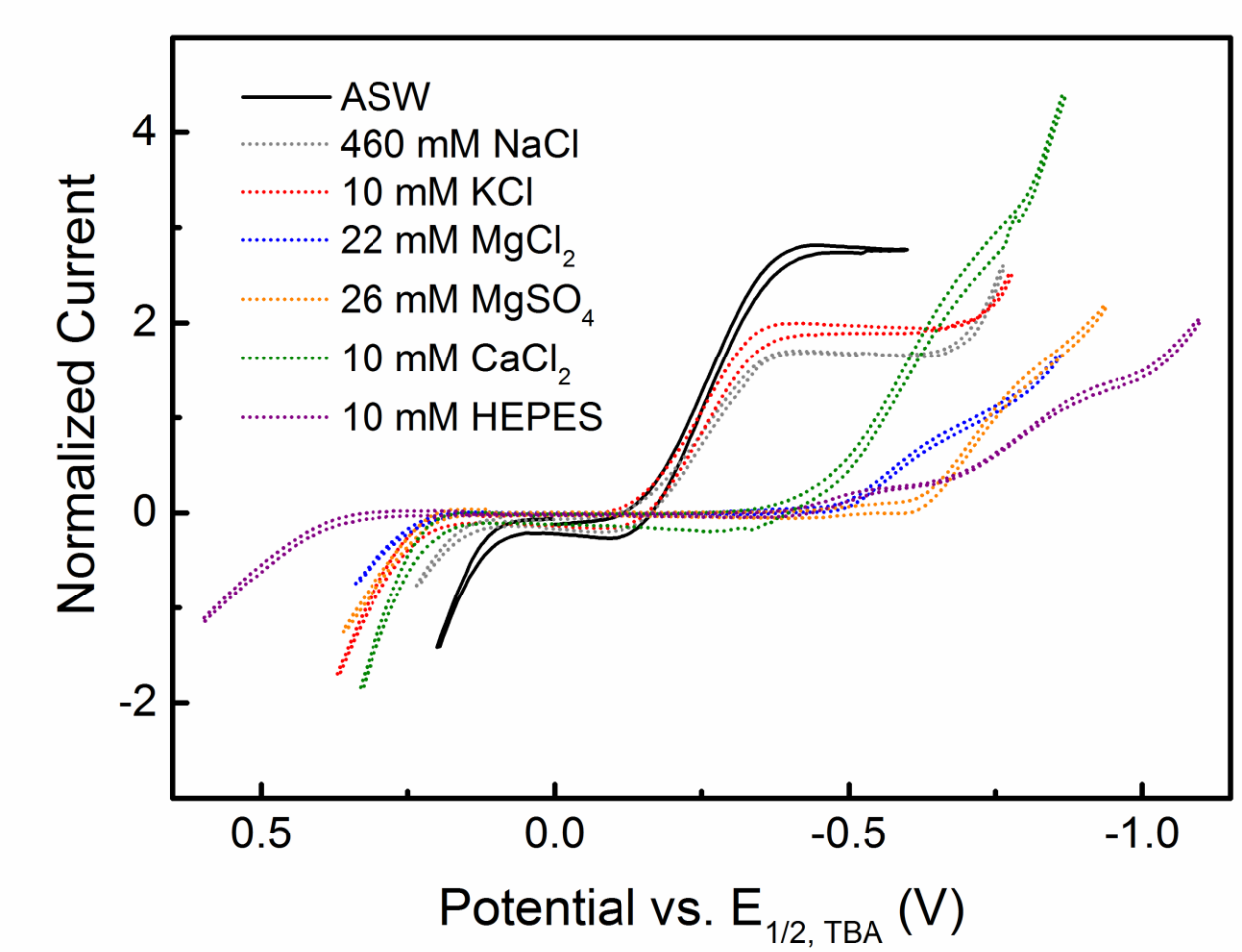

Figure 4.2. Cyclic voltammogram overlay of ASW and each component that makes up ASW, showing that ASW's assisted cation wave is composed mainly of K^+ and Na^+. Each CV was taken using a different electrode, so current is normalized to electrode radius.

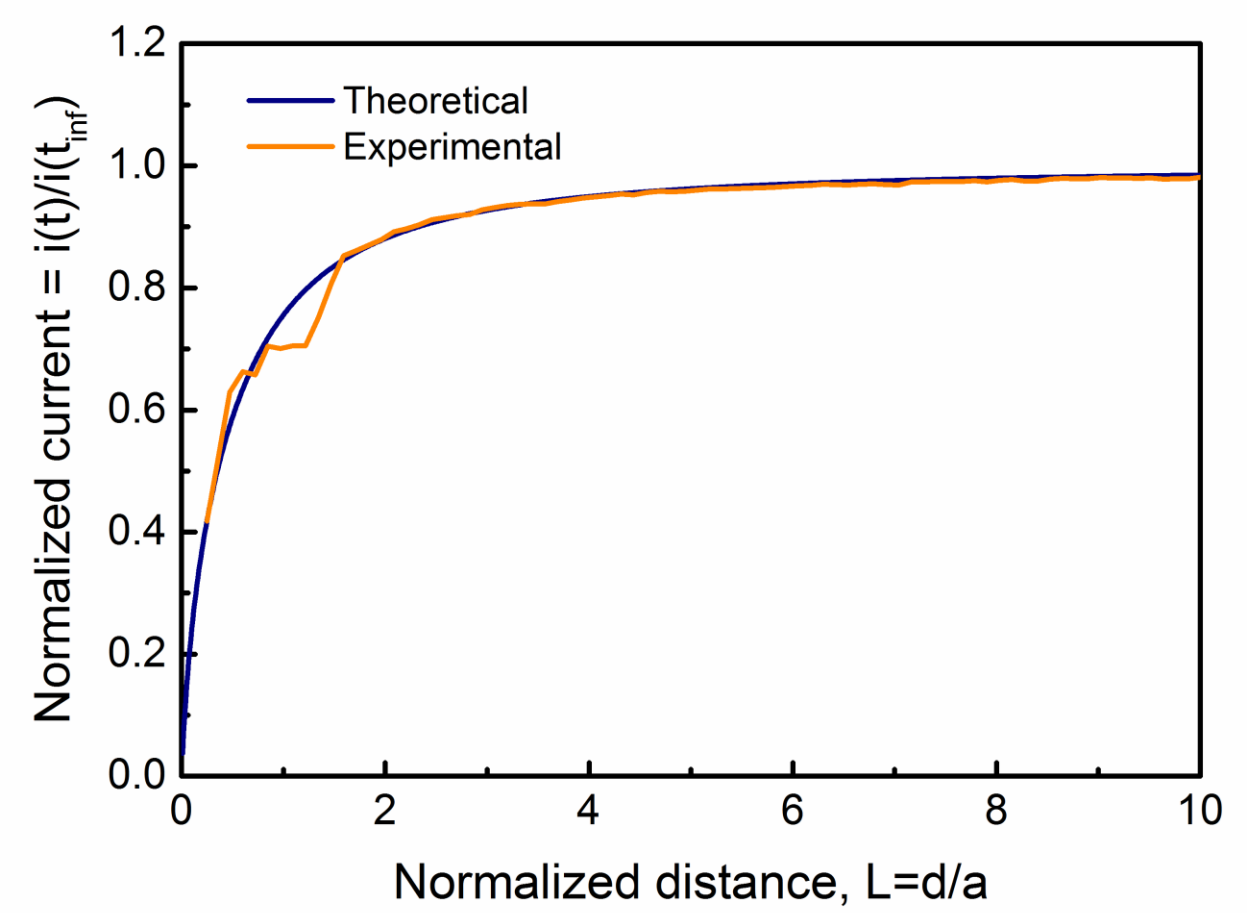

Figure 4.3. Approach curve using DB18C6 assisted transfer of ASW cations as a mediator at a pipet electrode with a radius of 48 nm.

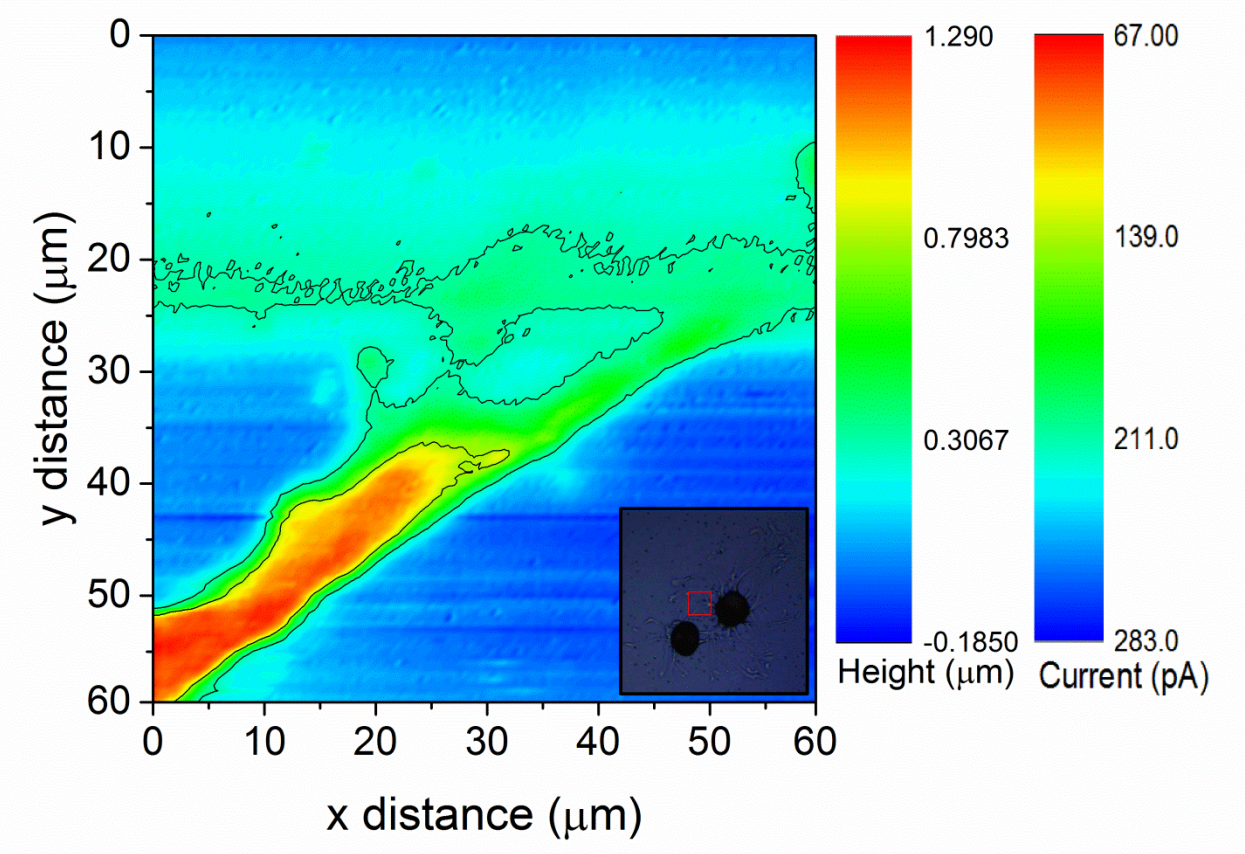

Figure 4.4. SECM image of an *A. californica* neuronal process, taken using a nanopipet with a radius of 855 nm. Inset: photograph of cells used for imaging (red box indicates region interrogated, each side of box = 60 µm).

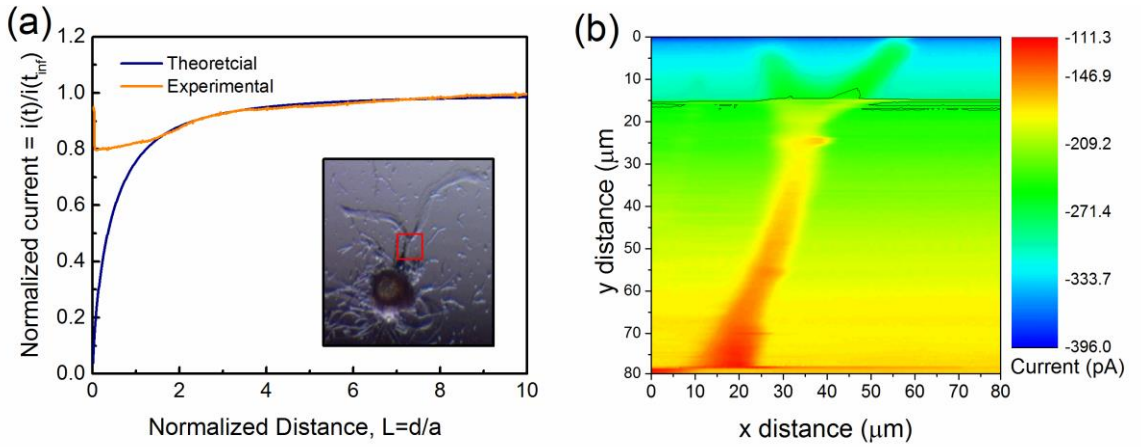

Figure 4.5. SECM images of cellular processes of a cultured *A. californica* neuron, using constant-height imaging. (a) shows the approach curve prior to imaging. Inset: photograph of the cell imaged (red box indicates region interrogated, each side of box = 80 µm) in (b), which shows possible indication of a tip crash during the SECM imaging process near y = 15 µm. Image was taken using a pipet electrode with a radius of 400 nm before approach, and the electrode approached at the top left corner of the image before scanning.

Table 4.1. Half-wave transfer potentials ($E_{1/2}$) of various neurotransmitters with respect to the $E_{1,2}$ of TBA. All analytes were detected using 1 mM DB18C6 present in the filling solution, according to cell 2.

Analyte	**$E_{1/2}$ vs. $E_{1/2,\ TBA}$ (V)**
acetylcholine	-0.443 ± 0.021
choline	-0.518 ± 0.003
tryptamine	-0.567 ± 0.004
glutamate	not detected in ASW
serotonin	not detected in ASW
dopamine	not detected in ASW (Ref. 2)
γ-aminobutyric acid	not detected in ASW
ascorbic acid	not detected in ASW (Ref. 2)

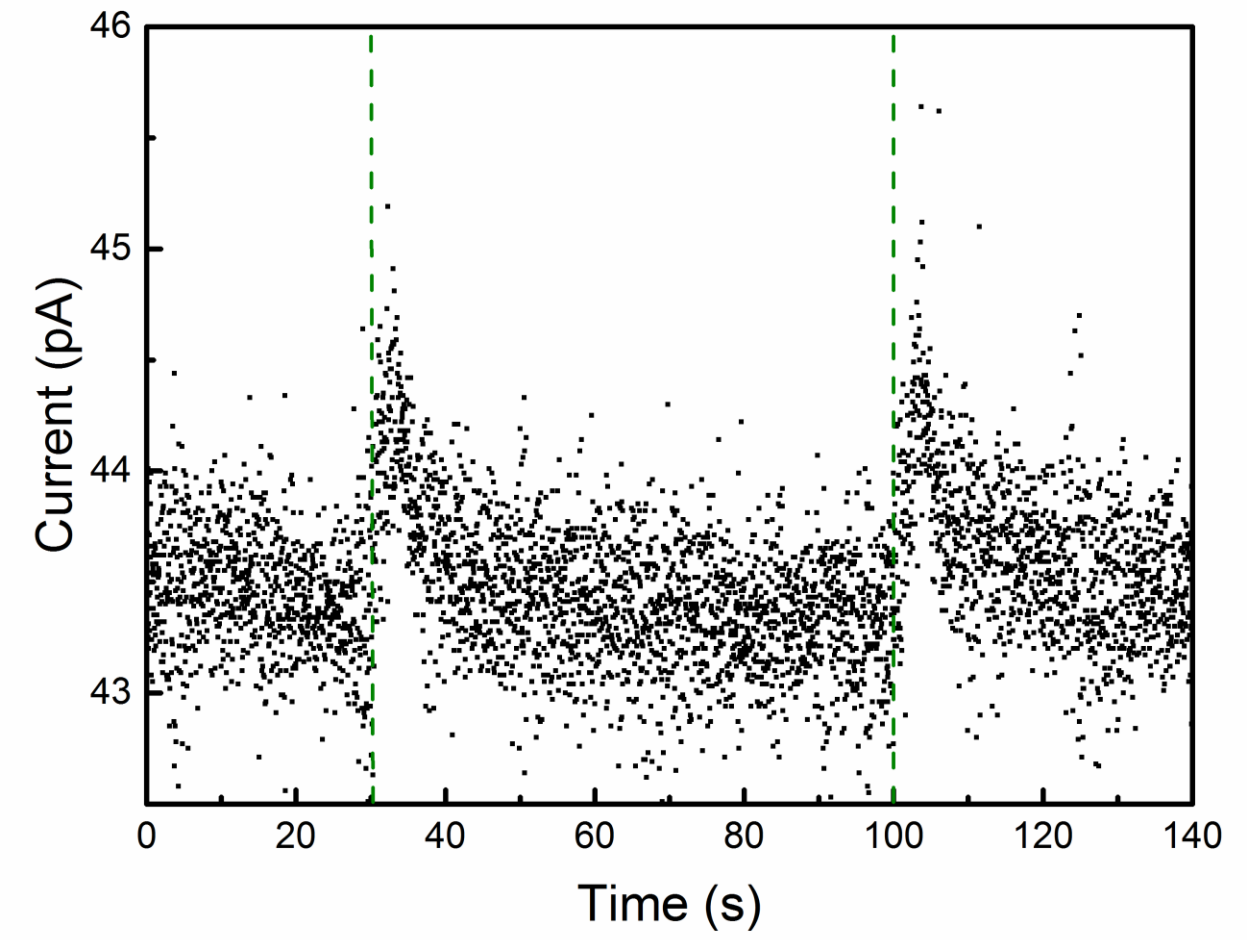

Figure 4.6. Chemical stimulation of an *A. californica* neuron with the pipet electrode placed inside the cell body. K^+ stimulation puffs are indicated by the dashed green lines. Potential applied to detection pipet = -0.42 V vs. $E_{1/2,\ TBA}$.

4.7 REFERENCES

1. M. L. Colombo, J. V. Sweedler and M. Shen, *Analytical chemistry*, **87**, 5095 (2015).
2. M. L. Colombo, S. McNeil, N. Iwai, A. Chang and M. Shen, *Journal of The Electrochemical Society*, **163**, H3072 (2016).
3. A. J. Bard, F. R. F. Fan, J. Kwak and O. Lev, *Analytical Chemistry*, **61**, 132 (1989).
4. A. J. Bard and M. V. Mirkin, *Scanning Electrochemical Microscopy*, Marcel Dekker, New York (2001).
5. Q. J. Chen, L. Luo, H. Faraji, S. W. Feldberg and H. S. White, *Journal of Physical Chemistry Letters*, **5**, 3539 (2014).
6. M. Shen, R. Ishimatsu, J. Kim and S. Amemiya, *Journal of the American Chemical Society*, **134**, 9856 (2012).
7. T. Sun, Y. Yu, B. J. Zacher and M. V. Mirkin, *Angewandte Chemie-International Edition*, **53**, 14120 (2014).
8. A. Schulte, M. Nebel and W. Schuhmann, in *Annual Review of Analytical Chemistry, Vol 3*, E. S. Yeung and R. N. Zare Editors, p. 299, Annual Reviews, Palo Alto (2010).
9. M. S. M. Li, F. P. Filice and Z. Ding, *Journal of Electroanalytical Chemistry*. (2016). DOI: 10.1016/j.elechem.2016.02.042
10. A. Kueng, C. Kranz and B. Mizaikoff, *Biosensors & Bioelectronics*, **21**, 346 (2005).
11. Y. Takahashi, T. Miyamoto, H. Shiku, R. Asano, T. Yasukawa, I. Kumagai and T. Matsue, *Analytical Chemistry*, **81**, 2785 (2009).
12. J. M. Liebetrau, H. M. Miller and J. E. Baur, *Analytical Chemistry*, **75**, 563 (2003).
13. L. P. Bauermann, W. Schuhmann and A. Schulte, *Physical Chemistry Chemical Physics*, **6**, 4003 (2004).
14. A. S. Cans and A. G. Ewing, *J. Solid State Electrochem.*, **15**, 1437 (2011).
15. D. M. Omiatek, Y. Dong, M. L. Heien and A. G. Ewing, *Acs Chemical Neuroscience*, **1**, 234 (2010).
16. L. J. Mellander, R. Trouillon, M. I. Svensson and A. G. Ewing, *Scientific Reports*, **2** (2012).
17. R. Trouillon and A. G. Ewing, *Chemphyschem*, **14**, 2295 (2013).
18. R. Trouillon and A. G. Ewing, *Acs Chemical Biology*, **9**, 812 (2014).
19. L. R. Squire, *Fundamental Neuroscience*, Elsevier/Academic Press (2013).
20. Castellu.V, H. Pinsker, Kupferma.I and E. R. Kandel, *Science*, **167**, 1745 (1970).
21. S. Arch, *Journal of General Physiology*, **60**, 102 (1972).
22. A. Y. Chiu, M. W. Hunkapiller, E. Heller, D. K. Stuart, L. E. Hood and F. Strumwasser, *Proceedings of the National Academy of Sciences of the United States of America*, **76**, 6656 (1979).
23. K. Ohnuma, M. D. Whim, R. D. Fetter, L. K. Kaczmarek and R. S. Zucker, *Journal of Physiology-London*, **535**, 647 (2001).
24. M. D. Whim, H. Niemann and L. K. Kaczmarek, *Journal of Neuroscience*, **17**, 2338 (1997).
25. W. T. Frazier, E. R. Kandel, Kupferma.I, R. Waziri and Coggesha.Re, *Journal of Neurophysiology*, **30**, 1288 (1967).
26. E. R. Kandel, W. T. Frazier and Coggesha.Re, *Science*, **155**, 346 (1967).
27. Y. Fan, S. S. Rubakhin and J. V. Sweedler, *Analytical Chemistry*, **83**, 9557 (2011).

28. J. A. Jing, J. V. Sweedler, E. C. Cropper, V. Alexeeva, J. H. Park, E. V. Romanova, F. Xie, N. C. Dembrow, B. C. Ludwar, K. R. Weiss and F. S. Vilim, *Journal of Neuroscience*, **30**, 16545 (2010).
29. R. Gillette, *Biological Bulletin*, **180**, 234 (1991).
30. M. L. Scott, C. K. Govind and M. D. Kirk, *Journal of Comparative Neurology*, **312**, 207 (1991).
31. M. Shen and M. L. Colombo, *Analytical Methods*, **7**, 7095 (2015).
32. C. Lefrou, *Journal of Electroanalytical Chemistry*, **592**, 103 (2006).
33. P. J. Rodgers, S. Amemiya, Y. X. Wang and M. V. Mirkin, *Analytical Chemistry*, **82**, 84 (2010).
34. G. Geblewicz and Z. Koczorowski, *Journal of Electroanalytical Chemistry*, **158**, 37 (1983).
35. C. Wei, A. J. Bard and M. V. Mirkin, *Journal of Physical Chemistry*, **99**, 16033 (1995).
36. Y. X. Wang, J. Velmurugan, M. V. Mirkin, P. J. Rodgers, J. Kim and S. Amemiya, *Analytical Chemistry*, **82**, 77 (2010).
37. E. F. Barrett, K. Morita and K. A. Scappaticci, *The Journal of Physiology*, **402**, 65 (1988).
38. C. Gonzalezgarcia, V. Cena, H. R. Keiser and E. Rojas, *Biochimica Et Biophysica Acta*, **1177**, 99 (1993).
39. J. Kehoe, *Journal of Physiology-London*, **204**, P11 (1969).
40. K. Sasaki, *Japanese Journal of Physiology*, **35**, 109 (1985).
41. N. E. Ziv and M. E. Spira, *Journal of Neuroscience*, **17**, 3568 (1997).
42. T. L. Ross, C. K. Govind and M. D. Kirk, *Journal of Neurophysiology*, **72**, 1897 (1994).
43. Y. Lee, Z. F. Ding and A. J. Bard, *Analytical Chemistry*, **74**, 3634 (2002).
44. D. O. Wipf, A. J. Bard and D. E. Tallman, *Analytical Chemistry*, **65**, 1373 (1993).
45. R. T. Kurulugama, D. O. Wipf, S. A. Takacs, S. Pongmayteegul, P. A. Garris and J. E. Baur, *Analytical Chemistry*, **77**, 1111 (2005).
46. F. O. Laforge, J. Velmurugan, Y. X. Wang and M. V. Mirkin, *Analytical Chemistry*, **81**, 3143 (2009).
47. M. A. Alpuche-Aviles and D. O. Wipf, *Analytical Chemistry*, **73**, 4873 (2001).
48. E. N. Ervin, H. S. White and L. A. Baker, *Analytical Chemistry*, **77**, 5564 (2005).
49. M. Ludwig, C. Kranz, W. Schuhmann and H. E. Gaub, *Review of Scientific Instruments*, **66**, 2857 (1995).
50. P. I. James, L. F. Garfias-Mesias, P. J. Moyer and W. H. Smyrl, *Journal of the Electrochemical Society*, **145**, L64 (1998).
51. D. Oyamatsu, Y. Hirano, N. Kanaya, Y. Mase, M. Nishizawa and T. Matsue, *Bioelectrochemistry*, **60**, 115 (2003).
52. H. Yamada, H. Fukumoto, T. Yokoyama and T. Koike, *Analytical Chemistry*, **77**, 1785 (2005).
53. F. Li, Y. Chen, P. Sun, M. Q. Zhang, Z. Gao, D. P. Zhan and Y. H. Shao, *Journal of Physical Chemistry B*, **108**, 3295 (2004).
54. T. J. Schroeder, J. A. Jankowski, J. Senyshyn, R. W. Holz and R. M. Wightman, *Journal of Biological Chemistry*, **269**, 17215 (1994).
55. I. M. Robinson, J. M. Finnegan, J. R. Monck, R. M. Wightman and J. M. Fernandez, *Proceedings of the National Academy of Sciences of the United States of America*, **92**, 2474 (1995).

56. Y. Okubo, H. Sekiya, S. Namiki, H. Sakamoto, S. Iinuma, M. Yamasaki, M. Watanabe, K. Hirose and M. Iino, *Proceedings of the National Academy of Sciences of the United States of America*, **107**, 6526 (2010).
57. Q. T. Nguyen, L. F. Schroeder, M. Mank, A. Muller, P. Taylor, O. Griesbeck and D. Kleinfeld, *Nature Neuroscience*, **13**, 127 (2010).
58. R. W. Holz, R. A. Senter and R. A. Frye, *Journal of Neurochemistry*, **39**, 635 (1982).

CHAPTER 5

CONCLUSIONS AND FUTURE DIRECTIONS

5.1 SUMMARY OF RESULTS

ITIES-based nanopipet electrodes provide a unique analytical platform for detecting ionic species that are both redox active and non-redox active. This quality gives them an advantage over their more traditional electrode counterparts, such as the carbon fiber electrode. Furthermore, fabrication of nanopipet electrodes is simple, even down to radii on the order of single to tens of nanometers.

The nanopipet electrodes shown here were able to detect acetylcholine, tryptamine, and serotonin in both qualitative and quantitative manners using cyclic voltammetry and amperometry. The diffusion coefficients and half-wave transfer potentials for each were reported. These three species are detected at separate potentials, with acetylcholine requiring the least amount of energy input, followed by tryptamine and then serotonin. Because of this, acetylcholine and tryptamine are detected in ASW, the biological medium for our model animal, *Aplysia californica*. However, ASW does not have a large enough potential window for sufficient detection of serotonin, therefore this species was detected in LiCl. The electrodes used to detect these three neurotransmitters used a simple organic electrolyte solution without the addition of an ionophore. In this case, they are selective against γ-aminobutyric acid, and ascorbic acid, and dopamine.

Dopamine was detected using similar nanopipet electrodes, simply with the addition of DB18C6 as an ionophore. Dopamine could be detected quantitatively due to the linear current response with respect to concentration. The diffusion coefficient and half-wave

transfer potentials were reported, neither of which were affected by changes in tip geometry at electrodes with radii on the order of hundreds of nanometers with varying taper angles. The observed diffusion coefficient of dopamine is decreased in the presence of increasing amounts of ascorbic acid, but is not affected by physiological levels of ascorbic acid. In all cases, regardless of diffusion coefficient, dopamine response is linear.

Nanopipets were used in biological studies involving cultured cells from *Aplysia californica*, in combination with SECM. The electrodes were lowered to a very small distance above the cells using probe approach curves, where high-resolution imaging could then be performed. The assisted transfer of ASW cations was used as a mediator and was found to be just as effective as an external mediator such as tetraethylammonium. Experiments involving chemical stimulation of the cells with K^+ were performed, and preliminary results indicate possible detection of release events. These results have been limited by the small amount of experiments performed to date, and so future work will be necessary to ensure reproducibility of results.

5.2 FUTURE WORK

Future imaging should be performed with the use of high resolution optical microscope for constant-height imaging or constant-distance imaging mode, where the electrode is maintained at a specified distance from the cell surface by means of a feedback mechanism. With small enough tips, SECM could potentially be employed to provide topographical images that give detailed information regarding the location of potential release sites. This precise location could then be interrogated using chemical stimulation, similar to the preliminary studies shown here.

The response at the detection electrode following stimulations needs to be well-characterized in many ways. Modifications to the experimental setup could provide assistance with this. For example, the addition of a lock-in amplifier could allow for more defined peak shapes due to higher sampling rates and higher signal-to-noise ratios. Furthermore, qualitative information regarding the releasate needs to be further explored. This could be done by examining cells with identified contents, such as the B1 and B2 neurons from *A. californica* buccal ganglia, which are known to release acetylcholine. Still, co-release of multiple species is possible, so control experiments will need to be performed as well. Once the identity of the detected species is known, it will be possible to quantify the amount of neurotransmitter detected based on the current level, and to analyze peaks for information regarding rise time and fall time, which could provide important information regarding the dynamics of release. In this case the distance of the electrode with respect to the release site will play an important role, and this information will need to be known for accurate analysis.

Overall, the results shown provide an indication that ITIES-based nanopipet electrodes can offer valuable information regarding neurotransmitter release from cultured cells. With the modifications described above in place, numerous studies may be performed to compare release dynamics with the addition various stimulants, modulators, or drugs.

APPENDIX A

INFORMATION SUPPORTING CHAPTER 2

Table A.1. Pulling parameters for nm orifice pipets using a P-2000 Laser-Based Micropipette Puller (Sutter Instrument, Novato, CA) with quartz glass capillaries (O.D. = 1.0 mm; I.D. = 0.70 mm; 10 cm length).

Heat	Fil	Vel	Del	Pul
725	4	55	130	100

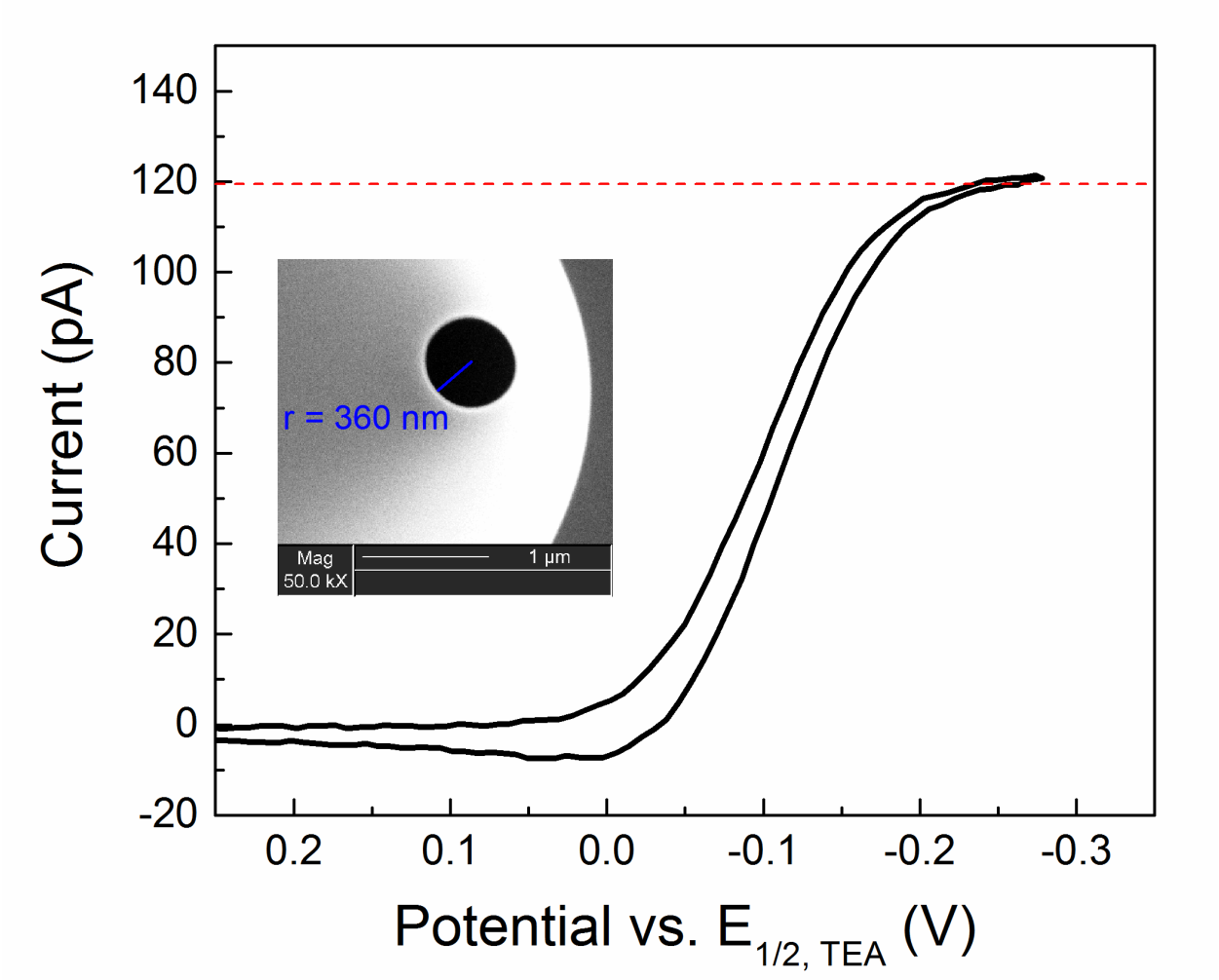

Figure A.1. SEM and cyclic voltammogram for one of the pipets used for calculating the diffusion coefficient of acetylcholine (ACh) in artificial sea water (ASW) via Cell 1. Concentration of ACh = 1 mM; steady state current = 120 pA (red dashed line). Inset: SEM image of pipet used, showing a radius of 360 nm. Calculated D_{Ach} = 7.02 x 10^{-6} cm^2/s.

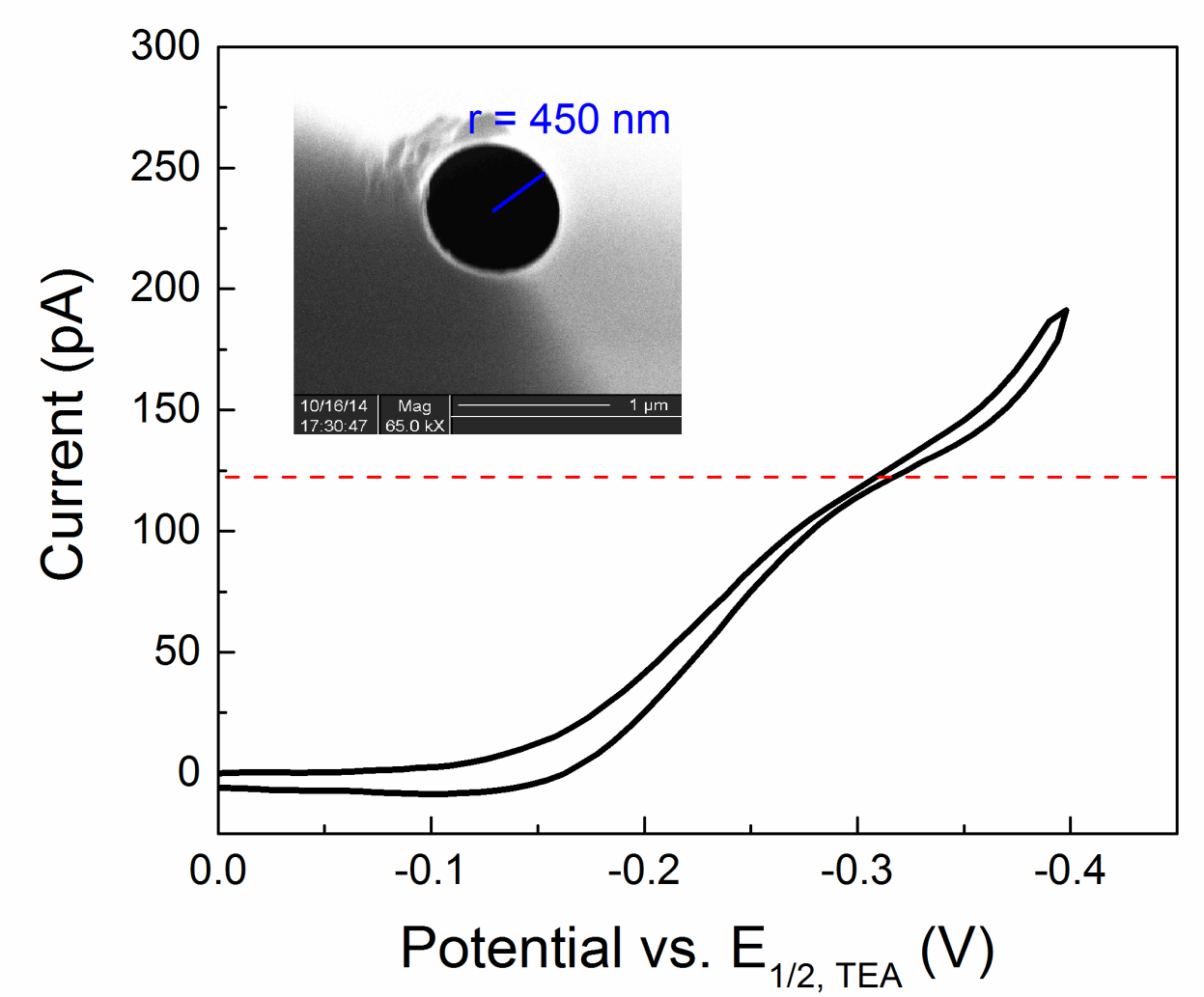

Figure A.2. SEM and cyclic voltammogram for one of the pipets used for calculating the diffusion coefficient of tryptamine (T) in artificial sea water (ASW) via Cell 1. Concentration of T = 1 mM; Steady state current = 126 pA (red dashed line); the process shown at more negative potentials is due to the transfer of ASW. Inset: SEM image of pipet used, showing a radius of 450 nm. Calculated $D_T = 5.90 \times 10^{-6}$ cm^2/s.

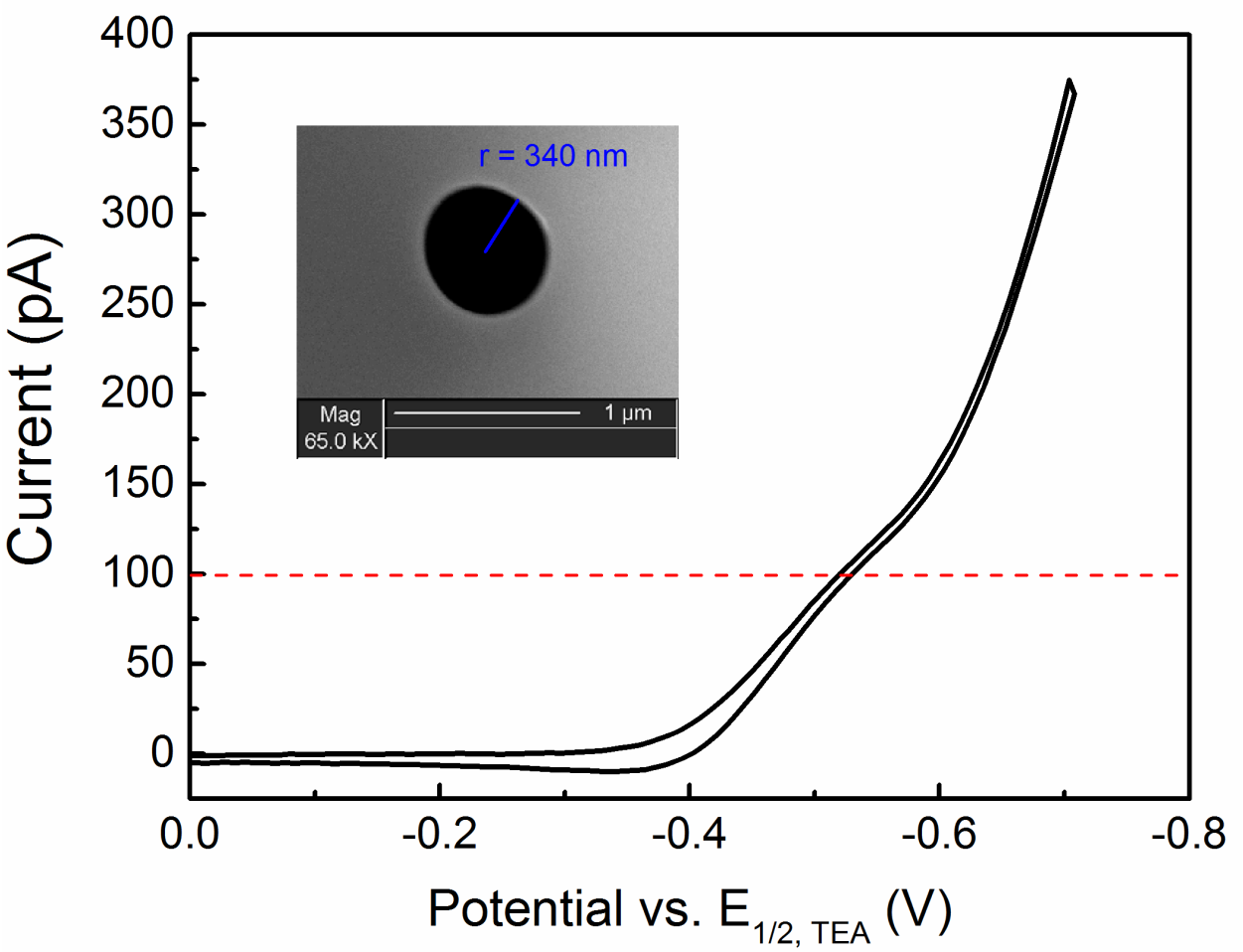

Figure A.3. SEM and cyclic voltammogram for one of the pipets used for calculating the diffusion coefficient of serotonin (5-HT) in 10 mM LiCl via Cell 2. Concentration of 5-HT = 1 mM; Steady state current = 100 pA (red dashed line); the process shown at more negative potentials is due to the transfer of LiCl. Inset: SEM image of pipet used, showing a radius of 340 nm. Calculated $D_{5\text{-HT}} = 6.20 \times 10^{-6}$ cm^2/s.

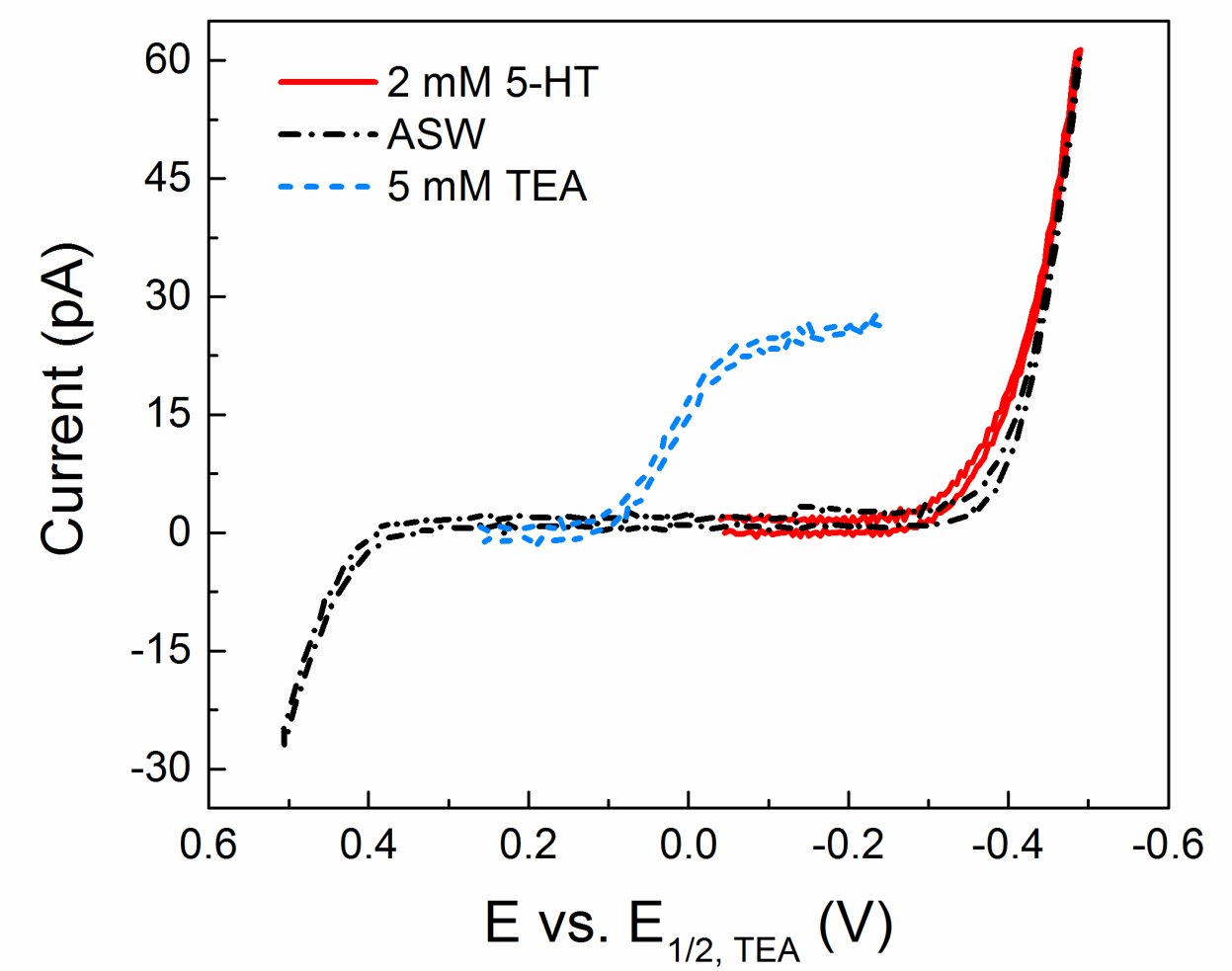

Figure A.4. Cyclic voltammogram of 2 mM serotonin (5-HT) in artificial sea water (ASW) using a pipet with a radius of 28 nm in Cell 3. Blue dashed line represents 5 mM TEA.

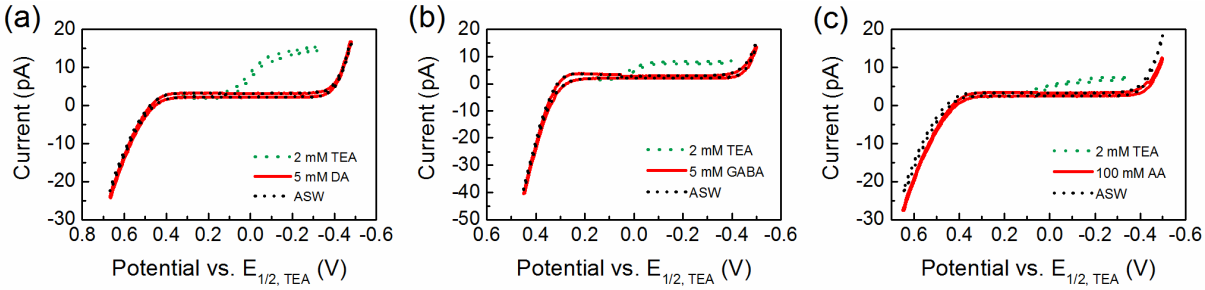

Figure A.5. Cyclic voltammograms of (a) 5 mM dopamine (DA), (b) 100 mM ascorbic acid (AA), and (c) 5 mM γ-aminobutric acid (GABA) in artificial sea water (ASW). Tetraethylammonium (TEA) was added at the end of each experiment to show that the probes used were working properly, ensuring that lack of signal from the possible interferents is because they do not transfer within the potential window of ASW.

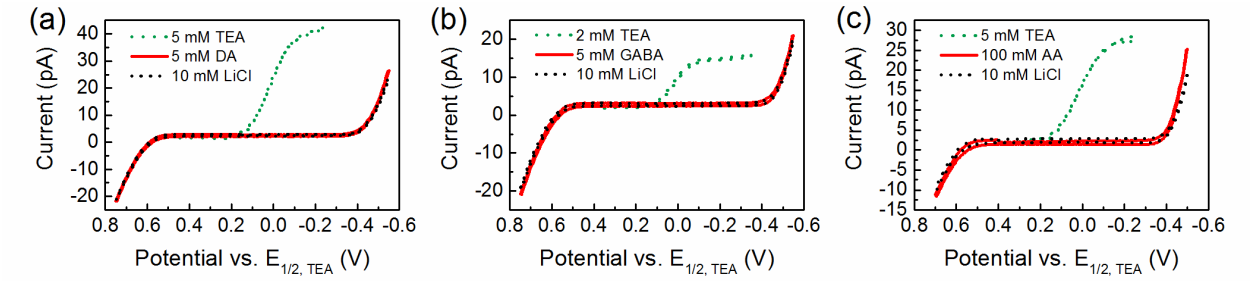

Figure A.6. Cyclic voltammograms of (a) 5 mM dopamine (DA), (b) 100 mM ascorbic acid (AA), and (c) 5 mM γ-aminobutric acid (GABA) in 10 mM LiCl. Tetraethylammonium (TEA) was added at the end of each experiment to show that the probes used were working properly, ensuring that lack of signal from the possible intereferents is because they do not transfer within the potential window of LiCl.

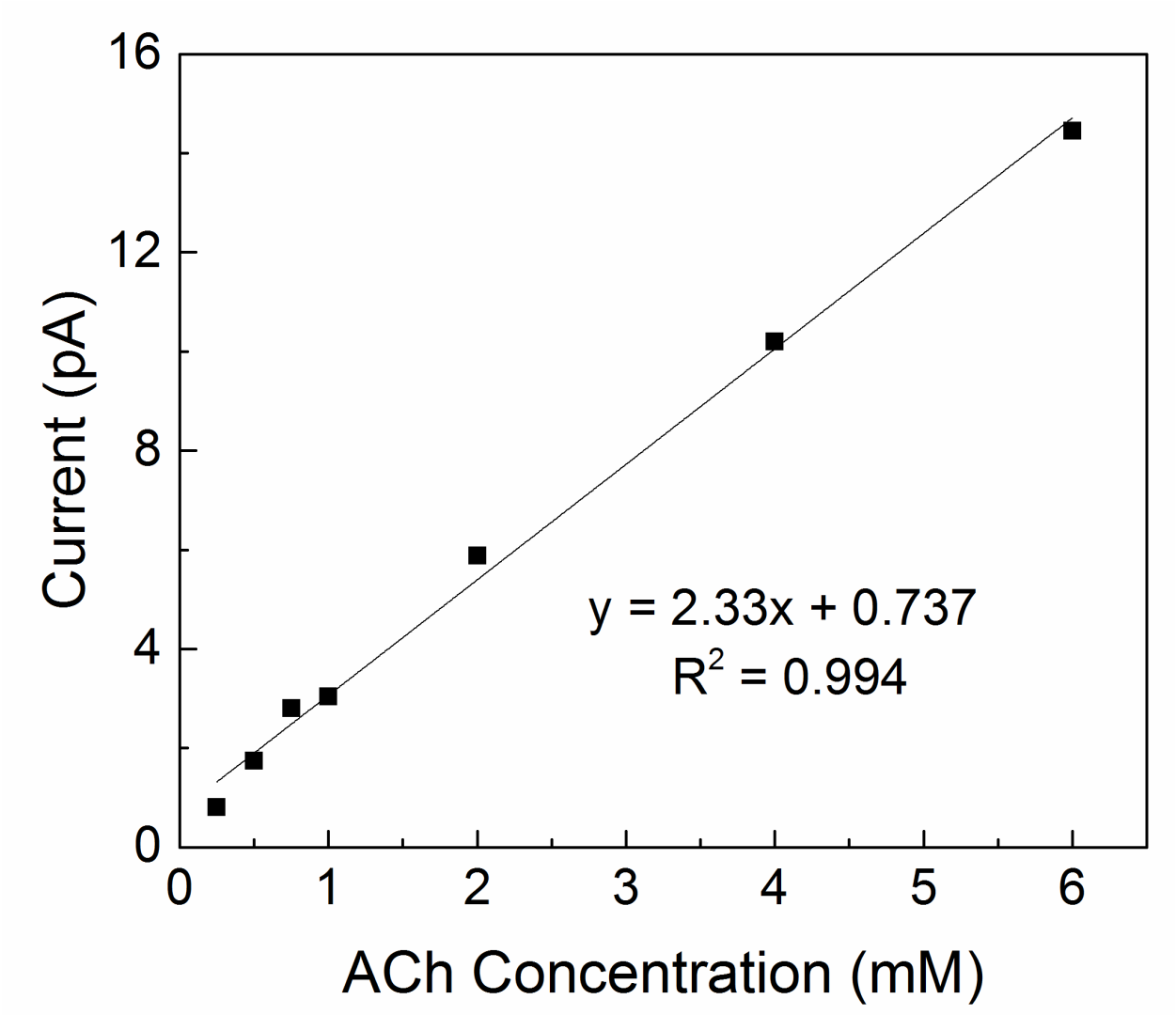

Figure A.7. Background subtracted calibration curve for cyclic voltammograms of 0.25 – 6 mM acetylcholine (ACh) using a pipet with a radius of 7 nm in Cell 1. Current was read at -0.25 V vs. $E_{1/2,\ TEA}$ in Figure 3a.

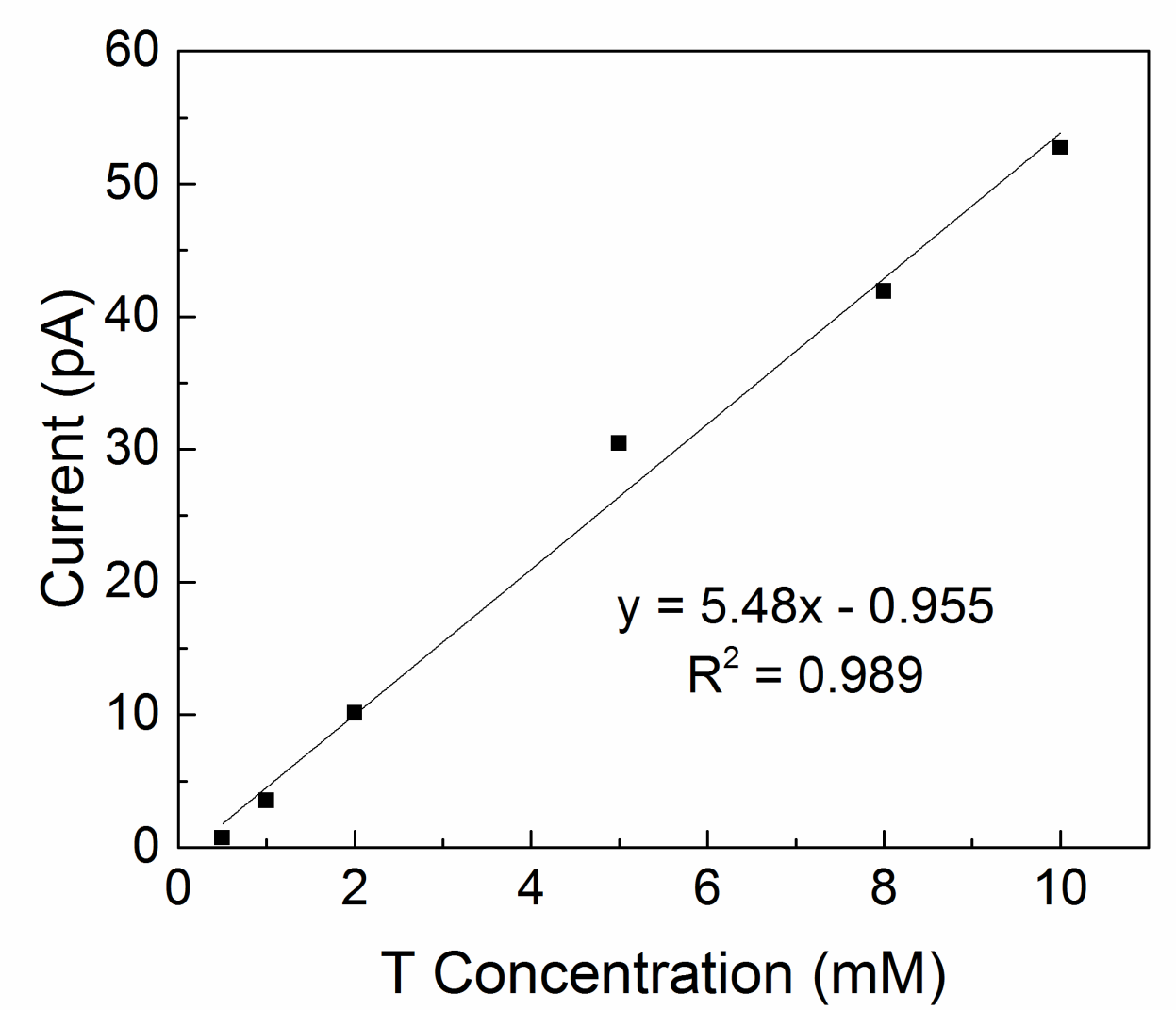

Figure A.8. Background subtracted calibration curve for cyclic voltammograms of 0.5 – 10 mM tryptamine (T) using a pipet with a radius of 19 nm in Cell 1. Current was read at -0.32 V vs. $E_{1/2,\ TEA}$ in Figure 3c.

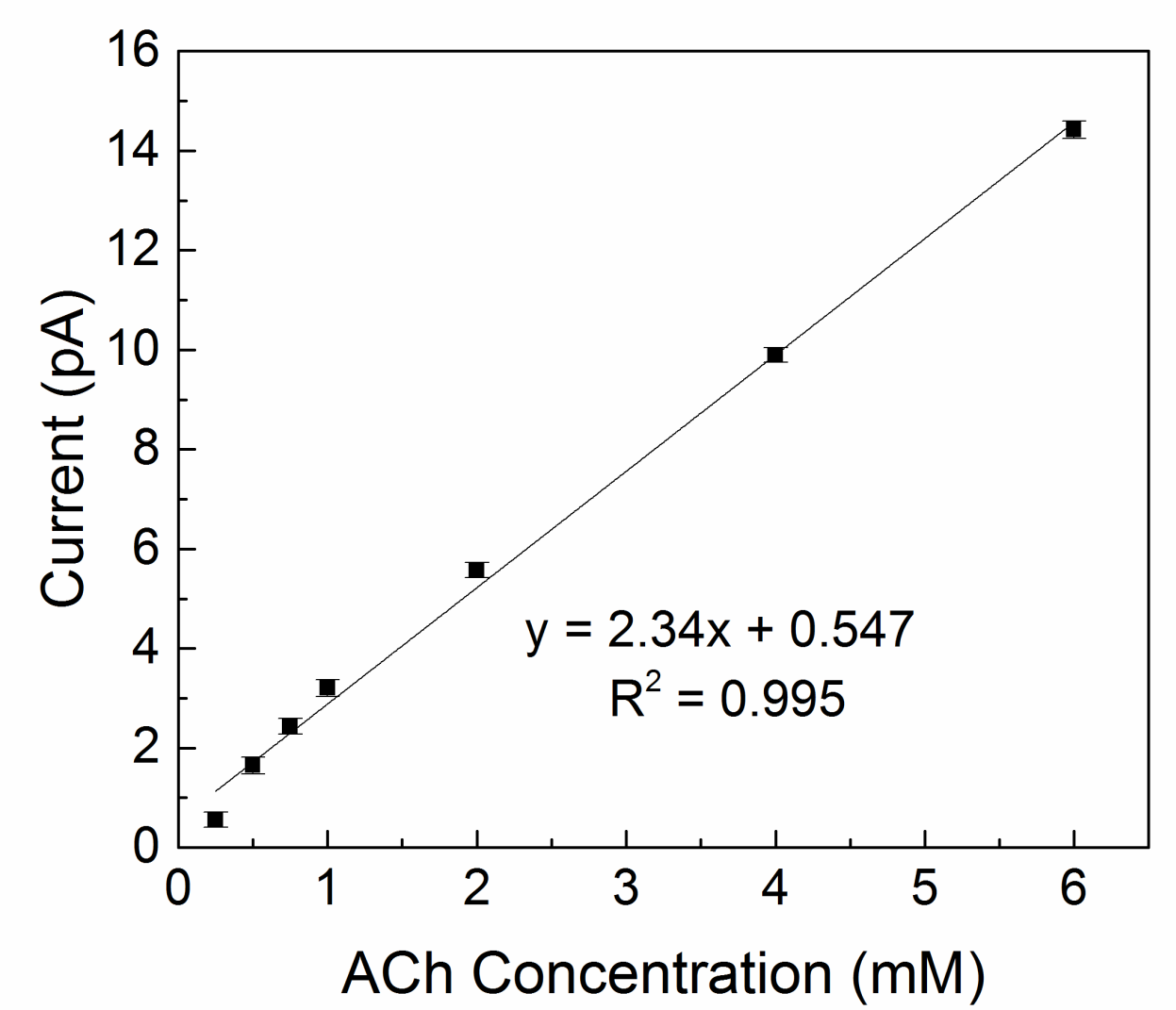

Figure A.9. Background subtracted calibration curve for amperometry of acetylcholine (ACh) based on Figure 3b. Applied potential = -0.25 V vs. $E_{1/2,\ TEA}$. Data points represent the average current over 50.0 s, and error bars represent standard deviation. Measurements were made using Cell 1.

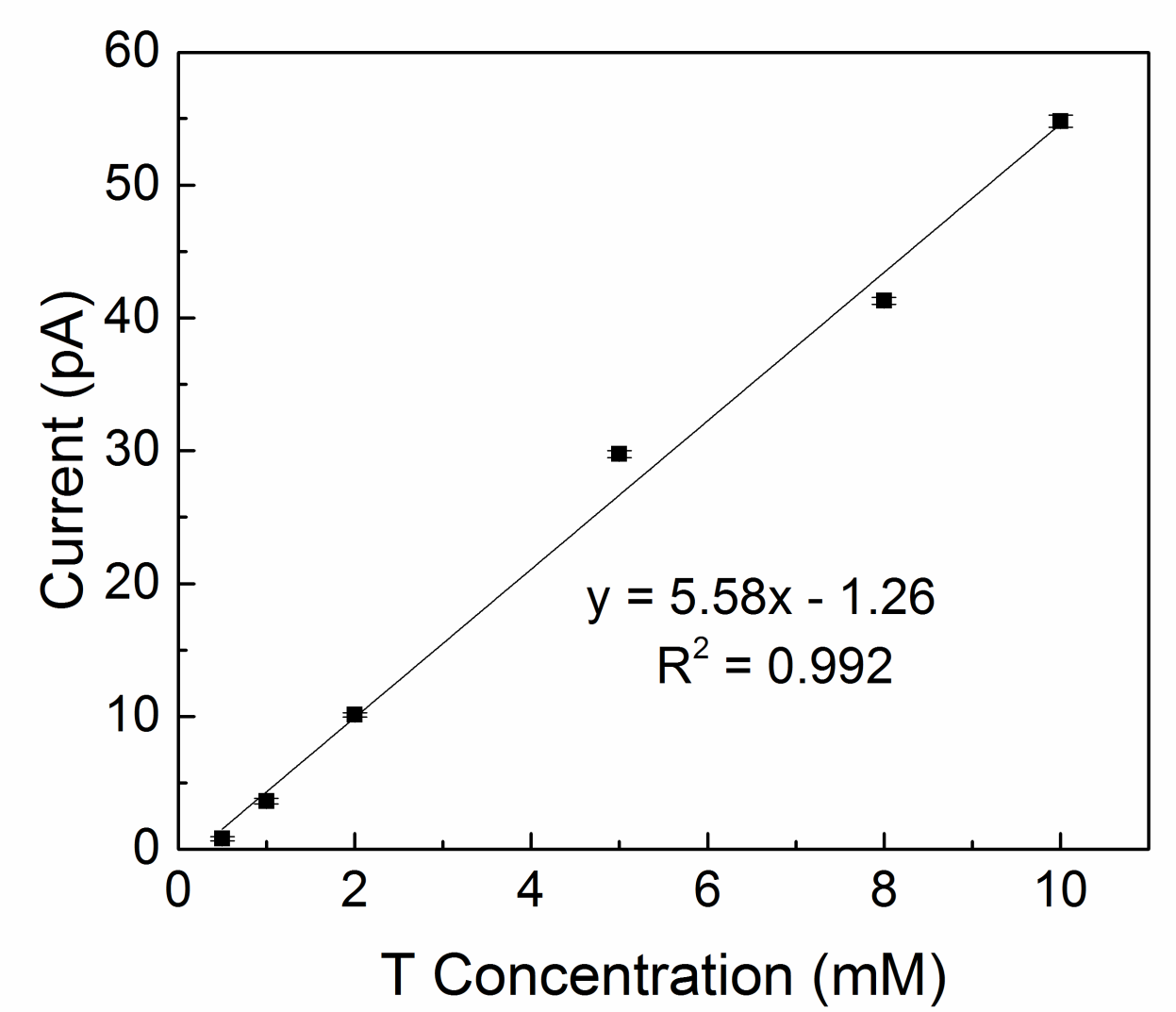

Figure A.10. Background subtracted calibration curve for amperometry of tryptamine (T) based on Figure 3d. Applied potential = -0.32 V vs. $E_{1/2,\ TEA}$. Data points represent the average current over 50.0 s, and error bars represent standard deviation. Measurements were made using Cell 1.

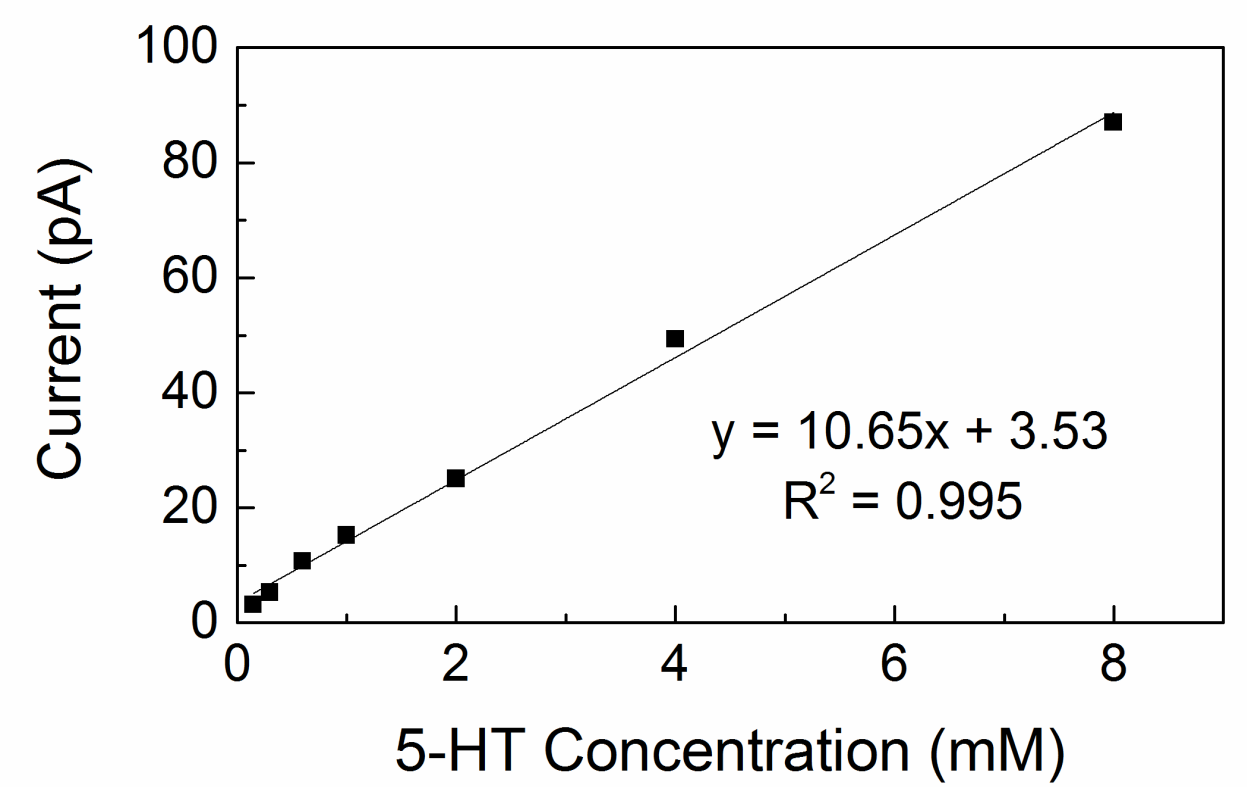

Figure A.11. Background subtracted calibration curve for cyclic voltammograms of 0.15 – 8 mM serotonin (5-HT) using a pipet with a radius of 35 nm in Cell 2. Current was read at -0.51 V vs. $E_{1/2,\ TEA}$.

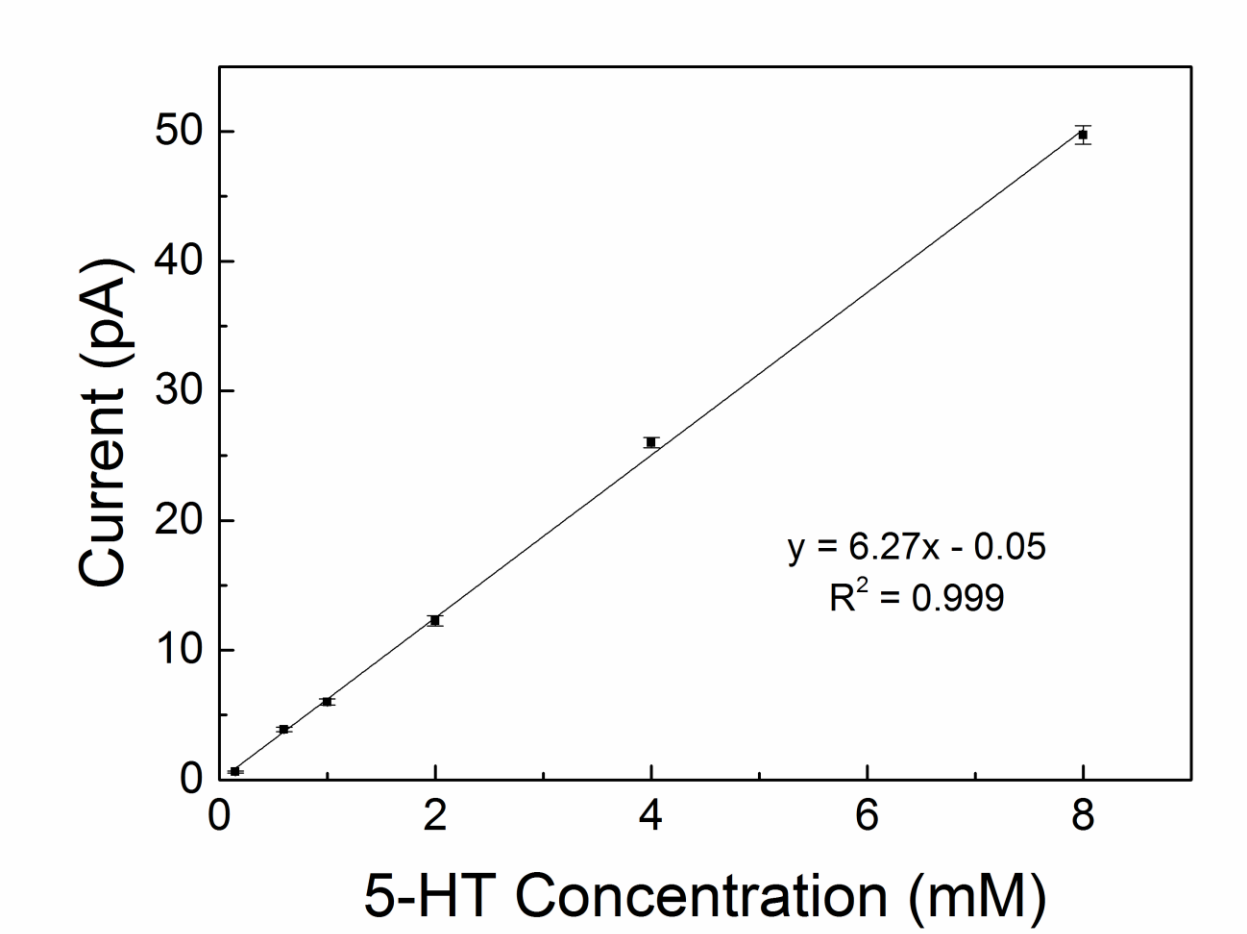

Figure A.12. Background subtracted calibration curve for amperometry of serotonin (5-HT) based on Figure 4b. Applied potential = -0.52 V vs. $E_{1/2,\ TEA}$. Data points represent the average current over 50.0 s, and error bars represent standard deviation. Measurements were made using a pipet with a radius of 21 nm using Cell 2.

APPENDIX B

INFORMATION SUPPORTING CHAPTER 3

Table B.1. pH of solution with addition of dopamine (DA) and ascorbic acid (AA) in a background solution of 10 mM $MgCl_2$.

Concentration (mM)	**pH**
0	6.18
2 AA	3.26
0.25 DA	3.27
0.5 DA	3.23
1 DA	3.36
2 DA	3.28
20 AA	2.60

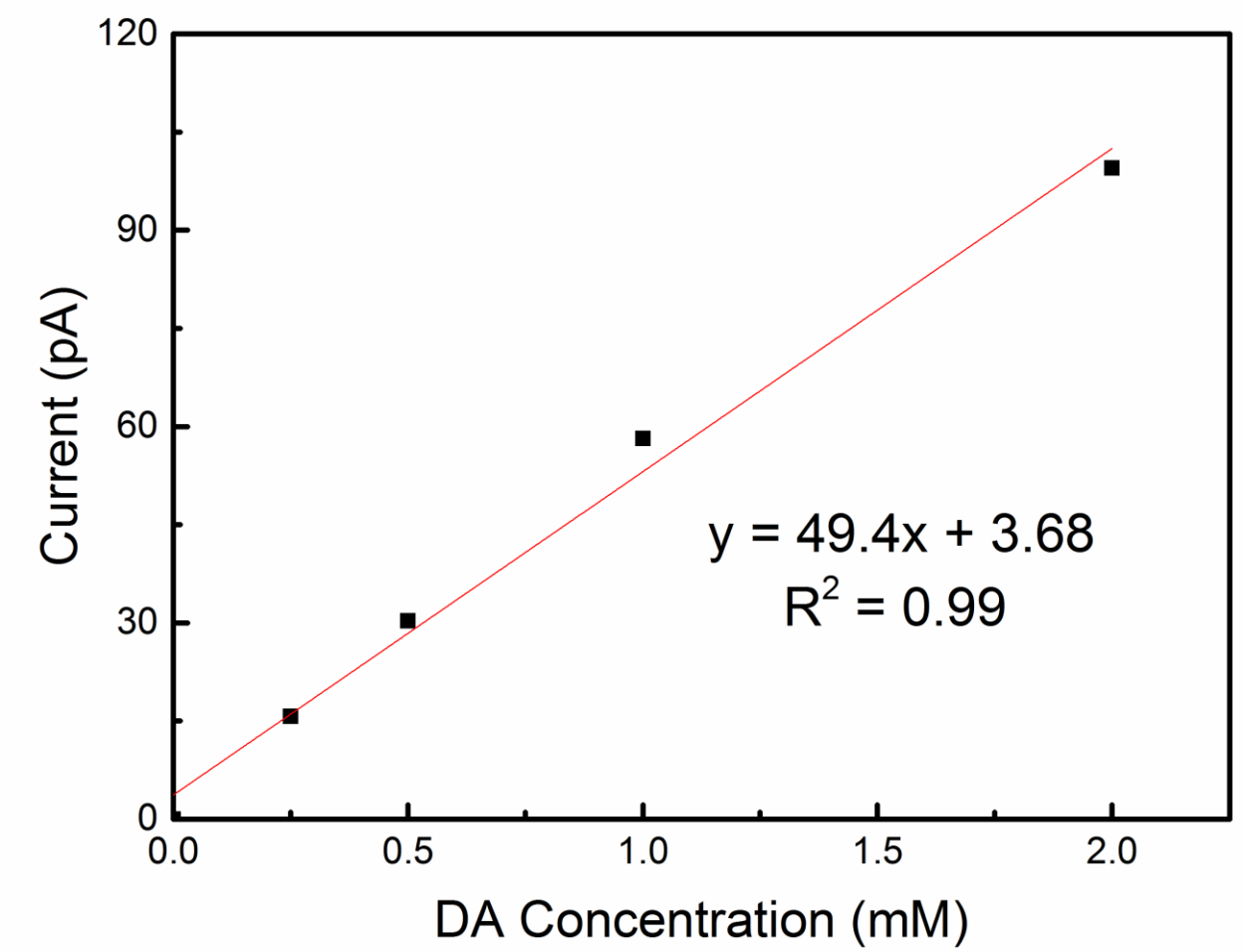

Figure B.1. Calibration curve corresponding to cyclic voltammogram overlays of 0.25 – 2 mM dopamine transfer shown in Figure 1a.

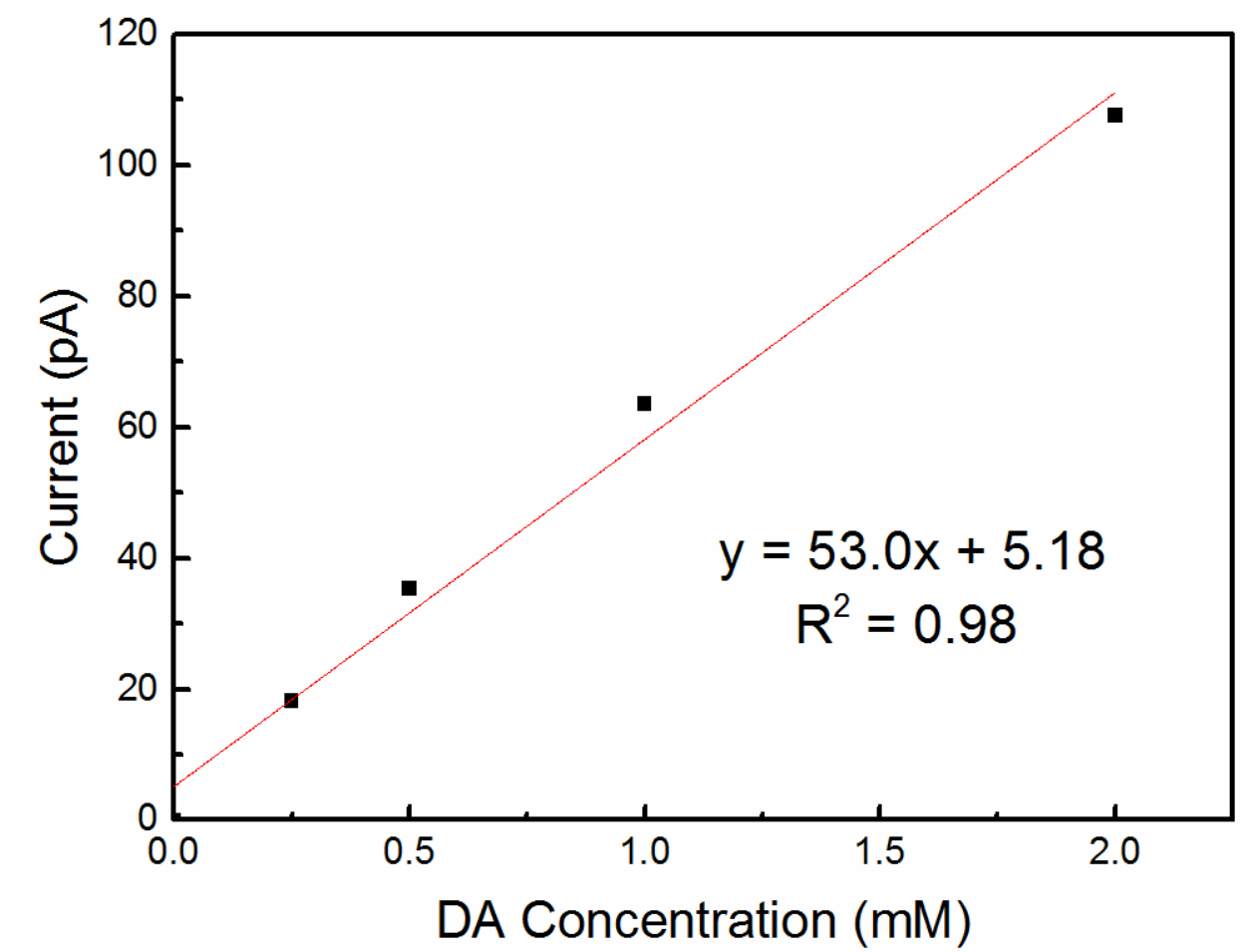

Figure B.2. Calibration curve corresponding to cyclic voltammogram overlays of 0.25 – 2 mM dopamine transfer shown in Figure 1b.

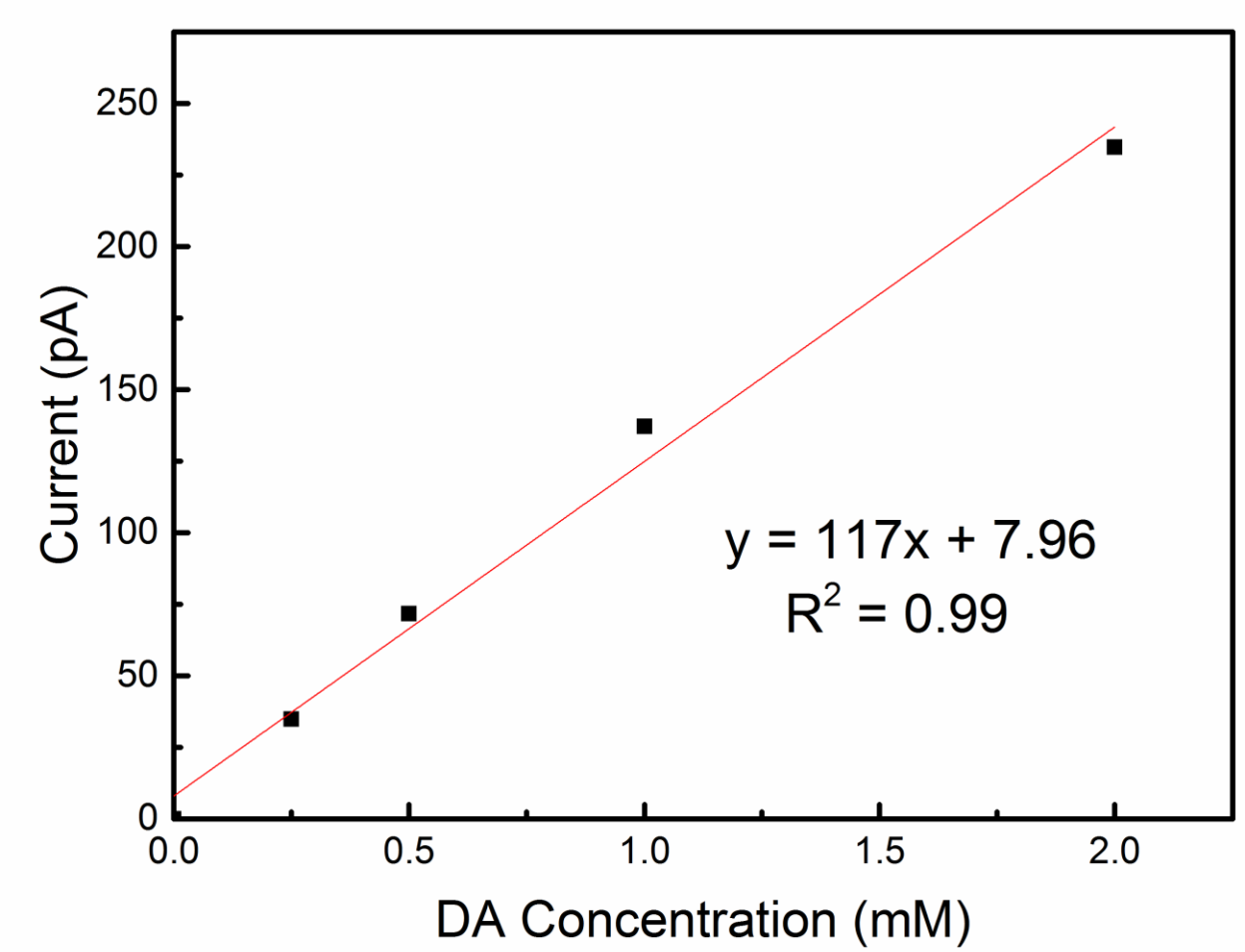

Figure B.3. Calibration curve corresponding to cyclic voltammogram overlays of 0.25 – 2 mM dopamine transfer shown in Figure 1c.

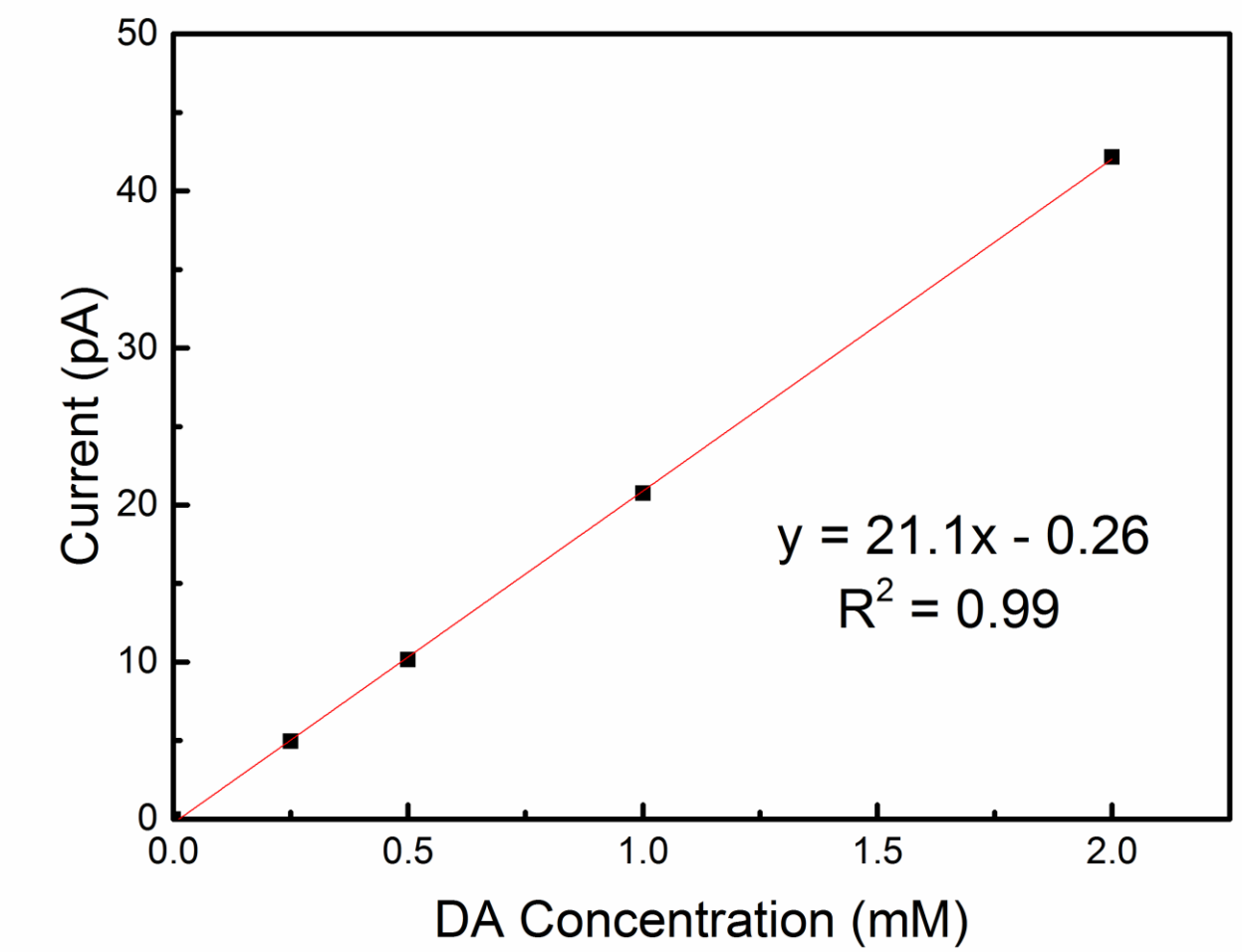

Figure B.4. Calibration curve corresponding to cyclic voltammogram overlays of 0.25 – 2 mM dopamine transfer shown in Figure 2a.

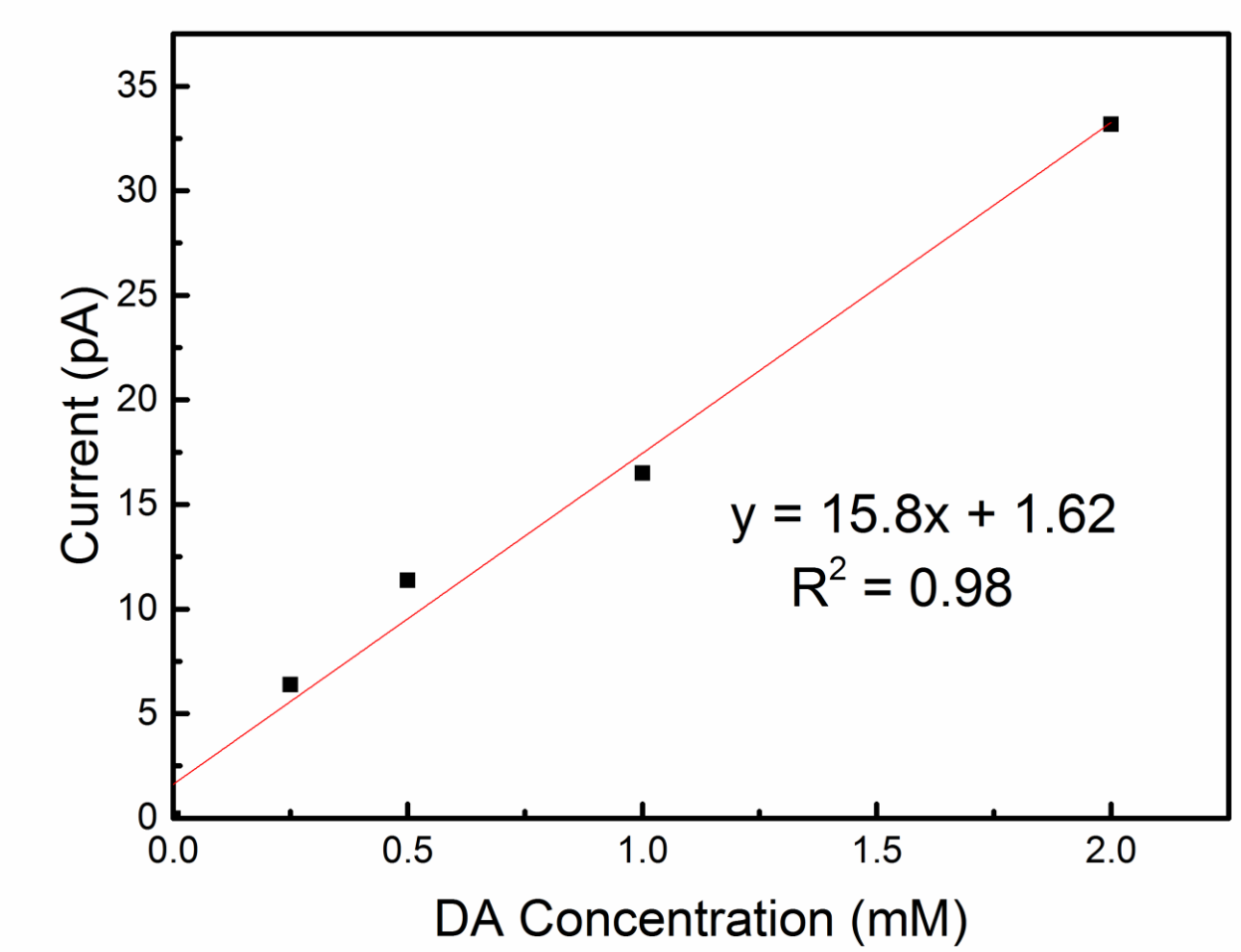

Figure B.5. Calibration curve corresponding to cyclic voltammogram overlays of 0.25 – 2 mM dopamine transfer shown in Figure 2b.

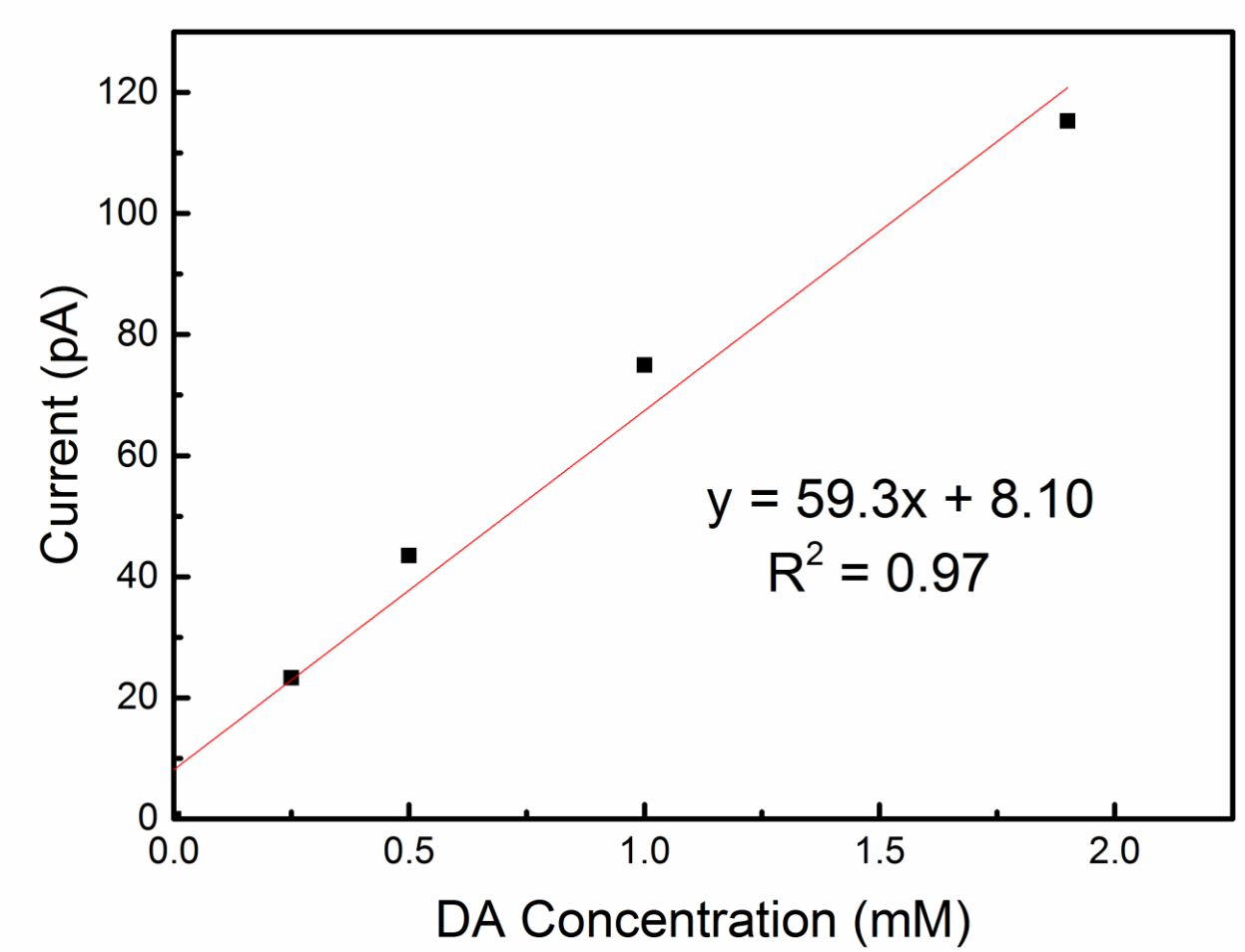

Figure B.6. Calibration curve corresponding to cyclic voltammogram overlays of 0.25 – 2 mM dopamine transfer shown in Figure 3.

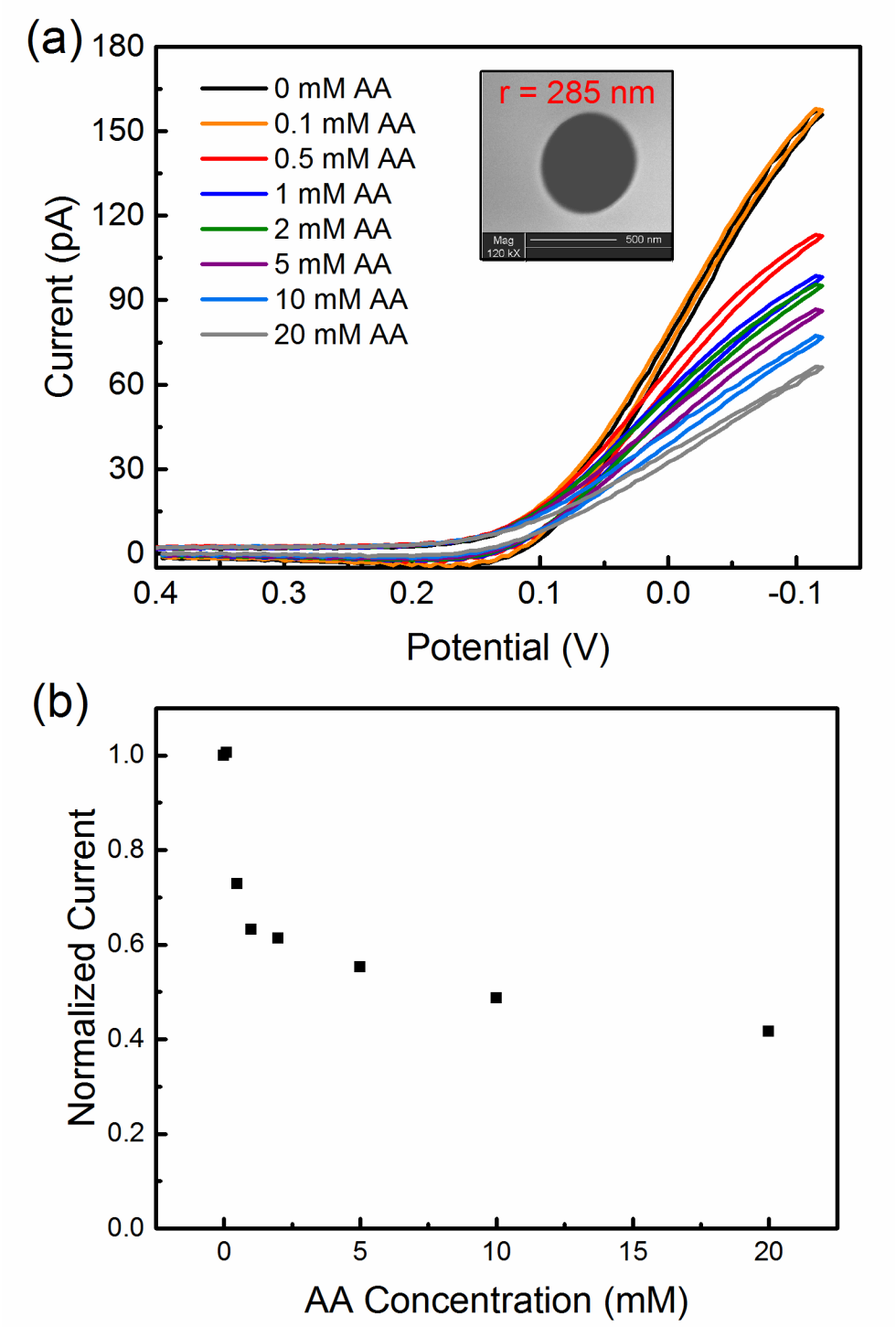

Figure B.7. (a) Cyclic voltammograms and (b) normalized current response of 2 mM DA with respect to additions of ascorbic acid ranging from 0.1 – 20 mM, using cell 2.